

**Blockade of Oncogenic NOTCH1 with the New SERCA Inhibitor CAD204520  
in T-cell Acute Lymphoblastic Leukemia**

Matteo Marchesini<sup>1, 10</sup>, Andrea Gherli<sup>1, 10</sup>, Anna Montanaro<sup>1</sup>, Laura Patrizi<sup>2</sup>, Claudia Sorrentino<sup>1</sup>, Luca Pagliaro<sup>1</sup>, Chiara Rompietti<sup>2</sup>, Samuel Kitara<sup>3</sup>, Sabine Heit<sup>4</sup>, Claus E. Olesen<sup>5</sup>, Jesper V. Møller<sup>5</sup>, Monia Savi<sup>6</sup>, Leonardo Bocchi<sup>6</sup>, Rocchina Vilella<sup>6</sup>, Federica Rizzi<sup>1,7</sup>, Marilena Baglione<sup>1</sup>, Giorgia Rastelli<sup>1</sup>, Caterina Loiacono<sup>1</sup>, Roberta La Starza<sup>2</sup>, Cristina Mecucci<sup>2</sup>, Kimberly Stegmaier<sup>3,8</sup>, Franco Aversa<sup>1</sup>, Donatella Stilli<sup>6</sup>, Anne-Marie Lund Winther<sup>9</sup>, Paolo Sportoletti<sup>2</sup>, Maike Bublitz<sup>4</sup>, William Dalby-Brown<sup>9</sup>, Giovanni Roti<sup>1, 11,\*</sup>

<sup>1</sup>University of Parma, Department of Medicine and Surgery, Parma, 43126, Italy

<sup>2</sup>University of Perugia, Department of Medicine, Hematology and Clinical Immunology, Perugia, 06123, Italy

<sup>3</sup>Department of Pediatric Oncology, Dana-Farber Cancer Institute, Harvard Medical School, Boston, Massachusetts, 02215, USA

<sup>4</sup>University of Oxford, Department of Biochemistry, Oxford, OX1 3QU, United Kingdom

<sup>5</sup>Aarhus University, Department of Biomedicine, 8000 Aarhus C, Denmark

<sup>6</sup>University of Parma, Department of Chemistry, Life Sciences and Environmental Sustainability, Parma, 43124, Italy

<sup>7</sup>INBB – Biostructures and Biosystems National Institute, Rome, 00136, Italy

<sup>8</sup>The Broad Institute, Cambridge, Massachusetts, 02142, USA

<sup>9</sup>Cado Biotechnology IvS, Copenhagen, Denmark

<sup>10</sup>These authors contributed equally to this work

<sup>11</sup> Lead contact

\*Correspondence: [giovanni.roti@unipr.it](mailto:giovanni.roti@unipr.it)

## SUMMARY

The identification of SERCA (Sarco/Endoplasmic Reticulum Calcium ATPase) as a target for modulating gain-of-function *NOTCH1* mutations in Notch-dependent cancers has spurred the development of this compound class for cancer therapeutics. Despite the innate toxicity challenge associated with SERCA inhibition, we identified CAD204520 a small molecule with better drug-like properties and reduced off-target  $\text{Ca}^{2+}$  toxicity compared to the SERCA inhibitor thapsigargin.

In this work, we describe the properties and complex structure of CAD204520 and show that CAD204520 preferentially targets mutated over wild type *NOTCH1* proteins in T-cell acute lymphoblastic leukemia (T-ALL) and mantle cell lymphoma (MCL). Uniquely among SERCA inhibitors, CAD204520 suppresses *NOTCH1* mutated leukemic cells in a T-ALL xenografted model without causing cardiac toxicity.

This study supports the development of SERCA inhibitors for Notch-dependent cancers and extends their application to cases with isolated mutations in the PEST degradation domain of *NOTCH1*, such as MCL or chronic lymphocytic leukemia (CLL).

## INTRODUCTION

Genetic alterations in Notch signaling have been described in the majority of human cancers (Lawrence et al., 2014). Most of the recurrent somatic mutations of NOTCH proteins (I-IV) are observed in the *NOTCH1* gene. *NOTCH1* encodes a single-pass transmembrane protein with transcription factor activity that acts in stem cell differentiation (Artavanis-Tsakonas et al., 1999; Pui et al., 1999), cell fate determination (Pui et al., 1999) and in tissue development processes (Penton et al., 2012). The NOTCH1 protein has several functional domains organized in evolutionarily conserved modules. The extra-cellular N-terminal domain is responsible for ligand binding through EGF-like calcium ( $\text{Ca}^{2+}$ ) dependent repeats, which are followed by three LNR modules that protect the extracellular portion from cleavage in the absence of ligand. The heterodimerization domain (HD) is a linker between the extracellular tail and the intracellular NOTCH active form (ICN1). Notch1 activation requires two sequential protein cleavage steps mediated by ADAM10/17 metalloproteases and the presenilin- $\gamma$ -secretase complex to release the intracellular portion of NOTCH1, ICN1, which translocates into the nucleus and mediates the activation of the Notch pathway (De Strooper et al., 1999; Kopan and Ilagan, 2009).

The involvement of NOTCH1 in the pathogenesis of T-cell acute lymphoblastic leukemia (T-ALL), an aggressive form of leukemia that mainly affects children, was initially discovered in 1991 (Ellisen et al., 1991). Ellisen and colleagues described a chromosome translocation, t(7;9), that juxtaposes the promoter elements of the



T-cell receptor- $\beta$  (TCRB) to the 3' end portion of the *NOTCH1* gene encoding its intracellular domain ICN1 (Ellisen et al., 1991). This fusion results in the overexpression of ICN1 causing the activation of genes that promote T-cell leukemogenesis. Similarly, activating *NOTCH1* mutations generate ligand-independent or proteasome resistant ICN1 polypeptides that sustain T-cell transformation and leukemia growth (Aster et al., 2008; Weng et al., 2004).

Although the frequency of mutations is highest in T-ALL, *NOTCH1* has emerged as one of the most frequently mutated genes (~5-20%) in chronic lymphocytic leukemia (CLL) (Di Ianni et al., 2009; Puente et al., 2011). The most frequent mutation, ~80%, is a 2-bp deletion in exon 34 that generates a premature stop codon (P2514fs\*4) leading to a truncation of the C-terminal PEST region. As in T-ALL these mutations cause an over-activation of Notch1 signaling because of the lack of its degradation (Arruga et al., 2014). Interestingly, additional studies reported a similar pattern of PEST mutations in mantle cell lymphoma (MCL) (Bea et al., 2013; Kridel et al., 2012) and in activated B-cell-like (ABC) diffuse-large B-cell lymphoma (6.1%) (Schmitz et al., 2018). PEST mutations identify genetic subtypes of B-cell lymphoma with a worse prognosis (Arruga et al., 2014; Baliakas et al., 2015; Inamdar et al., 2016; Schmitz et al., 2018), suggesting the need to extend targeting Notch1 in these aggressive forms of B-cell malignancies.

The Notch signaling pathway is also frequently activated in multiple types of solid tumors (Lobry et al., 2011; Stransky et al., 2011), such as melanoma, colorectal

carcinoma, and cholangiocarcinoma through mechanisms that differ from genetic variations (Roy et al., 2007; Wang et al., 2014). Paradoxically, mutations that inactivate the Notch pathway have been described in several human cancers as well (Klinakis et al., 2011; Stransky et al., 2011) showing that, depending on the cellular context, Notch signaling can be oncogenic or tumor suppressive and suggesting that fine-tuned inhibition of Notch signaling could be useful in those situations where Notch is activated.

The preponderance of oncogenic *NOTCH1* mutations in lymphoid malignancies has prompted the search for effective anti-Notch1 therapeutics (Baldoni et al., 2018; Roti and Stegmaier, 2011; Roti and Stegmaier, 2014). Because Notch activation relies on  $\gamma$ -secretase mediated proteolysis, inhibitors (GSI) had entered in clinical trials to treat relapsed T-ALL. However, the first generations of GSIs were poorly tolerated because of on-target gastro-intestinal toxicity (DeAngelo, 2006; Golde et al., 2013; van Es et al., 2005). As shown by Riccio and colleagues, the toxic effect of GSIs are a consequence of lack of substrate specificity of these molecules resulting in the combined inhibition of wild type NOTCH1 and NOTCH2 in intestinal progenitor cells (Riccio et al., 2008). Although few patients achieved a complete response, GSIs exhibited moderate clinical activity in some patients with solid tumor and leukemia (Knoechel et al., 2015). Recently, several studies demonstrated that combining GSIs with chemotherapy or other targeted agents increases the anti-cancer effects of these drugs (Groeneweg et al., 2014;

Mukherjee et al., 2016; Schott et al., 2013; Yuan et al., 2015), supporting the development of innovative anti-NOTCH1 therapeutics.

We have previously established that a small-molecule inhibitor of SERCA (Sarco/Endoplasmic Reticulum Calcium ATPase), thapsigargin, inhibits NOTCH1 and possesses anti-leukemia activity in a mouse model of human T-ALL. Importantly, thapsigargin preferentially inhibits the maturation of mutant NOTCH1 receptors compared to wild type NOTCH1 and NOTCH2 receptors. This selectivity provides a therapeutic window not observed before with other Notch modulators, including  $\gamma$ -secretase inhibitors or antibody-based approaches (Roti et al., 2013; Sorrentino et al., 2019). However, thapsigargin binding to SERCA results in an increase in cytosolic  $\text{Ca}^{2+}$  concentration and a depletion of  $\text{Ca}^{2+}$  stored in the endoplasmic reticulum (ER). Thus, the delivery of free thapsigargin to humans might cause cardiac toxicity due to a calcium ion shift. To overcome this limitation, we generated a thapsigargin pro-drug to deliver the small molecule in T-ALL. To this end, we took advantage of the dependency of ALL on folic acid (FA) and tagged folate to a permissive site on an active alcohol derivative of thapsigargin (8-O-debutanoylthapsigargin) via a cleavable ester linkage (JQ-FT) (Roti et al., 2017). However, an alternative approach to reduce the potential toxicity of thapsigargin is through the identification of SERCA inhibitors that retain the anti-Notch properties but lack  $\text{Ca}^{2+}$  related toxicities.

In this work, from a series of P-type ATPase inhibitors we optimized and characterized the effect of the selective SERCA modulator CAD204520 in *NOTCH1* mutated T-ALL. We demonstrate that CAD204520 exhibits a reduced  $\text{Ca}^{2+}$ -related toxicity but retains anti-Notch1 and anti-leukemia capacity both *in vitro* and *in vivo* in *NOTCH1* mutated T-ALL models. Furthermore, by extending the testing of CAD204520 in B-cell malignancies carrying clinically relevant PEST mutations, we demonstrate the potential of SERCA inhibition as a therapeutic approach against these cancers.

## RESULTS

### Identification of CAD204520 as a selective $\text{Ca}^{2+}$ ATPase inhibitor

P-type ATPases are a group of evolutionarily conserved proteins that transport a variety of charged substrates such as  $\text{H}^+$ ,  $\text{Na}^+$ ,  $\text{K}^+$ ,  $\text{Ca}^{2+}$ ,  $\text{Zn}^{2+}$ , and  $\text{Cu}^+$  or phospholipids across membranes (Bublitz et al., 2011). Since P-type ATPases control active ion transport across cellular membranes, their altered activity is associated with the development of pathophysiological conditions including cardiovascular, neurological, renal and metabolic diseases. Consequently, P-type ATPases are compelling therapeutic-targets. For example, the cardiac  $\text{Na}^+/\text{K}^+$ -ATPase inhibitor, digoxin (Hauptman and Kelly, 1999) and gastric  $\text{H}^+$ ,  $\text{K}^+$ -ATPase inhibitor, omeprazole (Sachs, 1997) are among the most clinically successful therapeutics in this target class (Burghoorn et al., 2002).

In recent years, P-type ATPases (e.g., SERCA) have emerged as potential dependencies in cancer (Yatime et al., 2009) and as mediators of chemotherapy resistance in solid tumors (Li et al., 2012; Samimi et al., 2004). Their importance for cell survival has furthermore sparked an interest in inhibiting P-type ATPases of pathogenic fungi and bacteria (Seto-Young et al., 1997). To identify potent P-type ATPase inhibitors in this context, Kjellerup and colleagues screened a library containing nearly 191 000 compounds for inhibition of the fungal  $\text{H}^+$ -ATPase (Kjellerup et al., 2017). A total of 407 compounds inhibited ATP hydrolysis activity of the  $\text{H}^+$ -ATPase by greater than 50% and were subsequently counter-screened for P-type ATPase specificity, by testing their effect on mammalian SERCA (rabbit

SERCA1a, that share 96.6% protein similarity with the human SERCA orthologues) and the pig Na<sup>+</sup>/K<sup>+</sup>-ATPase (Bublitz et al., 2018; Clausen et al., 2017; Kjellerup et al., 2017) (**Figure 1A**).

The initial hit compound, 2-(2-pyridyl)-6-(trifluoromethoxy)-1H-indole (**Figure 1B (I)**, **Figure S1A**) was a weak inhibitor of SERCA ATPase (IC<sub>50</sub> = 236 μM) but with an attractive low molecular weight. An extensive exploration of the chemical space occupied by the pyridine core was performed through a systematic replacement with commercially available alternative heteroaromatic and heterocyclic systems, as well pyridines substituted with small functional groups capable of picking up polar interactions. As a result, the piperidine analogue 2-(2-piperidyl)-6-(trifluoromethoxy)-1H-indole (**Figure 1B (II)**) was identified as the minimum pharmacophore with improved SERCA ATPase potency, selectivity against Na<sup>+</sup>/K<sup>+</sup>-ATPase and a reasonable ligand efficiency (LE) of 0.28. Options for diversity in substitution of indole C4-C7 were limited and C6-OCF<sub>3</sub> was “locked” to continue exploration of more promising points of substitution. Furthermore, indole N1 had been extensively explored in a closely related chemical program with an overlapping pharmacophore, and for reasons of concern about target selectivity it was decided not to explore the indole N1 chemical space with the identified Compound II. Conversely, Compound II was explored in R<sup>1</sup> of the indole system, and R<sup>2</sup> of the piperidine system (**Figure S1B**) for reasons detailed below.

Compounds with substitution on piperidine N1 (R<sup>2</sup>) with R<sup>1</sup>=H were subsequently produced and, among them, CAD204522, CAD307496, and CAD204521 (**Figure**

**1B**) showed various degree of  $\text{Ca}^{2+}$ -ATPase activity (**Table S1**). Interestingly, CAD204521 (**Figure 1B (III)**, **Table S1**) was closely related to a previously reported potent fungal  $\text{H}^{+}$ -ATPase inhibitor, Compound 7 (Bublitz et al., 2018). Similarly to Compound 7, CAD204521 showed an improved potency against  $\text{Ca}^{2+}$  ATPase but not a desired selectivity or drugability profile. Because indole C3 had the potential to provide  $\text{Ca}^{2+}$ -ATPase selectivity, we decided to explore indole  $\text{R}^1$  with  $\text{R}^2$ =p-bromobenzyl (derivatives of CAD204521, (IV)) (**Figure 1B**). For example, CAD204519 was by far the most potent inhibitor of  $\text{Ca}^{2+}$ -ATPase, however with an unfavorable  $\text{Na}^{+}/\text{K}^{+}$   $\text{Ca}^{2+}$  selectivity. Nevertheless, substitutions with certain hydrophilic groups on the  $\text{R}^2$  on piperidine N1 (**Figure 1B**, **Table S1**, CAD306750, CAD306749, CAD204520) increased the selectivity toward mammalian SERCA.

Notably, CAD204520 (**Figure 1B (V)**, **Figure S1C**) preferentially inhibited the  $\text{Ca}^{2+}$ -ATPase by reducing its ATP hydrolysis activity with an  $\text{IC}_{50} = 0.34 \pm 0.03 \mu\text{M}$  as compared to the  $\text{Na}^{+}/\text{K}^{+}$ -ATPase ( $\text{IC}_{50} = 8.30 \pm 0.94 \mu\text{M}$ ) and the  $\text{H}^{+}$ -ATPase ( $\text{IC}_{50}$  of  $26.90 \pm 2.98 \mu\text{M}$ ) (**Figure S1D**, **Table S1**). Furthermore, CAD204520 displayed the overall most promising drug properties of the synthesized compounds with a calculated LogP of 4.4 and LogD<sub>7.4</sub> of 2.2 (ACD/Labs 18.1.1). This compound was thus selected for further studies as a novel SERCA inhibitor.

To assess the binding mode of CAD204520 to SERCA, we then crystallized it in complex with SERCA and determined the crystal structure at 3.4 Å resolution. The crystals were of the same space group as previously reported thapsigargin-bound

SERCA (PDB:2AGV), and the overall conformation of SERCA bound to CAD204520 is very similar to the thapsigargin-bound form. The CAD204520 ligand binds to a groove at the membrane interface of SERCA, between the transmembrane helices M1, M2, M3 and M4 (**Figure 1C and 1D**) with two polar interactions to Asp59 on M1 (2.9 Å) and Asn101 on M2 (2.7 Å), and with several hydrophobic interactions involving Leu61, Val62, Ile307, Pro308, and Pro312 (**Figure 1C**). Interestingly, the CAD204520 binding groove is different from that of thapsigargin (**Figure S1E**), but similar to the binding of other SERCA inhibitors such as cyclopiazonic acid (CPA) (Laursen et al., 2009) (**Figure S1F**), 2,5-di-*t*-butyl-1,4-benzohydroquinone (BHQ) (Obara et al., 2005) (**Figure S1G**) and to that of the Compound 7 previously reported by Bublitz and colleagues (Bublitz et al., 2018) (**Figure S1H**). In fact, the indole system (core structure) of CAD204520 superposes very closely on the tetrahydrocarbazole core of Compound 7, including the central interaction of the indole N1 nitrogen with Asp59. The morpholinoethyl group, interacting with Asn101, occupies the same space as one of the two alternative positions found for the bromophenyl moiety of Compound 7 (**Figure S1H**). In contrast to Compound 7, however, there is no interaction with Asp245. Despite this similarity, CAD204520 does not induce the same overall SERCA conformation as Compound 7, but a conformation almost identical to thapsigargin-inhibited SERCA. The thapsigargin-binding site lies adjacent to the CAD204520 site, separated by M3 (**Figure S1I**).

Collectively these data show that CAD204520 selectively binds SERCA in the same binding pocket as BHQ, CPA and Compound 7. This pocket has been



identified as the pathway for  $\text{Ca}^{2+}$  ion entry into the pump from the cytosolic side of the membrane (Winther et al., 2013), and compound binding at this site locks SERCA in a  $\text{Ca}^{2+}$ -free (so-called ' $E_2$ ') conformation.

### **CAD204520 rescues T-ALL cells from thapsigargin resistance**

SERCA can be inhibited by different small molecules such as thapsigargin, BHQ, 1,3- dibromo-2,4,6-tris (methyl-isothio-uronium) benzene (Br<sub>2</sub>-TITU) and CPA. These compounds have specific binding sites in the ATPase protein and hence different inhibitory mechanisms (Christensen et al., 1993). A first question is whether CAD204520 binding to SERCA mimics thapsigargin ATPase inhibitory kinetics or, rather, the two molecules act independently as predicted by structural data.

To test our hypothesis, we took two different approaches. First, we generated a T-ALL cell line (ALL/SIL) resistant to thapsigargin by selecting cells growing under increasing concentration of this molecule. At days (~) 90, 120 and 150 T-ALL cells displayed respectively a 2x, 10x, 27x fold increased  $\text{IC}_{50}$  (**Figure S2A**). To rule out that this drug resistance was mediated by altered expression of the target, we demonstrated that naïve and resistant cell lines showed similar level of SERCA2 and SERCA3 proteins (**Figure S2B**). In order to evaluate for thapsigargin-induced gene mutations within the *ATP2A 1-3* genes, we performed whole exome sequencing and limited our analysis to single nucleotide exonic missense variation with a Phred-scaled quality score >30 (standard error = 1/1000 = 0.1%; accuracy 99.9%) (**Figure S2C**). Previous work had demonstrated that mutations occurring

in the third stalk (M3) segment of SERCA determine the sensitivity of the ATPase to thapsigargin (Yu et al., 1999; Yu et al., 1998; Zhong and Inesi, 1998). In particular, mutations in the M3 segment between Asp<sup>254</sup> and Leu<sup>260</sup> increase the thapsigargin concentrations required for inhibiting SERCA by more than three orders of magnitude (Horn et al., 2018; Zhong and Inesi, 1998) (**Figure S2D**). Interestingly, in ALL/SIL resistant cells we identified, within the Asp<sup>254</sup>-Leu<sup>260</sup> hotspot, a missense single nucleotide polymorphism (SNP) occurring in the *ATP2A2* exon 8 (c.G770T) causing a Glycine<sup>257</sup>→Valine mutation in the M3 helix (**Figure 2A** and **Figure S1I** highlighted in red). No mutations occurred in *ATP2A1* (**Figure 2A, top panel**) while missense mutations in *ATP2A3* were present both in the naïve and in the resistant lines indicating a pre-existing mechanism of allelic variance (**Figure 2A, bottom panel**). Similarly, no acquired mutations were identified in *SEC24A*, a gene involved in the ER-Golgi protein trafficking and previously identified as an essential mediator of thapsigargin-induced cell death in a genome-wide CRISPR/Cas9 screen in HAP1 cancer cells (Chidawanyika et al., 2018). According to our crystal structure, Gly<sup>257</sup> faces a hydrophobic part of CAD204520 at a distance that could probably accommodate a valine residue without interfering with CAD204520 binding (**Figure S1I**). The introduction of the bulky valine side chain will, however, very likely limit the freedom of movement of the neighbouring residue Phe<sup>256</sup>, which has to swing sideways in order to accommodate thapsigargin binding (**Figure S1E and S1I**), thus providing a potential explanation for the resistance effect.

Next, we treated ALL/SIL naïve and resistant cells at ALL/SIL IC<sub>50</sub> (as shown in the following sections), concentrations, and demonstrated that G<sup>257</sup>→V rescues ALL/SIL cells from thapsigargin induced cytotoxicity while it does not interfere with CAD204520 effects (**Figure 2B**). Accordingly, we hypothesize that because CAD204520 binds to SERCA in a pocket similar to that of CPA but distinct to that of thapsigargin, we anticipated that the combined inhibition might result in a synergistic effect with thapsigargin but not with cyclopiazonic acid. To avoid the limitations and biases associated with any one algorithm used to study drug-drug interactions, we used comprehensive approaches, including the Loewe additivity model, the Chou and Talalay index and the BRAID analysis. The Loewe additivity is a commonly used dose-effect-based model to quantify a zero-interactive state for the combination of two drugs (Loewe, 1953). The Chou-Talalay method (Chou, 2010) for drug combination is based on the median-effect equation and provides a mechanism-independent method for quantitative determination, combination index (CI), of drug interactions. A CI ranging from 0.9 to 1.1 is considered additive, a CI < 0.9 indicates synergy and a CI > 1.1 resistance. Finally, we used a response surface method, the Bivariate Response to Additive Interacting Doses (BRAID) model of combined action (Twarog et al., 2016; Twarog et al., 2018). A κ BRAID index > 0 shows synergy between the compounds tested. Unlike most methods that reduce combination analysis to a simple decision between synergy, additivity, and antagonism, surface models use non-linear optimization to fit a response surface model to the effects of combined compounds. We tested CAD204520 and thapsigargin both individually and in combinations at the indicated concentrations

for a total of sixty combinatorial points in T-ALL cell lines and in primary *NOTCH1* mutated T-ALL samples. We found that simultaneous exposure to CAD204520 and thapsigargin for 72 hours resulted in a robust synergistic inhibition of cell viability in T-ALL cells. Loewe, CI and BRAID models established a synergistic effect at low-dose combinations and support the notion that CAD204520 binds at a site within SERCA that is distinct from the thapsigargin binding sites (**Figure 2C-E**). Consistent with our hypothesis, combined CAD204520 and CPA treatment did not demonstrate the same degree of synergistic activity (**Figure S2E**).

Collectively, these data indicate that G257V mutation in the M3 helix of SERCA do not interfere with CAD204520 activity and that a greater anti-leukemia effect may be achieved by the simultaneous binding of CAD204520 and thapsigargin to their respective sites in SERCA.

### **CAD204520 suppresses leukemia growth in *NOTCH1* mutated T-ALL and MCL**

We previously demonstrated that SERCA inhibitors decrease T-ALL growth both *in vitro* and *in vivo* (Roti et al., 2013). To validate CAD204520 as a potential modulator of Notch-dependent cancers we initially tested the effect of CAD204520 in a panel of T-ALL or Mantle cell lymphoma (MCL) cell lines that contain activating mutations in the heterodimerization domain (HD) of *NOTCH1* and/or deletions in the degradation domain (PEST) (**Figure S3A**). *NOTCH1* mutated T-ALL (**Figure 3A**) (ALL/SIL, CTV-1, DND41, PF382, RPMI-8402) or MCL cell lines suppressed by GSI (REC-1) (**Figure 3B**) (Weng et al., 2004), were more sensitive to

CAD204520 as measured by inhibition of cell viability compared to *NOTCH1* wild type tumor cells (**Figure S3B-C**). Seventy-two hours of CAD204520 treatment triggered concentration-dependent apoptosis as determined by the increase of Annexin V/PI positive cells (**Figure 3C**) and the cleavage of PARP proteins (**Figure 3D**).

An additional phenotypic consequence of NOTCH1 inhibition with GSI is that T-ALL cells undergo cell cycle arrest (Weng et al., 2004). As shown in **Figure 3E** CAD204520 induced a G0/G1 arrest preferentially in *NOTCH1* mutated tumors (**Figure S3D**), and together with the data described above it supports the notion that CAD204520 inhibits lymphoid-derived cancer cells carrying clinically relevant *NOTCH1* HD or PEST mutations.

### **CAD204520 suppresses Notch1 signaling**

NOTCH receptors undergo several processing events including a first cleavage by a furin-like convertase (S1) in the *trans*-Golgi network that generates full-length heterodimers (Blaumueller et al., 1997; Logeat et al., 1998), ready to be conveyed to the plasma membrane (Le Borgne, 2006). The correct folding of these heterodimers requires  $\text{Ca}^{2+}$  that, in physiological condition, is tightly regulated across the endoplasmic reticulum (ER) storage by SERCA (Chemaly et al., 2018). To support the hypothesis that CAD204520-mediated SERCA inhibition impairs mutant NOTCH1 maturation, we evaluated the expression of NOTCH1 full-length and transmembrane portions of CAD204520-treated cells by western blotting. Lysates from T-ALL cell lines treated with 5  $\mu\text{M}$  CAD204520 for 24 hours were

immunoblotted with an antibody specific for the cytoplasmic portion of NOTCH1 that recognizes both unprocessed NOTCH1 (FL-N1) (~270 kDa) and the furin-processed transmembrane subunit (TM-N1) (~110 kDa). CAD204520 reduced the levels of the furin-processed transmembrane NOTCH1 subunit, but not the unprocessed full-length NOTCH1 precursor, in multiple T-ALL cell lines (**Figure 4A**). As expected by our structural data, combined CAD204520 and thapsigargin treatment resulted in an enhanced reduction in ICN1 and TM-NOTCH1 levels (**Figure S4A**).

In addition, we demonstrated that treatment of T-ALL with CAD204520 resulted in a concentration-dependent decrease in NOTCH1 expression on the cell surface by flow cytometry (**Figure 4B**). As expected, we did not observe this effect with a known GSI Notch inhibitor N-[N-(3,5-difluorophenacetyl)-1-alanyl]-(S)-phenylglycine (DAPT). Consistent with our hypothesis that CAD204520 affects NOTCH1 maturation rather than expression, NOTCH1 only decreases at the surface of the cells upon CAD204520 treatment, but co-localizes at the ER-Golgi intermediate compartment as shown by immunofluorescence co-localization studies (**Figure 4C, Figure S4B-E**). An immediate consequence of the decrement in NOTCH1 on the surface of the cells is the reduction of the catalytic activity of the  $\gamma$ -secretase complex because of the lack of NOTCH1 substrate. Here, we would expect a reduction in the level of ICN1. Indeed, CAD204520 ultimately leads to loss of ICN1 (**Figure 4D**) and results in the suppression of NOTCH1 target genes *MYC* and *DTX1* as measured by RT-PCR (**Figure 4E**). Furthermore, testing CAD204520 in MCL *NOTCH1* mutated cells yielded results comparable to the one

described in T-ALL, suggesting a conserved mechanism across different *NOTCH1* mutated cancers (**Figure S4D-F**).

In summary, these data show that CAD204520 inhibits Notch1 maturation demonstrating that SERCA inhibitors with a binding mode different from thapsigargin can efficiently suppress NOTCH1 maturation.

### **CAD204520 preferentially inhibits NOTCH1 mutated cancers**

SERCA inhibitors increase the Notch therapeutic index by targeting clinically relevant *NOTCH1* mutations in leukemia cells (Roti et al., 2013; Roti et al., 2017; Sharma et al., 2015). In fact, leukemia cells carrying *NOTCH1* alleles with heterodimerization domain mutations are more sensitive to SERCA inhibition than cells with wild type *NOTCH1* alleles (Roti et al., 2013; Roti et al., 2017).

To verify the hypothesis that CAD204520 preferentially targets mutant NOTCH1, we used two T-ALL cell lines carrying the same t(8;14)(q24;q32)/*TRAD@-MYC* translocation but different Notch mutational status (**Figure 5A and Figure S5A**). SKW-3/KE-37 harbors an isolated *NOTCH1* mutation in the PEST domain while MOLT16 is *NOTCH1* wild type (Minowada et al., 1989; Weng et al., 2004). First, we determined that the mutant T-ALL cell line was more sensitive to CAD204520 growth inhibition as measured by an ATP-based cell viability assay (**Figure S5B**). To validate this observation, we established a flow cytometry-based competition assay. SKW-3/KE-37 were transduced with a GFP (green fluorescent protein) lentiviral expressing vector and co-cultured with MOLT16 T-ALL cells in a 1:1 ratio.

Next, we treated SKW-3/KE-37-GFP and MOLT16 co-cultured cells with increasing concentrations of CAD204520 and demonstrated that the mutated T-ALL cell line, SKW-3/KE-37-GFP, was more sensitive to growth suppression compared to wild type MOLT16, as quantified by flow cytometric analysis of alive versus dead cells (**Figure 5B**). Analysis of caspase-3 and -7 activities indicates that the *NOTCH1* mutational status sensitizes cells to CAD204520-mediated apoptotic cell death (**Figure 5C**). Consistent with the hypothesis that SKW-3/KE-37 relies on Notch signaling for growth and survival, we observed a decrement of NOTCH1 protein only in mutant T-ALL cells compared to wild type (**Figure 5D**). To further support the preclinical development of CAD204520, we tested it (dose range 0.6-8  $\mu$ M) in a collection of T-cell lymphoblasts isolated from T-ALL patients. As shown in **Figure 5E**, CAD204520 preferentially affects T-ALL viability compared to normal lymphocytes. Primary blasts, derived from a patient suffering from a *NOTCH1* mutated T-ALL, exposed to 5  $\mu$ M CAD204520 rapidly underwent apoptosis (**Figure S5C**). In addition, T-ALL primary cases for which we confirmed a *NOTCH1* mutation (#1 *NOTCH1* ex 27, c.5101G>C p.A1701P; #2 *NOTCH1* ex 26, c.4793G>C p.1598P and *FBXW7* ex 9, c.1514G>T p.R505L) were more sensitive to CAD204520 compared to *NOTCH1* wild type B-cell ALL (**Figure 5F**). Collectively, these results indicate that CAD204520 retains anti-tumor activity preferentially in cells carrying *NOTCH1* alleles with heterodimerization domain (HD) or PEST mutations, holding great promise for CAD204520 future development against this indication.



### **Consequences of Ca<sup>2+</sup> release upon CAD204520 treatment**

A consequence of SERCA inhibition is the rise of intracellular Ca<sup>2+</sup> followed by the depletion of Ca<sup>2+</sup> stored in the ER. ER Ca<sup>2+</sup> exhaustion triggers a number of secondary events including the activation of the unfolded protein response pathway (UPR) (Wang and Kaufman, 2014) the activation of store-operated Ca<sup>2+</sup> channel (SOCE) (Parekh and Putney, 2005) and ultimately cell death (Orrenius et al., 2003).

To quantify the consequences of CAD204520 or thapsigargin treatment at the level of cytosolic Ca<sup>2+</sup>, we transferred ALL/SIL or DND41 in Ca<sup>2+</sup> free media and loaded with Indo-1 a ratiometric sensitive indicator fluorescent dye for measuring intracellular Ca<sup>2+</sup>. As shown in **Figure 6A** compared to DMSO, CAD204520 slightly increases cytosolic Ca<sup>2+</sup>. However, if compared to the thapsigargin effect, the extent of the increase appears modest with broad and flat peaks. In fact, thapsigargin causes a sharp rise in Ca<sup>2+</sup> concentration at ~200 seconds upon drugs injections. The next question is whether SERCA is still able to re-load Ca<sup>2+</sup> from the cytosol inside the ER upon CAD204520 treatment. This hypothesis would explain why the increase of Ca<sup>2+</sup> upon CAD204520 treatment is moderate and why thapsigargin triggers delayed on-target Ca<sup>2+</sup> effects such UPR activation and apoptosis (Lu et al., 2014). In this case we used a different approach and measured Ca<sup>2+</sup> Fluo-3 AM epifluorescence using an IonOptix system. This approach is ideal to measure fluctuations of ER Ca<sup>2+</sup>. As reported in **Figure 6B**, the peak fluorescence ( $f/f_0$ \_peak) was similar in the three groups of cells, indicating that the different compounds did not modify the Ca<sup>2+</sup> release from the

ER. Conversely, the fluorescence signal decay was significantly prolonged in thapsigargin-treated cells in comparison with both CAD204520 and DMSO (time<sub>50%-f/f0</sub>;  $P < 0.05$ ). In accordance with this finding, the fluorescence computed at 3, 5, and 10 min from the peak time (f/f0<sub>3min</sub>, 5min, and 10 min) or the area under the dose curve calculated within the same time frame (control vs. CAD204520  $\Delta$ mean=0.4188; control vs. thapsigargin  $\Delta$ mean=-2.658; CAD204520 vs. thapsigargin  $\Delta$ mean=-3.077), was significantly higher only in the thapsigargin group ( $P < 0.05$  and  $P < 0.0001$  respectively), suggesting that CAD204520 did not delay the cytosolic Ca<sup>2+</sup> re-uptake.

As previously mentioned, in addition to the effects on Ca<sup>2+</sup> dynamics, thapsigargin and thapsigargin analogs activate the ER related stress pathway of the UPR (Sehgal et al., 2017). To compare the effects of CAD204520 and thapsigargin on UPR activation we treated ALL/SIL, DND41 and RPMI-8402 at concentrations causing a similar ICN1 decrement (**Figure 6C and Figure S6A**). Interestingly, only thapsigargin sustained the expression of validated UPR markers such as P-eIF2 $\alpha$  and the ER chaperone BiP (Grp78) (**Figure 6C and Figure S6A**) or the proteolytic cleavage of ATF6 and its re-location in the nucleus (**Figure 6D and Figure S6B**).

Sustained Ca<sup>2+</sup> increase and UPR activation is associated with caspase mediated apoptosis and cell death in several tissue (Sovolyova et al., 2014) including cardiac cells (Liu and Dudley, 2015). For example, Ca<sup>2+</sup> release from the ER can induce delayed after-depolarizations leading to cardiac arrhythmias. Similarly, UPR

activation has been found to play a role in arrhythmogenesis during human heart failure by affecting cardiac ion channel expression (Dally et al., 2009). Thus, we hypothesized based on our  $\text{Ca}^{2+}$  dynamics studies that cardiac cells may be more tolerant to CAD204520 compared to thapsigargin treatment. To validate this hypothesis, we tested CAD204520 and thapsigargin in HL-1 cardiac cells and demonstrated that HL-1 are less sensitive to SERCA inhibition compared to a *NOTCH1* mutated cancer cell line confirming that SERCA represents a strong dependency in T-ALL (**Figure 6E, Figure S6C**). However, only cells treated with thapsigargin at  $\text{IC}_{50}$  concentrations displayed activation of the UPR pathway (**Figure 6F**) suggesting that CAD204520 further improves the therapeutic index of SERCA inhibitors because of its mild effect on  $\text{Ca}^{2+}$  dynamics and ER/UPR activation.

### **Modeling preclinical toxicity and efficacy of CAD204520 in a T-ALL leukemia model**

Because altered ER  $\text{Ca}^{2+}$  levels lead to heart failure (Yano et al., 2005), we measured the extent to which CAD204520 alters the function of heart cells. First, we isolated cardiomyocytes from Wistar rats and the cells were either untreated or incubated with CAD204520 or thapsigargin. The average diastolic sarcomere length (expressed in  $\mu\text{m}$ ) exhibited comparable values in all cell groups, independent of the treatment and the time of exposure to the inhibitors (Control:  $1.74 \pm 0.006$ ; CAD204520<sub>2hr</sub>:  $1.75 \pm 0.008$ ; CAD204520<sub>4hr</sub>:  $1.74 \pm 0.007$ ; Control:  $1.76 \pm 0.004$ ; Thapsigargin<sub>200nM</sub>:  $1.76 \pm 0.005$ ; Thapsigargin<sub>500nM</sub>:  $1.76 \pm 0.009$ ).

Compared to control cells, cardiomyocytes incubated with 5  $\mu$ M CAD204520 for 2 hours (CAD204520<sub>2hr</sub>) showed a reduced contractile efficiency, as reflected by the decrease in the rate of shortening ( $-dl/dt_{max}$ ; **Figure 7A**; -27%) and re-lengthening ( $+dl/dt_{max}$ ; **Figure 7B**; -25%), coupled with a lower fraction of shortening (FS; **Figure 7C**; -27%). A further slight decline (approximately an additional 10% decrease) in cell mechanical performance was observed after 4 hours exposure (*not shown*). In accordance with cell contractile properties, CAD204520<sub>2hr</sub> cardiomyocytes exhibited a modest (16%) decrease in the amplitude of the  $Ca^{2+}$  transient (**Figure S7A**) associated with a prolongation (+19%) of the time required for cytosolic  $Ca^{2+}$  removal (**Figure S7B (Tau)**). Choosing a thapsigargin dose for these comparative studies has been difficult due to the paucity of the *in vivo* studies reported in the literature. The dose selected for thapsigargin (200 nM) is in the mid-range of doses used by our group and others that assessed consequences of thapsigargin both *in vitro* and *in vivo* in different cancer models (Abdullahi et al., 2017; Ma et al., 2016; Roti et al., 2013). Nevertheless, thapsigargin induced a greater negative effect in treated cardiomyocytes. In fact, the rate of contraction, re-lengthening and the fraction of shortening were reduced by 77%, 89%, 66% respectively compared to control group suggesting that thapsigargin, at the tested concentrations, causes a marked impairment of cardiac cell mechanics (**Figure 7A-C**). The thapsigargin-induced cell damage altered  $Ca^{2+}$  dynamics, as shown in the representative tracing reported in **Figure S7C** hampering the measurement of  $Ca^{2+}$  transient parameters. Next, we evaluated the cytotoxic effect of CAD204520 on isolated cardiomyocytes by measuring the ability of the cells to produce ATP.

Interestingly CAD204520 treatment only minimally impacted the cellular metabolic capacity (10%) compared to vehicle treated cells suggesting CAD204520 does not induce marked effects on cardiomyocytes viability at the time and conditions tested (**Figure S7D**).

We then assessed the translational significance of our results. To explore the utility of the CAD204520 as an *in vivo* chemical probe, we performed a bioavailability and tissue distribution study (PK study) of CAD204520 in CD1 mice and found the compound to have a  $T_{1/2}$  of 11 hours, and  $C_{max}$  of 1.1 ng/mL (2.5  $\mu$ M) at  $T_{max}$  = 1 hour. Next, we completed a tolerability study in male and female BALB/c mice following administration of 30 mg/kg dose of CAD204520 BID by oral gavage for 21 days. Importantly, no adverse clinical symptoms or cardiac toxicity events were seen in animals dosed with vehicle or 30 mg/kg of CAD204520 (**Figure 7D**). Mice treated with double that dose (60 mg/kg) had mild reduction of weight (**Figure S7E**), without incurring cardiac failure, consistently with our *ex-vivo* results. Animals were sacrificed at day 21. No gross pathological abnormalities were detected on visceral organs including the heart, lungs, liver, brain or kidney observed in treated animals. With this dosing schedule, we determined a  $C_{max}$  within the range of CAD204520 for biological activities as established *in vitro* (1-10  $\mu$ M) and, therefore, initiated treatment studies of CAD204520 in a preclinical model of T-ALL.

To assess the *in vivo* efficacy of CAD204520 we established T-ALL derived xenografts from SKW-3/KE-37 human T-ALL cell line and confirmed leukemia engraftment by the quantification of hCD45 positive cells in peripheral blood (PB) of transplanted mice ( $0.3\% \pm 0.2$  circulating hCD45 (hCD45<sup>+</sup>) positive cells one week before the start of treatment). Then, we treated our cohort at a dose of 45 mg/kg twice a day at 8 hours intervals, for 4 days by oral gavage (**Figure S7F**). CAD204520 treatment resulted in a significant 56-fold reduction of the percentage of hCD45<sup>+</sup> SKW-3/KE-37 cells in circulating leukemic cells of xenotransplanted mice compared to the vehicle-administered control group ( $1.42\% \pm 2.6$  vs  $80.36\% \pm 4.5$ .  $P < 0.0001$ ) (**Figure 7E and Figure S7G**) and, consistently, a reduction of leukemic infiltration in the spleen (**Figure 7F and Figure S7H**). CAD204520-treated mice showed no decrease in body weight and no adverse effects on behavior. Importantly, no signs of acute cardiac toxicities (**Figure 7G**) or gastrointestinal metaplasia (**Figure 7H**) were documented. Furthermore, there were no changes in the complete blood counts between the control and treatment groups (**Figure 7I**).

Collectively these data demonstrate that CAD204520 reduces circulating leukemic cells without cardiac related toxicity during short-term treatment in leukemia xenograft models supporting further pre-clinical optimization in Notch1 dependent tumors.

## DISCUSSION

Although the prognosis of T-ALL has improved over the last two decades, the outcome of T-ALL patients with primary resistant or relapsed disease remains poor (Litzow and Ferrando, 2015; Marks and Rowntree, 2017). Therefore, current research goals are focused on the identification of targets to develop more effective and less toxic anti-leukemic agents (Follini et al., 2019; Roti and Stegmaier, 2011; Roti and Stegmaier, 2014; Starza et al., 2019).

Several studies strongly support the development of Notch inhibitors for targeted therapy in hematological malignancies and solid tumors where Notch signaling is deregulated (Brzozowa-Zasada et al., 2017). For example, pan Notch pathway antagonism with GSI reduces leukemia growth in mutant cancer cell lines and in mouse models (Palomero et al., 2006; Weng et al., 2004). Thus, modulators of Notch would be expected to have clinical efficacy particularly in T-ALL where recurrent *NOTCH1* mutations are common and cancer dependency has been well established. However, prolonged suppression of the canonical Notch pathway in normal tissue may cause dose-limiting gastrointestinal toxicity (DeAngelo, 2006) or increase the risk of skin cancers (Doody et al., 2015; Extance, 2010) underscoring the need for new therapeutic modalities to preferentially suppress the oncogenic signal. In recent years, we have pursued this approach and demonstrated that selective inhibitors of SERCA, such as thapsigargin and CPA, uniquely among Notch inhibitors preferentially affect mutated NOTCH1 proteins compared to the wild type ones (Roti et al., 2013; Roti et al., 2017).

Thapsigargin, a plant-derived sesquiterpene- $\gamma$ -lactone, has been used extensively as pharmacological tool to trigger  $\text{Ca}^{2+}$ -dependent and the UPR pathways in several disease models (Lytton et al., 1991). Because the increase of cytosolic  $\text{Ca}^{2+}$  and sustained UPR activation (ER stress) are important mediators of apoptosis, SERCA inhibitors have been considered for cancer therapies. (Mahalingam et al., 2013). However, large-scale isolation from *Thapsia* or scalable synthesis of thapsigargin is complex, requiring a 5- and 42-step process depending on the protocol used (Ball et al., 2007; Chen and Evans, 2017; Chu et al., 2017). Similarly, the synthesis of thapsigargin-based derivatives presents significant challenges. In fact, thapsigargin itself possesses a polyoxygenated 5-7-5 tricyclic core linked to four diverse ester groups and eight stereogenic centers not suitable for structural modeling (Ball et al., 2007; Ley et al., 2004). Structure-activity studies revealed that only few thapsigargin groups, for example the ester bond at O(8), can be hydrolyzed to generate intermediate derivatives that can be used for conjugation with a peptide (Andersen et al., 2015; Mahalingam et al., 2016) or with a cleavable ester linkage (Roti et al., 2017). In addition, modification of the thapsigargin ester acyl group, or of the lactone carbonyl, significantly reduces thapsigargin activity in cells or biochemical assays preventing their broad applicability in cancer (Quynh Doan and Christensen, 2015; Treiman et al., 1998).

A further limitation is that native thapsigargin is not tractable as a therapeutic agent due to expected  $\text{Ca}^{2+}$  shifts that can be prevented, for example, by creating inactive pro-drugs activated in a hysto-specif manner (Christensen et al., 2009; Doan et



al., 2015). This is the mode of action of mipsagargin, a thapsigargin derivative currently undergoing clinical trials for solid tumors (Mahalingam et al., 2013). Our group has developed JQ-FT, a folate-thapsigargin derivative that leverages the dependency of leukemia cells on folate metabolism to direct the inhibitor into T-ALL cells (Roti et al., 2017). Another strategy is to exploit analogues that possess an enhanced selectivity toward SERCA isoforms preferentially expressed in cancer cells (Arbabian et al., 2011; Denmeade and Isaacs, 2005) while keeping the activity of SERCA2a, the major cardiac isoform, unaffected (Clark et al., 2010; Dally et al., 2010; Lipskaia et al., 2010).

An alternative is the development of small molecules that retains SERCA inhibitory capacities but have only transient effects on cytosolic  $\text{Ca}^{2+}$  shifts. This idea emerged from recent studies from the laboratory of Moller and colleagues that challenged the consensus idea that the elevation of cytosolic  $\text{Ca}^{2+}$  - rather than the depletion of ER  $\text{Ca}^{2+}$  - led to the cell death induced by thapsigargin and analogues (Sehgal et al., 2017; Szalai et al., 2018). Contrary to what is generally thought, the rapid rise of cytosolic  $\text{Ca}^{2+}$ , as observed with thapsigargin, and its role in the short-term side effect on cardiac contractility, is not required for apoptosis following SERCA inhibition. It is rather the ER  $\text{Ca}^{2+}$ -depletion and sustained UPR activation that contributes to cell death (Sehgal et al., 2017).

The effect of a given SERCA inhibitor on cytosolic and ER  $\text{Ca}^{2+}$  levels depend strongly on its molecular mechanism of interaction with the ATPase. For example, the thapsigargin derivative substituted with a 12-aminododecanoyl linker, Boc-

8ADT, did not show measurable changes in  $\text{Ca}^{2+}$  levels even though it strongly inhibited SERCA-ATPase activity (Sehgal et al., 2017) leading to apoptosis in LNCaP cells (Dubois et al., 2013). This is probably due to the very slow binding kinetics of this compound leading to a slow net leakage of  $\text{Ca}^{2+}$  from the ER, which likely enables the maintenance of constant, stable cytosolic  $\text{Ca}^{2+}$  levels. Other possible causes for the lack of cytosolic  $\text{Ca}^{2+}$  peaks are a moderate decrease in SERCA's  $\text{Ca}^{2+}$  affinity or a residual  $\text{Ca}^{2+}$  transport activity in the presence of compound. It is tempting to speculate that other SERCA inhibitors that have advanced to clinical testing might have a similar mode of action. Curcumin, a small molecule derived from the turmeric spice that stabilizes SERCA in the E1 conformational state has been extensively tested in multiple cancer models and clinical trials (Wilken et al., 2011) without causing major cardiac events. Cisplatin is a widely used platinum-containing compound that among other effects inhibits SERCA and  $\text{Na}^+/\text{K}^+$ -ATPase simultaneously (Tadini-Buoninsegni et al., 2017). Given the large number of rotating bonds in CAD204520, slow binding kinetics to SERCA, as with Boc-8ADT, can also be anticipated. From our structural data, the interaction of CAD204520 with SERCA involves only two polar contacts, and one single hydrophobic contact within a distance of 3 Å. Overall the interaction looks surprisingly 'loose', perhaps indicating a concentration-dependent competition with  $\text{Ca}^{2+}$  binding and transport rather than an irreversible inhibition.

Our data also show that CAD204520 binds to SERCA differently from thapsigargin: it occupies a pocket between the trans-membrane helices M1, M2, M3 and M4 of

SERCA, whereas thapsigargin binds between M3, M5 and M7 (Brini and Carafoli, 2009). This observation agrees with our finding that thapsigargin, but not CPA, co-treatment enhances CAD204520's inhibitory effect, a feature that can be used for further medicinal chemistry optimization. In this regard however, CAD204520 maintains the same thapsigargin "property" to preferentially alter mutated NOTCH1 trafficking. Remarkably, this ability has not yet been explored in two of the most recently synthesized putative SERCA inhibitors: the natural tricyclic clerodane diterpene casearin J (De Ford et al., 2016) or the ethyl 2-amino-6-(3,5-dimethoxyphenyl)-4-(2-ethoxy-2-oxoethyl)-4H-chromene-3-carboxylate (CXL017) (Bleeker et al., 2013) both active in T-ALL cell lines.

The next question is whether CAD204520 activity has limitations *in vivo* due to  $\text{Ca}^{2+}$  shifts. For example, mice exposed to a thapsigargin analogue, L12-ADT, at 0.8 mg/kg die within 8 hours putatively from cardiac toxicity (Denmeade et al., 2003). Cardiac sarcoplasmic reticulum (SR)  $\text{Ca}^{2+}$  ATPase (SERCA2a) plays a central role in myocardial contractility. SERCA2a actively transports  $\text{Ca}^{2+}$  into the SR and regulates cytosolic  $\text{Ca}^{2+}$  concentration, SR  $\text{Ca}^{2+}$  load, and thus the rate of contraction and relaxation of the heart (Periasamy et al., 2008). The amount of  $\text{Ca}^{2+}$  release from the SR, dictating the extent of cell shortening, is also a steep function of SR  $\text{Ca}^{2+}$  content (Bassani et al., 1995). It follows that pharmacological inhibition of SERCA2a activity should reduce the amplitude of the calcium transient and the rate of SERCA-mediated  $\text{Ca}^{2+}$  removal, resulting in altered cardiomyocyte mechanics, as we observed in isolated unloaded ventricular myocytes exposed to

CAD204520 or thapsigargin. However, the impairment of cellular contractile performance and calcium dynamics was more pronounced after thapsigargin incubation compared to CAD204520 exposure (80-90% reduction in functional performance vs. 25-30%, on average) indicating that CAD204520 should have a better therapeutic window than thapsigargin *in vivo*.

An important question is whether and to what extent the depressed cardiomyocyte function secondary to pharmacological inhibition of SERCA2 activity would translate into decreased cardiac function *in vivo*. Based on previous experience from our group in a rat model of induced cardiomyopathy (Savi et al., 2017), a 20-30% decline in cellular mechanics *ex vivo* results in a comparable moderate hemodynamic impairment in the intact animal. In fact, while CAD204520 exerts an anti-leukemia effect *in vivo* it does not induce heart failure in the two different mouse models (Balb/c CD1 and IL2-NSG) used for this study.

While most *NOTCH1* mutations are found in the exon 26 and 27 coding for the HD region, mutations in the PEST domain are present in 20-30% of tumors resulting in an increased Notch activation due to the prolonged stabilization of ICN1 (Weng et al., 2004). Activating mutations clustered in the PEST sequence have been described in CLL and in MCL and several efforts are ongoing to target NOTCH1 in these diseases (Baldoni et al., 2018; Kridel et al., 2012). Our study demonstrates that CAD204520 is active in cell lines carrying a PEST mutation (SKW-3/KE-37). This result supports testing SERCA inhibitors in disease models with this recurrent abnormality such as CLL (Di Ianni et al., 2009) and MCL (Kridel et al., 2012). To

this end, we extended testing CAD204520 in REC-1 MCL cell line, one of the few representative models of NOTCH1 dependent MCL (Kridel et al., 2012) carrying a H2428Pfs\*7 PEST mutation. We showed that REC-1 is sensitive to CAD204520 inhibition compared to *NOTCH1* wild type MCL lines. In REC-1 CAD204520 reduces Notch activation with a mechanism similar to the one observed in T-ALL. Because in MCL *NOTCH1* mutations are associated with significantly shorter survival rates (Bea et al., 2013; Kridel et al., 2012) the development of Notch targeted therapy may represent an effective strategy to tackle this aggressive disease.

In conclusion, this study presents CAD204520 as an orally bioavailable SERCA inhibitor with tolerable off-target toxicity in NOTCH1 dependent tumors. This work provides a foundation for further development of novel drugs targeting Notch-dependent cancers. It also provides a deeper understanding of how different SERCA modulators affect cardiac tissue physiology.

## **SIGNIFICANCE**

Given its critical oncogenic role in several human cancers, Notch1 signaling has garnered increased attention as a potential therapeutic target. To date, several Notch modulators, including  $\gamma$ -secretase inhibitors, have shown therapeutic efficacy in preclinical cancer models. However, despite this promise, few of these candidates have been demonstrated to have a meaningful clinical benefit for

patients, in part due to tissue-dependent on-target toxicities from the simultaneous repression of both mutant and wild type Notch proteins.

The discovery of SERCAs as actionable modulators of Notch1 suggested a targeted approach to treat NOTCH1 dependent cancer including T-ALL, MCL and CLL. Uniquely among Notch modulators, SERCA inhibitors preferentially impair the clinically relevant class of oncogenic *NOTCH1* mutants compared to wild type. Thus, the development of tolerated SERCA modulators may uncover a therapeutic avenue for one of the most frequently mutated genes in human cancers.

## **ACKNOWLEDGEMENTS**

This work was supported by an AIRC Start-up Investigator Grant (n. 17107 G.R.), Fondazione Cariparma (3576/2017, 0180/2018 G.R.), Fondazione Grande Ale Onlus (G.R.), L'antica Torre di Melezzole (M.M.), Fondazione Umberto Veronesi Post-doctoral Fellowship (C.S.), Associazione Italiana contro le Leucemie-Linfomi e Mieloma ONLUS Parma chapter (A.G.), AIRC Investigator Grant 2018 (n. 21352 to P.S.), the Italian Ministry of Education, University and Research (Programma SIR n. RBSI14GPBL to P.S.), Fondazione Cassa di Risparmio di Perugia (project code: 2018. 0418.021) and Gilead fellowship program 2019 (R.L.S.), Progetti di Ricerca di Interesse Nazionale (PRIN) 2017 (project code: 2017PPS2X4 to C.M.), the National Cancer Institute R35 CA210030 and the Pan-Mass Challenge Team Crank (K.S.).

M.M. is a 2018 EHA-ASH Translational Training in Hematology scholar.

Authors thank Federico Quaini. M.D., Ph.D., Andrea Vecchi Ph.D. for technical assistance, Francesco Marchesini for art and design expertise, Antonio Cuneo, M.D. Ph.D and Chiara Liverani Ph.D. for critical suggestions, Sabrina Bonomini Ph.D. and Gabriella Sammarrelli Ph.D. for technical expertise, Niccolò Bolli M.D., Ph.D. for sequencing oversight, Pamela Criscuoli for administrative support and the physicians at the Hematology and BMT unit of the University of Parma.

## **AUTHOR CONTRIBUTIONS**

**Conceptualization and design:** MM, AG, WDB, AMW, MB, GR

**Methodology:** all authors

**Resources:** all authors

**Investigation:** all authors

**Formal analysis:** all authors

**Writing (original draft, review and editing):** WDB, AMW, MM, MB, GR

**Data curation:** WDB, AMW, PS, RLS, CM, FA, KS, MB, GR

**Funding acquisition:** PS, CM, RLS, KS, MM, GR

**Project administration:** MM, GR

**Supervision:** GR

## **DECLARATION OF INTERESTS**

William Dalby-Brown and Anne-Marie Lund Winther are CaDo Biotechnology IvS employees. The compounds studied are part of a patent application wholly owned by CaDo Biotechnology IvS, Denmark. Kimberly Stegmaier has previously consulted for Novartis and Rigel Pharmaceuticals and currently receives grant funding from Novartis on topics unrelated to this manuscript.



## FIGURE LEGENDS

### Figure 1: Identification, structure activity relationship (SAR) and co-crystal structure of CAD204520

A) Identification of CAD204520. 191,000 Small molecules were screened for inhibition of the fungal H<sup>+</sup>-ATPase Pma1. Molecules with an enzymatic inhibition of the H<sup>+</sup>-ATPase that exceed 50% were retained for subsequent hit validation. The 407 molecules were counter screened for (Pma1 over SERCA or Na<sup>+</sup>/K<sup>+</sup>) ATPase selectivity and minimum growth inhibitory capacity (MIC) < 150 µM. Hits were then characterized as described in (Kjellerup et al., 2017). From a subsequent hit optimization program (see panel B), CAD204520 was identified as the most promising candidate against mammalian Ca<sup>2+</sup>-ATPase (SERCA).

B) Structure activity relationship (SAR) of CAD204520.

C) Crystal structure of the SERCA-CAD204520 complex. Right panel: cartoon and surface representation of SERCA (light blue) with CAD204520 bound at the membrane interface (orange surface representation). Left panels: Close-up of the CAD204520 binding sites, as seen parallel to the membrane (upper panel) or along the membrane normal (lower panel). Dashed lines indicate polar interactions with Asp59 (2.9 Å) and Asn101 (2.7 Å). Nitrogen is shown in blue, oxygen in red, fluorine in cyan. Carbon is light blue for SERCA and orange for CAD204520.

D) Simulated annealing omit map (green mesh) of CAD204520 (orange), contoured at 3.0 sigma. Top panel, viewed roughly along the membrane plane, bottom panel, viewed roughly perpendicular to the membrane.

See also Figure S1 and Table S1

### **Figure 2: CAD204520 overcomes thapsigargin resistance in T-ALL**

A) Lollipop graphs showing sequenced mutations in the exonic region of *ATP2A1*, *ATP2A2* and *ATP2A3* genes. Allelic variants are depicted with a circle (black = synonymous; red = missense) relative to their amino acid position (gray bottom bar, aa) and to their protein domains (color coded). The length of the lollipop (# mutations) bar indicates if 0 = no mutations occur; 1 = mutations occur in one sample; 2 = mutation occur in both samples.

B) Effect of CAD204520 and thapsigargin and CAD204520 treatment in naïve and resistant ALL/SIL cells lines. Histograms show percentage of cell alive after 72 hours of treatment at indicated concentrations ( $\sim$ IC<sub>50</sub>). Error bar denotes the mean  $\pm$  SD of a minimum of three replicates. Statistical significance among groups (\*\*\*\* $P \leq 0.0001$ ) was determined by one-way ANOVA.

C) Surface plots analysis of ALL/SIL, DND41 and RPMI-8402 T-ALL cells lines and a primary *NOTCH1* mutated T-ALL sample treated with vehicle, CAD204520, thapsigargin, or CAD204520 plus thapsigargin. Each point represents and

independent measurement representative of three biological replicates. Plots were generated using the Combenefit script by MATLAB R201, which represents the Loewe (dose-effect based approach) analysis. A color scale bar represents the level of drugs antagonism or synergism.

D) Combination index analysis for the combinations of CAD204520 with thapsigargin in ALL/SIL, DND41 and RPMI-8402 T-ALL cell lines and a primary *NOTCH1* mutated T-ALL treated for three days. On the y axis is represented the combination index, on the x axis the fraction of cells inhibited.

E) BRAID index analysis for the combinations of CAD204520 with thapsigargin in ALL/SIL, DND41 and RPMI-8402 T-ALL cell lines and a primary *NOTCH1* mutated T-ALL treated for three days. A color scale bar represents the level of drugs antagonism or synergism. K index is indicated.

See also Figure S2

### **Figure 3: CAD204520 impairs T-ALL proliferation**

A) Effect of CAD204520 on cell viability after 72 hours of treatments in the indicated T-ALL cell lines. Error bars denote  $\pm$  SD of 2 replicates.

B) Effect of CAD204520 on cell viability after 72 hours of treatments in the indicated MCL cell lines. Error bars denote  $\pm$  SD of 2 replicates.

C) Effect of CAD204520 treatment on induction of apoptosis. Annexin V/propidium iodide staining of T-ALL cells following 72 hours of treatment with the indicated concentrations of CAD204520. A minimum of 20,000 events was collected for each condition.

D) Western immunoblot showing expression of cleaved PARP in *NOTCH1* mutated cell lines (ALL/SIL, DND41, RPMI-8402 and REC-1) cells treated at the indicated concentrations of CAD204520 for 24 hours.  $\beta$ -Actin was used as a loading control.

E) Effect of CAD204520 treatments on cycling ALL/SIL, DND41, RPMI-8402 and REC-1 cells. Percentage of DNA content following four days of treatment with the indicated concentrations of CAD204520 on each cell cycle phase is indicated. A minimum of 20,000 events was collected for each condition.

See also Figure S3

#### **Figure 4: CAD204520 modulates Notch1 signaling**

A) Effect of CAD204520 treatment for 24 hours on NOTCH1 (N1) processing and activation in T-ALL cell lines all with heterodimerization mutations (DND41 and ALL/SIL (L1594P $\Delta$ PEST), and RPMI-8402 (ins1584PVELMPPE). The blot was incubated with an antibody against the C-terminus of NOTCH1 that recognizes

both the furin-processed NOTCH1 transmembrane subunit (TM) and the unprocessed NOTCH1 precursor (FL).

B) Effect of 24 hours of CAD204520 and GSI (DAPT) treatments on NOTCH1 cell surface staining as assessed by flow cytometry.

C) Effect of CAD204520 and GSI (DAPT) treatment (24 hours) on the subcellular localization of NOTCH1. Immunofluorescence images of permeabilized ALL/SIL incubated with anti-Notch1 (C20-Red) and anti-Golgin (Green) are shown. Co-localization is indicated by yellow signal. Bar indicates 100  $\mu$ m magnification.

D) Western immunoblot showing the expression of cleaved NOTCH1 (ICN1) in ALL/SIL, DND41 and RPMI-8402 cells treated at the indicated concentration of CAD204520 for 24 hours. HSP90 was used as a loading control.

E) CAD204520 treatment for 24 hours downregulates expression of NOTCH1 target genes in ALL/SIL, DND41 and RPMI-8402 T-ALL cells as assessed by qRT-PCR. Error bars indicate the mean  $\pm$  SD of 4 replicates. Data were analyzed using the  $\Delta\Delta$ CT method and plotted as a percentage relative to the control gene *RPL13A*. Statistical significance ( $***P \leq 0.001$ ;  $****P \leq 0.0001$ ) was determined by one-way ANOVA using Bonferroni's correction for multiple comparison testing. GSI (DAPT) was used as a positive control.

See also Figure S4

**Figure 5: *NOTCH1* mutation sensitizes T-ALL cells to CAD204520 inhibition**

A) Interphase and metaphase FISH, with the LSI MYC probe, show split signals between der(8) (red signal) and der(14) (green signal), in the MOLT-16 (left) and SKW-3/ KE-37 (right) cell lines . (b) SKW-3/ KE-37 has two der(8).

B) Left: cell-based competition assay. SKW-3/KE-37 and MOLT16 were transduced with a GFP containing vector or an empty control vector respectively and co-cultured 1: 1 ratio. Right: normalized effect of CAD204520 on cellular viability in co-cultured SKW-3/KE-37-GFP and MOLT16 cells treated for 72 hours. Error bars denote the mean  $\pm$  SD of 2 replicates for vehicle-treated (DMSO) cells and for CAD204520-treated cells. Statistical significance ( $*P \leq 0.05$ ) was determined by one- way ANOVA using Bonferroni's correction for multiple comparison testing.

C) Caspase 3/7 luminescence fold induction in SKW-3/KE-37 and MOLT16 cells. Error bars denote the mean  $\pm$  SD of 6 replicates for vehicle-treated (DMSO) cells and for CAD204520-treated cells. Statistical significance ( $***P \leq 0.001$ ) was determined by one-way ANOVA using Bonferroni's correction for multiple comparison testing.

D) Effect of CAD204520 treatment for 24 hours on NOTCH1 (N1) processing and activation in SKW-3/KE-37 and MOLT16 cell lines. The immunoblot was stained with an antibody against the C-terminus of NOTCH1 that recognizes the furin-processed NOTCH1 transmembrane subunit (TM) and the unprocessed NOTCH1 precursor (FL) and HSP90 was used as a loading control.

E) Effect of the CAD204520 in primary T-ALL cells (n=9) or isolated lymphocytes (n=6). The whisker plot represents the effect of small molecules on cellular viability calculated using the area under the curve (AUC) model of log-transformed dose-responses data using GraphPad V7. The line in the whisker diagram represents the AUC median. The upper edge (hinge) indicates the 75<sup>th</sup> percentile of the data set, and the lower hinge the 25<sup>th</sup> percentile. The ends of the vertical line show the minimum and the maximum data values. Statistical significance (\*\* $P \leq 0.001$ ) was determined by a non-parametric t-test (Mann-Whitney).

F) Normalized effect of the CAD204520 in primary *NOTCH1* mutated T-ALL cells (n=2) or primary B-ALL (n=2) on cellular viability. Error bars denote the mean  $\pm$  SD of 4 replicates. Statistical significance comparing each T-ALL vs. B-ALL case to each dose (\*\* $P \leq 0.001$ ; \*\*\*\* $P \leq 0.0001$ ) was determined by a non-parametric t-test (Mann-Whitney).

See also Figure S5

**Figure 6: Effects of CAD204520 on Ca<sup>2+</sup> and UPR activation**

A) Indo-1 AM fluorescence traces of T-ALL cells loaded with 5  $\mu$ M of Indo-1 AM and treated with DMSO, CAD204520 1 $\mu$ M, or thapsigargin 1 $\mu$ M. Baseline and post-treatment fluorescence is indicated by a black arrow. Cells were acquired for a minimum of ten minutes a LSR Fortessa X20 flow cytometer.

B) Time course of ER calcium release and reuptake traces recorded in DMSO, CAD204520 and thapsigargin T-ALL treated cells. Each trace is representative of five (DMSO) or four (CAD204520 and thapsigargin) independent experiments. In green the area under the curve (AUC). Values are reported as mean  $\pm$  SEM; *f/f0<sub>peak</sub>*: peak fluorescence normalized to baseline fluorescence; *time<sub>50%-f/f0</sub>*: time at 50% of fluorescence signal decay measured from the peak time; *f/f0<sub>3min</sub>*, *5min*, and *10 min*: fluorescence computed at 3, 5, and 10 minutes from the peak time. \**P* < 0.05 vs DMSO; # *P* < 0.05 vs 1 $\mu$ M CAD204520. Statistical significance was determined by a Kruskal-Wallis test and differences among groups were determined by a Mann-Whitney non-parametric t-test.

C) Effect of CAD204520 and thapsigargin treatment for 24 hours in ALL/SIL and DND41 cell lines. The blot was stained with an antibody against the C-terminus of NOTCH1 that recognizes the furin-processed NOTCH1 transmembrane subunit (TM) and the unprocessed NOTCH1 precursor (FL), an antibody that recognizes



the cleaved NOTCH1 (ICN1), P-eIF2 $\alpha$ , total eIF2 $\alpha$ , BiP and HSP90 used as a loading control.

D) Effect of CAD204520 and thapsigargin treatment for 24 hours on ATF6 in ALL/SIL cell line. Immunofluorescence of permeabilized ALL/SIL cells stained with ATF6 (green) is shown. Cell nuclei were stained with DAPI (blue). Scale bar: 100  $\mu$ m.

E) Effects of CAD204520 (left) and thapsigargin (right) on cell viability after 72 hours of treatments in HL-1 and ALL/SIL cell lines. Error bars denote  $\pm$  SD of a minimum of 2 replicates.

F) Effect of CAD204520 and thapsigargin treatment for 24 hours in HL-1 cell lines. The blot was stained with BiP and  $\beta$ -Actin used as a loading control.

See also Figure S6

### **Figure 7: Effects of CAD204520 on preclinical model of T-ALL**

A-C left panels. Effect of CAD204520 treatment on rat cardiomyocyte mechanics. Single experiments are represented by two dots interconnected by a solid line. Specifically, the line between dots connects the quantification of Maximal Rate of Shortening (A:  $-dl/dt_{max}$ ), Maximal Rate of re-Lengthening (B:  $+dl/dt_{max}$ ), and Fraction of Shortening (C: FS%), before and after the CAD204520 (5  $\mu$ M) or

thapsigargin (200 nM) treatment compared to control (Control). A-C right panels: Mean percentage effect of CAD204520 (CAD204520<sub>2hr</sub>) and thapsigargin (Thapsigargin<sub>200nM</sub>) on the same cardiac functions. Graph bars: mean  $\pm$  SD of the 6 CAD204520 treated cardiomyocyte groups and mean  $\pm$  SD of the 2 thapsigargin treated cardiomyocyte groups. Statistical significance comparing CAD204520 treated cells vs. thapsigargin treated cells (\*\*  $P \leq 0.001$ ; \*  $P \leq 0.05$ ) was determined by a non-parametric t-test (Mann-Whitney).

D) Effect of daily 30 mg/Kg administration of CAD204520 on body weight. Error bars denote the mean  $\pm$  SD of 6 replicates (3 male and 3 female mice). Statistical significance (n.s.) was determined by a 2-way ANOVA analysis.

E) Effect of CAD204520 on T-ALL leukemia burden in a SKW-3/KE-37 xenografted murine model. Anti-leukemic activity of CAD204520 assessed by measuring hCD45<sup>+</sup> cells after 4 days of CAD204520 treatment (45 mg/kg/OS BID) or vehicle (tween-80 0.5% w/v and HPMC 1.0% w/v). Representative dotplot showing the effect of CAD204520 on T-ALL growth in a SKW-3/KE-37 murine model. A minimum of 20,000 events was collected for each condition.

F) Immunohistochemical analysis of the spleen in a SKW-3/KE-37 xenografted murine model treated with CAD204520 45 mg/kg or vehicle for 4 days. The spleen of all mice was examined; representative results for one control animal and one

CAD204520 treated animal are shown. Formalin-fixed, paraffin-embedded tissue sections were stained with hCD45. Scale bars: 20  $\mu$ m.

G) Representative images of hematoxylin/eosin stained sections of the left ventricle from SKW-3/KE-37 xenograft treated with CAD204520 45 mg/kg or vehicle. CAD204520 treatment did not affect the gross structural components of the myocardium neither induced focal areas of damage. Well aligned myofibers in the absence of myocytolytic necrosis or interstitial inflammatory infiltrates are shown at higher magnification (inset). Scale bars: low magnification = 0.2 mm; high magnification (insets) = 0.05 mm.

H) Representative images of hematoxylin/eosin stained histological section of the small intestines from SKW-3/KE-37 xenograft treated with CAD204520 45 mg/kg or vehicle. Compared to controls, intestinal villi and crypts appear to be well preserved in CAD204520-treated animals. At higher magnification (inset), no morphological changes in goblet cells and enterocytes were observed in CAD204520-treated mice. Scale bars: low magnification = 0.2 mm; high magnification (insets) = 0.05 mm.

I) Effect of CAD204520 on cell blood count WBC, hemoglobin and platelets in a SKW-3/KE-37 murine model after 4 days of CAD204520 treatment (45 mg/kg/OS BID) or vehicle (tween-80 0.5% w/v and HPMC 1.0% w/v). Error bars denote the mean  $\pm$  SD of 8 CAD204520 treated animals or the mean  $\pm$  SD of 8 replicates

vehicles treated mice. Statistical significance for treated vs. vehicle (n.s.) was determined by non-parametric t-test (Mann-Whitney).

See also Figure S7

## **STAR METHODS**

## **RESOURCE AVAILABILITY**

## **LEAD CONTACT**

Further information and requests for resources and reagents may be directed to and will be fulfilled by the lead contact, Giovanni Roti (giovanni.roti@unipr.it).

## **MATERIALS AVAILABILITY**

All unique/stable reagents generated in this study are available from the lead contact with a completed material transfer agreement.

## **EXPERIMENTAL MODEL AND SUBJECT DETAILS**

### **Animals**

NOD-*scid* IL2Rgamma<sup>null</sup> (NSG) mice (The Jackson labs, RRID: IMSR\_JAX:005557) for efficacy studies were maintained in specific pathogen-free facilities at the “Preclinical Research Services Center” (Ce.Se.R.P) at the University of Perugia (08/2018-UT of 07/24/2018). Animal procedures were approved by the University of Perugia IACUC following the DL 26/2014 and 2010/63/EU guidelines for the protection of animals used for scientific purposes. Pharmacokinetics (PK) and tolerability studies were performed at Aurigene Discovery Technologies, India. In-house breed CD1 (ICR) or BALB/cAnNCr mice

for pharmacokinetics (PK) and tolerability studies were maintained in individually ventilated cages at the Aurigene facility in Hyderabad in India.

To assess effect of CAD204520 on the cardiac mechanics, cardiomyocytes were isolated from 12-14 week-aged Wistar rats (*Rattus norvegicus*, Charles River Laboratory, RRID: RGD\_13508588) of  $362 \pm 5$  g in weight. Animals were housed in a temperature-controlled room (22–24 °C), with a 12 hours light cycle (light on from 7.00 AM to 7.00 PM) with unrestricted food and water supply. Experiments were performed under the Veterinary Animal Care and Use Committee of the University of Parma-Italy and conform to the National Ethical Guidelines of the Italian Ministry of Health (Prot. N° 614/2016-PR) and the Guide for the Care and Use of Laboratory Animals (National Institute of Health, Bethesda, MD, USA, revised 1996).

### **Yeast cells**

*Saccharomyces cerevisiae* RS72 yeast cells (ATCC #9763) for the biochemical ATPase assay were pre-cultured in 100 ml sterile SGAH medium (7.04 g/L yeast nitrogen base, 19.8 g/L galactose, 64 mg/L adenine, 64 mg/L histidine) for 3 days at 25°C and 150 rpm. The pre-culture was transferred to 500 mL sterile SGAH medium and further incubated for 3 to 4 days. 100 mL from the cell culture was transferred to 1 L YPAD medium (10 g/L yeast extract, 20 g/L bacto-peptone, 20 g/L glucose, 20 mg/L adenine) and incubated at 25°C for 18-20 hours.

### **Cell Lines**

Human cell lines DND41 (source: male), MOLT16 (source: female), REC-1 (source: male), Mino (source: female), PF382 (source: female), RPMI-8402 (source: female), SKW-3/KE-37 CTV-1 (source: male), HBS2 (source: male), Loucy (source: female) and PEER (source: female) were purchased from Leibniz-Institut DSMZ-German collection of microorganisms and cell cultures (Germany); the identity of ALL/SIL (source: male) was confirmed by PCR sequencing for known *NOTCH1* mutations and short tandem repeat (STR) loci profiling and they were kindly provided by Stegmaier laboratory. MAVER-1 (source: male) cells were a gift from the Muraro laboratory (C.R.O. National Cancer Institute, Aviano, Italy). Cells were cultured in RPMI 1640 (Fisher Scientific, Waltham MA, USA #MT10040CV) with 10% or 20% fetal bovine serum (FBS) (Thermo Fisher Scientific, Waltham MA, USA, Waltham MA, USA, #10270-106) and 1% penicillin-streptomycin (Fisher Scientific, Waltham MA, #3MT30002CI) and incubated at 37°C with 5% CO<sub>2</sub>. 293T (source: human primary embryonal kidney cell line 293 (ACC 305)) cells were purchased Leibniz-Institut DSMZ-German collection of microorganisms and cell cultures (Germany) and cultured in DMEM (Fisher Scientific, Waltham MA, USA #11965-084) with 10% FBS and 1% penicillin-streptomycin and incubated at 37°C with 5% CO<sub>2</sub>. HL-1 cardiac muscle cell line was a kind gift from the Miragoli laboratory (University of Parma, Parma, Italy). HL-1 cells were plated on a gelatin layer derived from bovine skin/fibronectin (1mg/ml)(Sigma-Aldrich, St. Louis, MO, USA, #G9391 and #F-1141) coated T25 flask and cultured in Claycomb medium (Sigma-Aldrich, St. Louis, MO, USA, #51800C) with 10% FBS, 1% penicillin-streptomycin, 2mM L-Glutamine (Thermo

Fisher Scientific, Waltham MA, USA, Waltham MA, USA, # 25030081), 0,1mM Norepinephrine [(±)- Arterenol] plus L-Ascorbic acid, sodium salt (Sigma-Aldrich, St. Louis, MO, USA, #A0937 and #A7506) and incubated at 37°C with 5% CO<sub>2</sub>. Cytogenetic, FISH and mutation analysis was completed according to validated methods as previously described (La Starza et al., 2016; La Starza et al., 2014).

### **Primary samples**

T-ALL lymphoblasts were obtained from patients with leukemia under an approved protocol at the Parma University Hospital (n.18249/18/05/2017) and according to the declaration of Helsinki guidelines for the protection of human rights. Peripheral blood (PB), and bone marrow (BM) samples were collected at the time of diagnosis, and we retained samples with blasts >85%. Mononuclear cells were isolated by density gradient centrifugation using LSM-lymphocyte separation medium (Cappel™ MP Biomedicals, LLC, Ohio, USA #50494). Lymphocytes were isolated from peripheral blood mononuclear cell PBMC by using a CliniMACS Prodigy (Miltenyi Biotec, Bergisch Gladbach, Germany) and cultured for a short time using the same growth conditions described above.

## **METHOD DETAILS**

### **Preparation, crystallization and structure determination of the SERCA-CAD204520 complex**

Rabbit sarcoplasmic reticulum (SR) membranes containing SERCA were prepared from rabbit hind leg muscle as previously described (Andersen et al., 1985). Briefly,



muscle tissue was dissected and minced in 10 mM KCl, 2.5 mM K<sub>2</sub>HPO<sub>4</sub>, 2.5 mM KH<sub>2</sub>PO<sub>4</sub>, 2 mM EDTA, followed by centrifugation at 4 °C for 20 min and 6.400 x g, supernatant filtered and spun at 9.700 x g for 20 min. SR membranes were sedimented by a 60 min centrifugation at 47.800 x g at 4 °C. Membranes were homogenised and washed successively with buffers B (1 M sucrose, 50 mM KCl), C (1 M KCl, 3.4 mM MgATP pH 7.0), D (50 mM KCl), and E (0.3 M sucrose, 5 mM Hepes pH 7.4). Finally, washed membranes were extracted twice with extraction buffer (0.3 M sucrose, 0.5 M KCl, 1 mM EDTA, 10 mM Tris, 0.01 mM CaCl<sub>2</sub>, 1.25 mM MgCl<sub>2</sub>, pH7.9, 0.5 mg/ml DOC, 0.5 mg/ml DTT) followed by centrifugation at 4 °C and 181.000 x g for 75 min. The pellet was then washed with 5 mM TAPS pH 7.5, 0.3 M sucrose, 0.5 M KCl, 0.5 mM MgCl<sub>2</sub>, 10 µM CaCl<sub>2</sub>, and finally resuspended and flash frozen in buffer E. SERCA membranes were resuspended and gently homogenized in 100 mM MOPS-Tris pH 6.8, 80 mM KCl, 3 mM MgCl<sub>2</sub>, 4 mM EGTA and 20% (v/v) glycerol. CAD204520 was added to the membrane preparation at a final concentration of 0.5 mM and incubated overnight at 4 °C. The following day, 0.4 mM TNPATP were added and incubated for 15 minutes (min) prior to the solubilization of the protein with C<sub>12</sub>E<sub>8</sub> at a detergent/protein ratio of 1.5:1 (w/w). After 10 min incubation and centrifugation (TLA-100.3 rotor, 50,000 rpm, 30 min, 4 °C), the concentration of solubilized protein was usually 10–12 mg/mL. Co-crystallization of SERCA with CAD204520 was carried out using hanging drop equilibration at room temperature (RT) with protein/buffer in a 1:1 ratio. The best diffracting crystals were obtained with crystallization buffer consisting of 10% glycerol, 14% PEG 6000, 100 mM NaCl and 6% MPD. Data

were collected at 100 K and a wavelength of 0.976 Å at beam line I03 at the Diamond Light Source (DLS) in Didcot, UK. The data were processed using XDS (Kabsch, 2010) and AIMLESS (Evans and Murshudov, 2013) and the structure was determined by molecular replacement in PHASER (McCoy, 2007) using a SERCA crystal structure with matching space group (pdb: 4UU0) (Drachmann et al., 2014). PHENIX (Adams et al., 2010) was used for refinement, ligand fitting and model validation and COOT for model building (Emsley and Cowtan, 2004). Figures were prepared with Pymol (Molecular Graphics System, Version 2.0 Schrödinger, LLC).

<sup>a</sup> values in parentheses refer to the highest resolution shells as indicated

<b>Data collection</b>	
No. of data sets combined	2
Wavelength (Å)	0.97625
Space group	P 41 21 2
Unit cell Dimensions (Å)	a = 71.63 b = 71.63 c = 588.31
Resolution (Å) <sup>a</sup>	58.83 - 3.40 (3.67 - 3.40)
No. unique reflections <sup>a</sup>	22,672 (4,468)
I/σ <sup>a</sup>	9.3 (1.6)
CC (1/2) <sup>a</sup>	100 (65.2)
R <sub>pim</sub> (%) <sup>a</sup>	7.7 (77.9)
Completeness (%) <sup>a</sup>	100 (100)
Multiplicity <sup>a</sup>	36.6 (32.2)
<b>Refinement</b>	
Resolution (Å)	54.52 - 3.40
No. reflections (refinement)	22,530
No. reflections (R-free)	1,138
R <sub>work</sub> / R <sub>free</sub> (%)	22.81 / 25.54
No. atoms	7749

Protein	7671
TNP-ATP	46
CAD204520	31
K <sup>+</sup>	1
Average B-factors (Å <sup>2</sup> )	
Protein	118.07
TNP-ATP	155.59
CAD204520	130.33
K <sup>+</sup>	138.60
R.m.s. deviations	
Bond lengths (Å)	0.003
Bond angles (°)	0.72
Ramachandran	
favored / allowed / outliers (%)	90.32 / 8.97 / 0.71

<sup>a</sup> values in parentheses refer to the highest resolution shells as indicated

## Synthesis pathways

CAD307496 (2-[1-[3-(3-pyridyl)propyl]-2-piperidyl]-6-(trifluoromethoxy)-1H-indole) was prepared through the following intermediates:

(a) Intermediate 2-[2-(2-pyridyl)ethynyl]-5-(trifluoromethoxy)aniline: 2-Bromo-5-(trifluoromethoxy)aniline (6.21g, 24,2 mM), 2-ethynylpyridine (2.50g, 24.2 mM) and potassium carbonate (8.38g, 60.6 mM) in NMP (50 mL) were degassed with argon. Pd(DtBPF)Cl<sub>2</sub> (474mg, 0,73 mM ) was added and the reaction heated under argon to 120°C for 1 hour 45 min. The reaction cooled and diluted with water, extracted with 1:1 cHexane/EtOAc (3x 150 ml), washing each extract well with water. The combined extracts were dried, evaporated, and columned on 100 g SNAP cartridge eluting with 0-60% EtOAc/cHexane, using 20 column volumes to yield 750 mg of title compound as a brown solid. This was used without further purification.

(b) Intermediate 2-(2-pyridyl)-6-(trifluoromethoxy)-1H-indole: To 2-[2-(2-pyridyl)ethynyl]-5-(trifluoromethoxy)aniline (950mg, 3,41 mM) was added potassium 2-methylpropan-2-olate (383.13 mg, 3,41 mM) in DMF (50 mL) and the mixture was stirred at RT overnight. The reaction was quenched with 0.4 mL HOAc concentrated in vacuo, dissolved in diethyl ether and washed with sat.  $\text{NaHCO}_3$  and water. The organic phase was dried, evaporated, columned on 50 g SNAP cartridge eluting with 20-60% DCM/cHexane using 20 column volumes to yield 510 mg of the title compound as a yellow solid.

(c) Intermediate A (2-(2-piperidyl)-6-(trifluoromethoxy)-1H-indole): 2-(2-pyridyl)-6-(trifluoromethoxy)-1H-indole (4.18 g, 15,02 mM) in ethanol (100 mL) and 1M HCl in methanol (45 ml) hydrogenated over  $\text{PtO}_2$  (300 mg, 1.32 mM) at RT and pressure on 9.35. The mixture was warmed after 1 hour to 40°C and left overnight after which additional  $\text{PtO}_2$  (300 mg, 1.32 mM) was added and the reaction was stirred for another 5 hours. The catalyst was removed by filtration, and the filtrate evaporated to a white solid foam. This was taken up in DCM, and crystallized upon standing. The solid was broken up with diethyl ether and filtered to yield 3.7 g of title compound. The product may be converted to the hydrochloride by standard methods known to those skilled in the art.

(d) Intermediate 3-(3-bromopropyl)pyridine: To a stirring solution of 3-(3-pyridyl)propan-1-ol (0.14 g, 1 mM) in dichloromethane (2 mL) at 0°C was added carbon tetrabromide (0.5 g, 1,5 mM) then triphenylphosphine (0.42 g, 1,6 mM) portion wise, carefully. The reaction mixture was then stirred at 0°C for 2 hours.

The material was applied to a DCM-wetted 5g SCX-2 cartridge; washed with DCM then eluted with 0.5 M DIPEA in DCM to yield a pink solution used in the next step.

(e) To 2-(2-piperidyl)-6-(trifluoromethoxy)-1H-indole hydrochloride (100 mg, 0.31 mM) was added 3-(3-bromopropyl)pyridine (10 mL, mixture of the bromide and DIPEA in DCM and prepared described above; 0.34 mM). The reaction mixture was stirred at RT for 1 hour and then left to stand overnight. The reaction mixture was heated at 45°C and the DCM allowed to evaporate to concentrate the mixture after which DMF (1 mL) and DIPEA were added. A MDAP purification returned 35 mg of gum-like material which was run through a 2g SCX-2 cartridge yielding the title product after evaporation in 29 mg (23%) with satisfactory purity. QC-LC-MS (99.2%). LC-MS (ESI): (M+H)+ = 404.1.

Intermediate A was used to produce additional compounds in a fashion similarly to that used in the preparation of CAD307496.

**CAD204522:** From Intermediate A and commercially available 4-(2-Chloroethyl)morpholine (CAS 3240-94-6). Yield 61%. QC-LCMS (ESI): (m/z) (M+H)+ = 398.1, (M-H)- = 396.3.

**CAD204521:** Intermediate A and commercially available 4-bromobenzaldehyde (CAS 1122-91-4) was added followed by HOAc (0.02 ml, 0.35 mM) and sodium triacetoxyborohydride (74.55mg, 0.35 mM). The reaction mixture was stirred for 1 hour and run through a MeOH-wetted SCX-2 cartridge, washed with methanol, and then eluted with 2M NH<sub>3</sub> (aq). Yield 28%. QC-LCMS (ESI): (m/z) (M+H)+ = 453.0, (M-H)- = 451.1.

**CAD204631:** (3-(2-{1-[(4-bromophenyl)methyl]piperidin-2-yl}-6-(trifluoromethoxy)-1H-indol-3-yl)propan-1-ol): Intermediate 5-(2-pyridyl)pent-4-yn-1-ol: To 2-bromopyridine (2g, 12.7 mM), bis-triphenylphosphine palladium dichloride (1.1g, 1,58 mM) and CuI (301 mg, 1,58 mM) in triethylamine (50 mL, 358,7 mM) under argon was added dropwise pent-4-yn-1-ol (3.53 mL, 38 mM) and the mixture was heated to 50°C for 21.5 hours after which the reaction was cooled, evaporated almost to dryness, and then partitioned between water and ethyl acetate. The phases were separated and the aqueous phase extracted with ethyl acetate. The combined organics were dried (sodium sulfate), filtered, and evaporated. The crude product was purified by column chromatography (Isolera, 100 g column; 0-100% ethyl acetate in cyclohexane to provide 3.98 g (78%) of the title product as a yellow liquid.

(a) Intermediate 3-[2-(2-pyridyl)-6-(trifluoromethoxy)-1H-indol-3-yl]propan-1-ol: 5-(2-Pyridyl)pent-4-yn-1-ol (3.98 g, 24,7 mM), 2-bromo-5-(trifluoromethoxy)aniline (6.32 g, 24.7 mM), potassium carbonate (8.53 g, 61.7 mM) and Pd(DtBPF)Cl<sub>2</sub> (805 mg, 1.23 mM) in 1-methyl-2-pyrrolidinone (100 mL) were degassed then heated at 120°C under argon for 18 hours. The reaction mixture was split in two and each fraction passed through a MeOH-wetted SCX-2 cartridge (70 g); which were washed with methanol and then eluted with 2M ammonia in methanol. The ammonia fractions were evaporated and the crude product (8.3 g) was further purified on a Isolera (330 g column; 0-100% ethyl acetate in cyclohexane to yield 4.47g (54%) in accordance with the title compound.

(b) Intermediate B (3-[2-(2-piperidyl)-6-(trifluoromethoxy)-1H-indol-3-yl]propan-1-ol): A solution of 3-[2-(2-pyridyl)-6-(trifluoromethoxy)-1H-indol-3-yl]propan-1-ol (2.76 g, 8,21 mM) and PtO<sub>2</sub> (200 mg, 0,880 mM) in ethanol (100 mL) and 1M HCl in MeOH (24.62 mL, 24,62 mM) was degassed before placing under a H<sub>2</sub> atmosphere at RT for 4.5 hours. The reaction mixture was filtered through celite, the filterpad washed with additional ethyl acetate after which the filtrate was evaporated to give 4.02 g of a brown oil. The crude product was purified columned on Isolera (100 g column; 0-10% (2N ammonia in methanol) in DCM) to provide 2.48 g (88%) of a brown solid consistent with the title structure.

(c) From Intermediate B and commercially available 4-bromobenzaldehyde (CAS 1122-91-4) and a procedure similar to CAD204521. Yield 78%. QC-LCMS (ESI): (m/z) (M+H)<sup>+</sup> = 511.1, (M-H)<sup>-</sup> = 509.1.

**CAD204520** (4-[2-[2-[3-propyl-6-(trifluoromethoxy)-1H-indol-2-yl]-1-piperidyl]ethyl]morpholine) dihydrochloride was prepared through following intermediates:

(a) Intermediate 2-Pent-1-ynylpyridine: A slurry of 2-bromopyridine (8 g, 50.63 mM) and pent-1-yne (4.14 g, 60.76 mM) in triethylamine (141.16 mL, 1012.7 mM) degassed with argon added bis-triphenylphosphine palladium dichloride (1776.96 mg, 2.53 mM) and CuI (964.3 mg, 5.06 mM) was warmed to 50°C overnight. The reaction mixture was diluted with diethyl ether and washed with water. The crude product was dried and evaporated, columned on 100 g SNAP cartridge eluting with 0-20% EtOAc/cHexane, using 15 column volumes to yield a black oil which was used without further purification.

(b) Intermediate 3-Propyl-2-(2-pyridyl)-6-(trifluoromethoxy)-1H-indole: 2-Bromo-5-(trifluoromethoxy) aniline (3879 mg, 15.15 mmol), 2-pent-1-ynylpyridine (2200 mg, 15.15 mM) and potassium carbonate (5235 mg, 37.88 mM) in NMP (20 mL) were degassed with argon. Pd(dtbpf)Cl<sub>2</sub> (494 mg, 0.760 mmol) was added and the reaction heated under argon to 120°C overnight. The reaction mixture was then diluted with water, extracted with 1:3 EtOAc/cHexane, and subsequently diethyl ether. The combined extracts were dried, evaporated and columned on 100 g SNAP cartridge eluting with 0-10% EtOAc/cHexane to yield 2.225 g of product.

(c) Intermediate E: (2-(2-Piperidyl)-3-propyl-6-(trifluoromethoxy)-1H-indole hydrochloride): 3-Propyl-2-(2-pyridyl)-6-(trifluoromethoxy)-1H-indole (2.23 g, 6.95 mM) in ethanol (50 mL) and 1M HCl in methanol (21 mL) was hydrogenated over PtO<sub>2</sub> (450 mg, 2.00 mM) at 40°C for 7 hours after which the reaction mixture was left overnight at RT, in a hydrogen atmosphere. The reaction mixture was filtered, evaporated and taken up in 20 mL DCM. A white precipitate formed when 50 mL diethyl ether was added to give after drying 1.066 g (42%) of product. The mother liquor was columned after evaporation on a SNAP (50g) cartridge eluting with 0-10% NH<sub>3</sub> in MeOH/DCM, using 15 column volumes. Fractions containing products were combined and evaporated to dryness to yield 0.544 g (23%) of title compound as the free base providing a combined yield of 66%.

(d) 4-[2-[2-[3-propyl-6-(trifluoromethoxy)-1H-indol-2-yl]-1 piperidyl]ethyl]morpholine dihydrochloride: 2-(2-Piperidyl)-3-propyl-6-(trifluoromethoxy)-1H-indole (140 mg, 0.430 mM), 4-(2-chloroethyl)morpholine hydrochloride (87.81 mg, 0.470 mM) and sodium bicarbonate (108.11 mg, 1.29



mM) in methyl alcohol (2 mL) was refluxed under argon for 75 min. The reaction mixture was filtered and concentrated, loaded onto an elute 5 g cartridge and eluted with EtOAc, then 5% MeOH/DCM. The crude product was further purified by Xselect CSH 5 micron C18 prep column (19x250 mm) HPLC eluting with 10-60% MeCN/water (+0.1% HCO<sub>2</sub>H) to yield a product which was taken up in MeCN, 1M HCl (aq) and freeze dried to yield a white solid, 70 mg (31%) QC-LCMS (ESI): (m/z) (M+H)<sup>+</sup> = 440.2, (M-H)<sup>-</sup> = 438.2.

**CAD204519:** From Intermediate E and commercially available 4-bromobenzaldehyde (CAS 1122-91-4) and a procedure similar to CAD204521. Yield 26%. QC-LCMS (ESI): (m/z) (M+H)<sup>+</sup> = 495.0 (M-H)<sup>-</sup> = 493.1.

**CAD306750:** (1-{[(4-fluorophenyl)methyl]amino}-3-{2-[3-propyl-6-(trifluoromethoxy)-1H-indol-2-yl]piperidin-1-yl}propan-2-ol):

(a) Intermediate F: 1-Chloro-3-[2-[3-propyl-6-(trifluoromethoxy)-1H-indol-2-yl]-1-piperidyl]propan-2-ol: 2-(Chloromethyl)oxirane (163 mg, 1,76 mM) was dissolved in dichloromethane (1mL) and methyl alcohol (0.5 mL) and 2-(2-piperidyl)-6-(trifluoromethoxy)-1H-indole (Intermediate E, 500mg, 1.76mmol) was added. The reaction mixture was stirred at RT for 19 hours after which the reaction mixture was evaporated and columned on the Isolera (50 g cartridge, 0-5% (2N ammonia in methanol) in DCM) (yield 74%).

(b) Intermediate (1-{[(4-fluorophenyl)methyl]amino}-3-{2-[3-propyl-6-(trifluoromethoxy)-1H-indol-2-yl]piperidin-1-yl}propan-2-ol): From Intermediate F and commercially available 4-fluorobenzylamine (CAS 140-75-0) and sodium iodide (25.9 mg, 0.17 mM) in N,N-dimethylformamide (1mL) was heated at 70°C

for 22 hours after which the reaction was poured into water and extracted with EtOAc. The organic phases were dried (sodium sulfate), filtered and evaporated. The crude material was purified using Isolera column chromatography (0-10% (2N ammonia in methanol) in DCM). The crude product was further purified using preparative HPLC (C18, Xselect, 20-80% MeCN in water plus 0.1% formic acid). Yield 33%. QC-LCMS (ESI): (m/z) (M+H)<sup>+</sup> = 508.1, (M-H)<sup>-</sup> = 506.2. The product is a 1:1 mixture diastereomer.

**CAD306749:** This compound was produced in a similar way as CAD306750 from Intermediate F and commercially available 1-(3-Bisphenyl)methanamine (CAS 177976-49-7). Yield 19%. QC-LCMS (ESI): (m/z) (M+H)<sup>+</sup> = 566.2 (M-H)<sup>-</sup> = 564.2

**CAD305666:** (2-[2-[1-[(4-bromophenyl)methyl]-2-piperidyl]-6-(trifluoromethoxy)-1H-indol-3-yl]ethanol):

(a) Intermediate 2-[2-(2-pyridyl)-6-(trifluoromethoxy)-1H-indol-3-yl]ethanol: Was prepared similar to CAD204631 step (a). Yield 52%.

(b) Intermediate 2-[2-(2-piperidyl)-6-(trifluoromethoxy)-1H-indol-3-yl]ethanol was prepared similar to intermediate B (step (b) for CAD204631) Yield 45%.

(c) Intermediate 2-[2-[1-[(4-bromophenyl)methyl]-2-piperidyl]-6-(trifluoromethoxy)-1H-indol-3-yl]ethanol was obtained using Intermediate 2-[2-(2-piperidyl)-6-(trifluoromethoxy)-1H-indol-3-yl]ethanol and commercially available 4-bromobenzaldehyde (CAS 1122-91-4) and a procedure similar to CAD204521. Yield 87%. QC-LCMS (ESI): (m/z) (M+H)<sup>+</sup> = 497.1 (M-H)<sup>-</sup> = 495.1.

**CAD204630:** (2-[1-[(4-bromophenyl)methyl]-2-piperidyl]-3-isopentyl-6-(trifluoromethoxy)-1H-indole hydrochloride):

(a) Intermediate 3-isopentyl-2-(2-pyridyl)-6-(trifluoromethoxy)-1H-indole: By a method similar to that of CAD204631 step (a) above using commercially available 2-Bromo-5-(trifluoromethoxy)aniline (CAS 887267-47-2) and 2-(5-methylhex-1-ynyl)pyridine. Yield 60%.

(b) Intermediate 3-isopentyl-2-(2-piperidyl)-6-(trifluoromethoxy)-1H-indole: By a method similar to intermediate B (step b for CAD204631). Yield 56%.

(c) 2-[1-[(4-bromophenyl)methyl]-2-piperidyl]-3-isopentyl-6-(trifluoromethoxy)-1H-indole hydrochloride: By a method similarly to that of CAD204521 employing commercially available 4-bromobenzaldehyde (CAS 1122-91-4). Yield 62%. QC-LCMS (ESI): (m/z) (M+H)<sup>+</sup> = 523.1 (M-H)<sup>-</sup> = 521.1. Note: Many of the compounds are racemates i.e. of enantiomers or diastereomers. The pure enantiomer was not isolated.

### **ATPase preparation**

Heat competent *Saccharomyces cerevisiae* RS72 yeast cells (Cid et al., 1987) were transformed using a lithium acetate, single-stranded carrier DNA/polyethylene glycol method and with a yeast multicopy vector (Hill et al., 1986) containing the full-length cDNA of the *S. cerevisiae* plasma membrane H<sup>+</sup>-ATPase isoform *PMA1* under control of the *PMA1* promoter. Transformed yeast cells were pre-cultured in 100 ml sterile SGAH medium (7.04 g/L yeast nitrogen base, 19.8 g/L galactose, 64 mg/L adenine, 64 mg/L histidine) for 3 days at 25°C and 150 rpm. The pre-culture was transferred to 500 mL sterile SGAH medium and further incubated for 3 to 4 days. 100 mL from the cell culture was transferred to 1

L YPAD medium (10 g/L yeast extract, 20 g/L bacto-peptone, 20 g/L glucose, 20 mg/L adenine) and incubated at 25°C for 18-20 hours. Recombinant yeast was harvested by 2-3 min of centrifugation at 3.000 x g and 4°C, followed by 2 times wash in milli-Q water. Harvested cells were incubated in 10% glucose for 10 min, on a shaking table, and centrifuged at 3.000 x g and 4°C. Cells were re-suspended in homogenisation buffer (50 g/L glucose, 28.3% glycerol, 0,1 M Tris-HCl pH 7.25, 10 mM EDTA pH 8.0, 50 mM KCl, 1mM DTT, 200 µM PMSF, 2 µg/ml Pepstatin A), and disrupted with 165 g glass beads (500 µm) by runs in a BeadBeater (Biospec). The disrupted cells were centrifuged at 4°C for 5 and 15 min at 1.400 x g and 12.000 x g, respectively. The supernatant was collected and centrifuged at 251.000 x g for 1 h with 112 µM phenylmethylsulfonyl fluoride (PMSF) and 1.1 µg/mL Pepstatin A. The resulting pellet was re-suspended in GTEK<sub>20</sub> buffer (20% glycerol, 10 mM Tris-HCl pH 7.25, 25 mM KCl, 0.5 mM EDTA pH 8.0, 1 mM DTT, 0.2 mM PMSF, 2 µg/ml Pepstatin A) and centrifuged for 45 min at 251.000 x g and 4°C. Pellet was then re-suspended in STKED<sub>20</sub> buffer (200 g/L sucrose, 40 g/L glucose, 50 mM Tris-HCl pH 7.25, 50mM KCl, 1 mM EDTA pH 8.0, 1 mM DTT, 0.2 mM PMSF, 2 µg/ml Pepstatin A), homogenised and diluted with STKED<sub>20</sub> buffer. The plasma membranes were recovered at the interface of a 43%/53% (wt/wt) step sucrose gradient containing sucrose in 50 mM Tris-HCl pH 7.25, 50 mM KCl, 1 mM EDTA, 1 mM DTT. Centrifugation was done for 16 h at 154.000 x g and 4°C. The plasma membrane fraction was collected and diluted with GTEK<sub>20</sub> buffer and centrifuged for 1 hour at 274.000 x g. Pellet was collected and homogenised in GTEK<sub>20</sub> buffer and stored at -80°C.

Sarco/Endoplasmic reticulum (SR)  $\text{Ca}^{2+}$ -ATPase was provided in SR membranes purified by extraction with a low concentration of deoxycholate (DOC) as described above. The pig kidney  $\text{Na}^{+}/\text{K}^{+}$ -ATPase purification included a mild SDS treatment of isolated microsomes followed by a washing step and was kindly performed by Natalya Fedosova, Aarhus University and prepared as described in (Klodos et al., 2002). In brief, pieces of outer medulla were extracted and cut in pieces and further suspended and homogenized in ISE-buffer (25 mM imidazole, 250 mM sucrose, 1 mM EDTA pH 7.4). Microsomes were isolated by differential centrifugations. The final pellet was suspended and homogenized in ISE-buffer and stored at  $-20^{\circ}\text{C}$ .

### **ATP hydrolysis inhibition**

ATPase activity was determined by measuring the amount of liberated phosphate from ATP hydrolysis. The ATPase assay was performed in 96 well plates in a final reaction volume of 60  $\mu\text{L}$ . 0.1-0.2  $\mu\text{g}$ /well of DOC extracted SERCA membrane or the  $\text{Na}^{+}/\text{K}^{+}$ -ATPase was used, while 1-2.5  $\mu\text{g}$ /well was used of the Pma1 membrane preparation. Reactions including protein membrane preparation and exogenously added compounds in a  $\frac{1}{2}$  log dilution concentration range from 333  $\mu\text{M}$  or 166  $\mu\text{M}$  to 0.005  $\mu\text{M}$ . We conducted the enzymatic reactions in the following buffers; Pma1 buffer: 17.5 mM MOPS-NaOH pH 7, 7 mM  $\text{MgSO}_4$ , 44 mM  $\text{KNO}_3$  (vacuolar ATPase inhibitor), 22 mM  $\text{NaN}_3$  (mitochondrial ATPase inhibitor), 0.22 mM  $\text{Na}_2\text{MoO}_4$  (acid phosphatase inhibitor); SERCA buffer: 9 mM MOPS-NaOH pH 7, 2.7 mM  $\text{MgCl}_2$ , 0.1 mM  $\text{CaCl}_2$  and 72 mM KCl.  $\text{Na}^{+}/\text{K}^{+}$ -ATPase buffer: 30 mM MOPS-NaOH pH 7, 40 mM NaCl, 4 mM  $\text{MgCl}_2$  and 20 mM KCl. Reactions were

started by the addition of Na-ATP to a final concentration of 2.5 mM (Pma1 and Na<sup>+</sup>/K<sup>+</sup>-ATPase) or 5 mM (SERCA), followed by 30 min incubation at 30 °C. The amount of liberated phosphate was determined calorimetrically after addition of STOP solution (mixture of L-ascorbic acid, ammonium heptamolybdate tetrahydrate, and HCl to give final concentrations of 65 mM, 2.2 mM, and 189 mM, respectively) with 5 min incubation at RT followed by addition of arsenite solution (mixture of NaAsO<sub>2</sub>, sodium citrate dihydrate, and acetic acid to give final concentrations of 3.1 mM, 28 mM, and 141 mM, respectively). We measured absorption at 860 nm after additional 30 min incubation at RT.

### **Cell Viability, apoptosis and DNA content assays**

ATP-based cell viability was determined using the CellTiter-Glo viability assay (Promega Corporation, Madison, WI, USA #G7573) and luminescence was measured using a Victor X4 (Perkin Elmer, Waltham, MA, USA). Apoptotic rate was quantified by staining cells with Annexin V and propidium iodide using a flow-cytometry commercial kit (eBioscience™ Annexin V Apoptosis Detection Kit APC, Waltham MA, USA, # 88-8007-74). Cells were analyzed by flow cytometry with a FACScan flow cytometer (Beckman Culture-Cytomics FC 500, Life Sciences Division, Indianapolis, USA) and FlowJo V10 (Tree Star LLC, Ashland, OR, USA) analytical software. Cellular DNA content was assessed by staining with propidium iodide (50 g/ml) and analyzed by flow cytometry. At least 20,000 events were acquired and all determinations were replicated at least twice.

### **Cell competition assay**

SKW-3/KE-37-GFP and MOLT16 were co-cultured at 1:1 ratio in RPMI 1640, 10% FBS, 1% P/S medium.  $1 \times 10^6$  cells per condition were treated with CAD204520 at the following concentrations 2.5 and 5  $\mu$ M and DMSO at 0.005% and 0.01% respectively and incubated at 37°C. After 72 hours, T-ALL cells were washed in PBS, and stained with a LIVE/DEAD Fixable Far Red Dead Cell Stain (Invitrogen, Life Technologies, Carlsbad, CA, USA, #L34973) for 30 min. Fluorescent signal was assessed by flow-cytometry [Beckman Culture-Cytomics FC 500 (Life Sciences Division, Indianapolis, USA) and FlowJo V10 (Tree Star LLC, Ashland, OR, USA) analytical software]. A minimum of 20,000 events was collected for each biological sample. Experiments are representative of two independent experiments.

### **Compound sources**

We obtained the compounds for this study from the following sources: DAPT (N-[N-(3,5-difluorophenacetyl)-1-alanyl]-(S)-phenylglycine) (Selleckchem, Houston, TX USA, #S2215), thapsigargin (Enzo Biochem, Inc., USA #BML-PE180-0005).

### **Compound treatment of cell lines and primary cells**

Cells were seeded in 384-well plates (Corning Life Sciences Plastic, Bedford MA, USA, #3570) at the final concentration of  $0.02 \times 10^6$ /mL per condition. Small molecules were added with a nanometric dispenser Tecan D300e (Tecan Trading AG, Switzerland), and cellular viability was assessed after 72 hours of drug

treatment using a CellTiter-Glo ATP assay (Promega Corporation, Madison, WI, USA, #G7573). IC<sub>50</sub> and the area under the curve (AUC) were calculated using GraphPad Prism software (La Jolla, CA, USA).

### **Intracellular calcium measurement**

Cytosolic Ca<sup>2+</sup> concentration was measured using the Indo-1 AM probe (ThermoFisher Scientific, Waltham MA, USA, #I1223). Cells were washed twice with a calcium free solution (D-PBS Life Technologies, Carlsbad, CA, USA, #10010015) and loaded at 37°C in 5% CO<sub>2</sub> for 30 min with 5 µM of Indo-1 AM. Then, cells were washed twice with D-PBS and equilibrated in RPMI 1640 (Thermo Fisher Scientific, Waltham MA, USA, Waltham MA, USA #MT10040CV) with 10% fetal bovine serum (FBS) (Sigma-Aldrich, St. Louis, MO, USA, #F2442-500ML) and 1% penicillin-streptomycin (Thermo Fisher Scientific, Waltham MA, USA, #3MT30002CI) for 5 min at 37°C. Baseline fluorescence of Indo-1 AM loaded cells was acquired for 1 min LSR Fortessa X20 flow cytometer (BD Biosciences, San Jose, CA, USA). Subsequently DMSO (0.1%), CAD204520 1 µM, or Thapsigargin 1 µM were added and measurement was resumed for a total of 10 min. Data analysis was performed using FlowJo V10 (Tree Star LLC, Ashland, OR, USA) analytical software.

ER Ca<sup>2+</sup> release and re-uptake was measured with the IonOptix system (IonOptix, Milton, MA, USA). Ca<sup>2+</sup> signals were detected by epifluorescence after loading T-ALL cells (ALL/SIL, DND41) with Fluo-3-AM (10 µM; Invitrogen, Carlsbad, CA, USA) in PBS (Gibco, Thermo Fisher Scientific, Waltham, MA, USA) for 20 min, at



room temperature. After removing the fluorophore, cells were washed with PBS for 30 min and then placed ( $1 \times 10^6$ ; 1ml volume) in a chamber mounted on the stage of an inverted microscope (Nikon-Eclipse TE2000-U, Nikon Instruments, Florence, Italy). The recording started with measurement of baseline fluorescence. Then, 1  $\mu$ M CAD204520, 1  $\mu$ M thapsigargin, or DMSO (0.1%) were manually added with a pipette, and the recording was continued for up to 15 min (during the first 7 min: 5 seconds of recording followed by 5 seconds of rest; in the remaining 8 min: 5 seconds of recording followed by 30 seconds of rest). Excitation length was 480 nm, with emission collected at 535 nm. The following parameters were evaluated: (i) peak fluorescence normalized to baseline fluorescence ( $f/f_0$ \_peak), (ii) time at 50% of fluorescence signal decay, measured from the peak time ( $\text{time}_{50\%}-f/f_0$ ), and normalized fluorescence computed at 3, 5, and 10 min from the peak time ( $f/f_0$ \_3min,  $f/f_0$ \_5min, and  $f/f_0$ \_10 min).

### **Western blot**

Protein lysates for western blotting were incubated with antibodies specific for  $\gamma$ -secretase-cleaved NOTCH1 (Val1744, #4147 or #2421 Cell Signaling, Beverly, MA, USA) or the C-terminus of NOTCH1 (#SC-6014 (C-20), Santa Cruz Biotechnology, Santa Cruz, CA, USA). Cleaved form of Poly (ADP-ribose) polymerase was detected using an antibody specific for the cleaved peptide of PARP (#9541, Cell Signaling, Beverly, MA, USA). The expression of SERCA isoforms in ALL/SIL were detected using SERCA2 (#9580, Cell Signaling, Beverly, MA, USA) and SERCA3 (#sc-81759, Santa Cruz Biotechnology, Santa Cruz, CA,

USA) antibodies. Loading controls were performed with antibodies specific for  $\beta$ -Actin, (#BK3700S, Cell Signaling, Beverly, MA, USA), GAPDH (#137179, Santa Cruz Biotechnology, Santa Cruz, CA, USA) or HSP90 (# sc-69703 (4F10)), Santa Cruz Biotechnology, Santa Cruz, CA, USA). Effects on the endoplasmic reticulum stress pathway (ER stress) we used the following antibodies: BiP, (#BK3177S), phospho-eIF2 $\alpha$  (Ser51) (#9721S), eIF2 $\alpha$  (#9722S) (Cell Signaling, Beverly, MA, USA). Blots were developed using species specific fluorescent antibodies obtained from LI-COR (Biosciences, Lincoln, NE, USA) such as IRDye 680LT Goat anti-Mouse IgG (#925-68020); IRDye 800CW goat anti-rabbit IgG (#925-32211); IRDye 680RD goat anti-rabbit IgG (#925-68071). Cell surface NOTCH1 was evaluated by staining non-permeabilized cells with monoclonal anti-human NOTCH1 antibody (#FAB5317P, R&D, Minneapolis, MN, USA).

### **Indirect immunofluorescence microscopy**

DND41, REC-1 and ALL/SILL cells were resuspended in PBS, spotted on immunofluorescence slides (Thermo Fisher Scientific, Waltham, MA) by a cytopspin centrifuge (CR2000, Small Prime Centrifuge, Centurion) fixed for 10 min in 4% paraformaldehyde (#28908, Thermo Fisher Scientific, Waltham MA, USA), permeabilized in 0.2% Triton X-100 for 5 min, and blocked in 5% bovine serum albumin for 1 hour. Then, the cells were incubated with primary antibodies against full length NOTCH1 (#SC-6014 (C-20) Santa Cruz Biotechnology, Santa Cruz, CA, USA or #ab44986 (A6) Abcam, Cambridge, United Kingdom), GOLGA1

(#SAB1409131, Sigma-Aldrich, St. Louis, MO, USA), and ATF6 (#37149, Abcam, Cambridge, United Kingdom).

Alexa Fluor 488 (#A11029, Invitrogen, Carlsbad, CA, USA) and Alexa Fluor 568 (#A11036, Invitrogen, Carlsbad, CA, USA) were used as secondary antibodies and cells were incubated 1 hour at room temperature protected by the light. Nuclei were stained with DAPI (#D9542, Sigma-Aldrich, St. Louis, MO, USA). Coverslips were mounted with Prolong Gold Antifade reagent (#P36934, Thermo Fisher Scientific, Waltham MA, USA). Images were captured using a EVOS FL microscope (Thermo Fisher Scientific, Waltham MA, USA) and analyzed using ImageJ software (<http://rsbweb.nih.gov/ij/>).

### **Real-time RT-PCR**

Primers and probes for real-time RT-PCR were obtained from Applied Biosystems (Foster City, CA, USA) (*RPL13A* #Hs01926559\_g1, *MYC* #Hs00153401\_m1, *DTX1* #Hs00269995\_m1). The data were analyzed using the  $\Delta\Delta CT$  method and plotted as percentage of transcript compared to vehicle.

### **Whole exome sequencing**

DNA was extracted from about  $10 \times 10^6$  ALL/SIL o ALL/SIL thapsigargin resistant using a Promega Maxwell® kit as per the manufacturer's protocol (Promega Corporation, Madison WI, USA, #AS1010).

A total amount of 1.0  $\mu$ g genomic DNA per sample was used as input material for the DNA library preparation. Sequencing libraries were generated using Agilent

SureSelect Human all exon kit (Agilent Technologies, CA, USA) following manufacturer's recommendations and index codes were added to each sample. Briefly, fragmentation was carried out by hydrodynamic shearing system (Covaris, Massachusetts, USA) to generate 180-280bp fragments. Remaining overhangs were converted into blunt ends via exonuclease/polymerase activities and enzymes were removed. After adenylation of 3' ends of DNA fragments, adapter oligonucleotides were ligated. DNA fragments with ligated adapter molecules on both ends were selectively enriched in a PCR reaction. After PCR reaction, library hybridizes with liquid phase with biotin labeled probe, after which streptomycin-coated magnetic beads are used to capture the exons of genes. Captured libraries were enriched in a PCR reaction to add index tags to prepare for hybridization. Products were purified using AMPure XP system (Beckman Coulter, Beverly, USA) and quantified using the Agilent high sensitivity DNA assay on the Agilent Bioanalyzer 2100 system and sequenced with Hiseq PE 150 (Illumina®, San Diego, CA, USA). Paired-end clean reads were aligned to the reference genome (hg38) with Burrows-Wheeler aligner (B.W.A.). SAMtool was used to sort and index the original BAM files and Picard marked duplicates reads. Coverage and depth was calculated based on the final BAM files. If a read or reads pair were mapped to multiple positions, B.W.A. will choose the most likely position. If two or more likely position were present B.W.A. will choose one randomly. This multiple hit strategy has significant impact on SNP, INDEL and CNV detection, and variant calling accuracy. Following genomic variant detection, we performed annotation of

variants with the tool ANNOVAR (Wang et al., 2010) in multiple aspects, including protein coding changes, affected genomic regions, allele frequency etc.

### **Virus production and transduction of T-ALL cell lines**

$3 \times 10^6$  293T were plated in 10 cm plates and maintained in DMEM media (Life Technologies, Carlsbad, CA, USA, #11965118), 10% fetal bovine serum (FBS) (Sigma-Aldrich, St. Louis, MO, USA, #F2442-500ML), 1% penicillin-streptomycin (Thermo Fisher Scientific, Waltham MA, #3MT30002CI) and incubated at 37°C with 5% CO<sub>2</sub>, until sub confluent. Cells were transfected with 2 µg of pCMV-VSV-G envelope vector, Delta 8.9 packaging plasmid and pXPR-011-GFP, a vector expressing a green fluorescent protein (GFP), according to the FuGENE 6 protocol (Promega Corporation, Madison WI, USA, #E2691). The tissue culture medium was changed to RPMI 1640 24 hours post-transfection, and viral supernatant was harvested and filtered (0.2 µm) 48 hours post-transfection.  $4 \times 10^6$  SKW-3/KE-37 T-ALL cells were resuspended in 100 µL of RPMI 1640 and spin-infected for 1 hour at 37°C with 100 µl lentivirus particles and 8 µg/mL polybrene (Sigma-Aldrich, St. Louis, MO, USA). Cells were selected 48 hours later with 1 µg/mL puromycin (Sigma-Aldrich, St. Louis, MO, USA).

### **Cardiomyocyte isolation and treatment**

Individual left ventricular (LV) myocytes were enzymatically isolated by collagenase perfusion, following a procedure previously described (Meraviglia et al., 2018). Briefly, after sacrifice, the rat heart was rapidly removed, mounted on a

Langendorff apparatus and perfused at 37°C with the following sequence of solutions: solution 1: calcium-free solution for 5 min containing the following (expressed in mM/L): 126 NaCl, 22 dextrose, 5.0 MgCl<sub>2</sub>, 4.4 KCl, 20 taurine, 5 creatine, 5 Na pyruvate, 1 NaH<sub>2</sub>PO<sub>4</sub>, and 24 HEPES (pH = 7.4, adjusted with NaOH); solution 2: solution 1 plus 0.1 mM Ca<sup>2+</sup>, 1 mg/ml type 2 collagenase (Worthington Biochemical, USA), and 0.1 mg/ml type XIV protease (Sigma, Milan, Italy) for about 15 min, and solution 3: solution 1 plus 0.1 mM Ca<sup>2+</sup> (enzyme-free) for 5 min. All solutions were gassed with 100% O<sub>2</sub>. Afterward, the LV was minced and shaken for 5 min. The cells were filtered through nylon net and re-suspended in the low calcium solution for 30 min, then slowly brought to a final calcium concentration of 1 mM (maintenance solution).

A total of 8 rats (male) were scarified for these experiments. Specifically, cardiomyocytes isolated from the heart of 6 rats were either untreated (Control group) or incubated with 5 µM CAD204520 for 2 hours (CAD204520<sub>2hr</sub>) or 4 hours (CAD204520<sub>4hr</sub>) and then used for recording cell mechanics (IonOptix, Milton, MA, USA) (Bocchi et al., 2018; Meraviglia et al., 2018). Cardiomyocytes isolated from additional 2 rats were incubated with thapsigargin, at two different concentrations, 200 nM or 500nM for 2 hours and then submitted to the same experimental protocol (Control number of cells n=63; Thapsigargin<sub>200nM</sub>, n=28; Thapsigargin<sub>500nM</sub>, n=25. Left ventricular myocytes were placed in a chamber mounted on the stage of an inverted microscope (Nikon-Eclipse TE2000-U, Nikon Instruments, Florence, Italy) and superfused (1 mL/min at 37°C) with a Tyrode solution containing (in mM): 140 NaCl, 5.4 KCl, 1 MgCl<sub>2</sub>, 5 HEPES, 5.5 glucose,

and 1 CaCl<sub>2</sub> (pH 7.4, adjusted with NaOH) (Sigma-Aldrich, Milan, Italy). The cells were field stimulated at a frequency of 0.5 Hz by constant current pulses (2 milliseconds in duration, and twice diastolic threshold in intensity; MyoPacer Field Stimulator, IonOptix). Load-free contraction of myocytes was measured with the IonOptix system, which captures sarcomere length dynamics via a Fast Fourier Transform algorithm. The following parameters were computed: mean diastolic sarcomere length, fraction of shortening (FS), and the maximal rates of shortening ( $-dl/dt_{\max}$ ) and re-lengthening ( $+dl/dt_{\max}$ ). Steady-state contraction of myocytes was achieved before data recording by means of a 10 seconds conditioning stimulation. Sampling rate was set at 1 kHz. In a fraction of cells from each experimental group, calcium transients were measured simultaneously with cell motion, after loading the myocytes with Fluo-3 AM (10  $\mu$ mol/L; Invitrogen, Carlsbad, CA, USA) for 30 min. Excitation wavelength was 480 nm, with emission collected at 535 nm. Fluo3 signals were expressed as normalized fluorescence ( $f/f_0$ : fold increase). The time course of the fluorescence signal decay was described by a single exponential equation, and the time constant (Tau) was used as a measure of the rate of intracellular calcium clearing. Only rod-shaped myocytes exhibiting cross striations and no spontaneous contractions were selected for physiological measurements. Cardiomyocyte subgroups were washed three times with low-calcium solution and centrifuged (42 x g for 5 min). After removing the supernatant, the pellet was stored at -80 °C for intracellular ATP content detection (as described below).

### **Intracellular ATP content detection**

The intracellular content of ATP was measured by the luminescence ATP-lite assay (PerkinElmer, Waltham, MA, USA, #6016943) according to the manufacturer's protocol, using an EnSpire® multimode plate reader (PerkinElmer, Waltham, MA, USA). Briefly, a frozen pellet of cardiomyocytes (both untreated or incubated with 5  $\mu$ M CAD204520 for 2 or 4 hours) was re-suspended in 1 mL of PBS, and then 20  $\mu$ L of this suspension were further diluted 20 times in PBS. 100  $\mu$ L of each diluted sample were lysed and assayed for ATP content in triplicate, as previously detailed (Bocchi et al., 2018). The raw luminescence data were normalized for the total protein content measured by the DC Protein assay kit (Bio-Rad, Hercules, CA, USA).

### **In vivo studies**

In brief 6 male, 7-9 weeks old CD1 (ICR) in-house breed mice (Aurigene, India) were treated with 30 mg/Kg/diem CAD204520 in fed state by oral gavage dissolved in Tween-80 0.5% w/v (Sigma-Aldrich, Missouri, USA) and hydroxypropyl-methylcellulose (HPMC) 1.0% w/v (Shin-Etsu Chemical Co., Tokyo, Japan) to model PK and biodistribution data. Samples from the plasma and brain were collected at eight time points (5 min to 24 hours). CAD204520 concentration was assessed by LC/MS-MS method and PK parameters ( $T_{max}$ ,  $C_{max}$ ,  $T_{1/2}$ , AUC, etc.) were calculated with Analyst 1.6.1 software using a one-compartment model. Lambda Z PK parameters was reviewed by LD ADME consult (Copenhagen, Denmark) to model multiple doses PO infusion and time-concentration data. For tolerability studies, 6-8 weeks BALB/cAnNCr mice per group (3 male and 3 female)



were treated BID with 30 mg/Kg CAD204520 or vehicle (see above) by oral gavage at 8 hours interval. CAD204520 and vehicle were administered from day 1 to day 21 by oral route. Daily body weight measurement before dosing and adverse events were recorded. Animals were sacrificed on day 21. In a subsequent experiment, 6 BALB/cAnNCr mice per group (3 male and 3 female) were treated with 30 mg/Kg CAD204520 (BID) for 7 days and for the remaining of the study (day 7 to day 21) with 60 mg/Kg (BID).

To generate NOTCH1-dependent T-ALL tumors in mice,  $10 \times 10^6$  SKW-3/KE-37 cells were transplanted via the retro-orbital venous sinus in adult (10-12 weeks old) non-irradiated NSG mice (day 0) (Baldoni et al., 2018). Once disease was established at day 12 after transplant, animals were divided into two treatment groups of eight mice each (3 male and 5 female): vehicle [tween-80 0.5% w/v (Sigma-Aldrich, Missouri, USA) and hydroxypropyl-methylcellulose (HPMC) 1.0% w/v (Shin-Etsu Chemical Co., Tokyo, Japan)] or 30 mg/kg BID of CAD204520. Animals were treated with either vehicle or CAD204520 at 30 mg/kg BID (PO) for 4 days. Antileukemic activity of CAD204520 was assessed by measuring human CD45<sup>+</sup> expression (clone HI30, BD Biosciences, New Jersey, USA) on peripheral blood blast cells by flow cytometry (FACS CANTO, BD Biosciences, San Jose, CA, USA) and by quantification of hCD45<sup>+</sup> cells in formalin-fixed, paraffin-embedded spleen sections [(clones 2B11 + PD7/26 Dako, Agilent, Stevens Creek Blvd Santa Clara, CA, USA)]. Complete blood count was performed using an XE-2100 hematology automated analyzer (Dasit). Formalin-fixed, paraffin-embedded heart and gut sections were stained using hematoxylin and eosin. Images were acquired

at different magnifications using a Leica DM750 microscope (Leica Microsystems, Wetzlar, Germany).

## **QUANTIFICATION AND STATISTICAL ANALYSIS**

Assumption of normal distribution was not determined and *P*-value was calculated by non-parametric t-test (Mann-Whitney) by comparing treated samples to untreated controls. Significance across groups was determined by one-way or two-way ANOVA using Bonferroni correction for multiple comparisons testing when appropriate. Statistics were performed using GraphPad Prism software. Graphs show means and standard deviation ( $\pm$ SD) as indicated in the figure legends. Statistical significance, group size, and experimental details are described in the figure legends and/or in the method details.

## **DATA AND CODE AVAILABILITY**

The model and structure factors for the SERCA-CAD204520 complex structure reported in this paper have been deposited in the Protein Data Bank: code 6YAA.

## REFERENCES

- Abdullahi, A., Stanojic, M., Parousis, A., Patsouris, D., and Jeschke, M. G. (2017). Modeling Acute ER Stress in Vivo and in Vitro. *Shock* 47, 506-513.
- Adams, P. D., Afonine, P. V., Bunkoczi, G., Chen, V. B., Davis, I. W., Echols, N., Headd, J. J., Hung, L. W., Kapral, G. J., Grosse-Kunstleve, R. W., *et al.* (2010). PHENIX: a comprehensive Python-based system for macromolecular structure solution. *Acta Crystallogr D Biol Crystallogr* 66, 213-221.
- Andersen, J. P., Lassen, K., and Moller, J. V. (1985). Changes in Ca<sup>2+</sup> affinity related to conformational transitions in the phosphorylated state of soluble monomeric Ca<sup>2+</sup>-ATPase from sarcoplasmic reticulum. *J Biol Chem* 260, 371-380.
- Andersen, T. B., Lopez, C. Q., Manczak, T., Martinez, K., and Simonsen, H. T. (2015). Thapsigargin--from Thapsia L. to mipsagargin. *Molecules* 20, 6113-6127.
- Arbabian, A., Brouland, J. P., Gelebart, P., Kovacs, T., Bobe, R., Enouf, J., and Papp, B. (2011). Endoplasmic reticulum calcium pumps and cancer. *Biofactors* 37, 139-149.
- Arruga, F., Gizdic, B., Serra, S., Vaisitti, T., Ciardullo, C., Coscia, M., Laurenti, L., D'Arena, G., Jaksic, O., Inghirami, G., *et al.* (2014). Functional impact of NOTCH1 mutations in chronic lymphocytic leukemia. *Leukemia* 28, 1060-1070.
- Artavanis-Tsakonas, S., Rand, M. D., and Lake, R. J. (1999). Notch signaling: cell fate control and signal integration in development. *Science* 284, 770-776.
- Aster, J. C., Pear, W. S., and Blacklow, S. C. (2008). Notch signaling in leukemia. *Annu Rev Pathol* 3, 587-613.
- Baldoni, S., Del Papa, B., Dorillo, E., Aureli, P., De Falco, F., Rompietti, C., Sorcini, D., Varasano, E., Cecchini, D., Zei, T., *et al.* (2018). Bepridil exhibits anti-leukemic activity associated with NOTCH1 pathway inhibition in chronic lymphocytic leukemia. *Int J Cancer* 143, 958-970.
- Baliakas, P., Hadzidimitriou, A., Sutton, L. A., Rossi, D., Minga, E., Villamor, N., Larrayoz, M., Kminkova, J., Agathangelidis, A., Davis, Z., *et al.* (2015). Recurrent mutations refine prognosis in chronic lymphocytic leukemia. *Leukemia* 29, 329-336.
- Ball, M., Andrews, S. P., Wierschem, F., Cleator, E., Smith, M. D., and Ley, S. V. (2007). Total synthesis of thapsigargin, a potent SERCA pump inhibitor. *Org Lett* 9, 663-666.
- Bassani, J. W. M., Yuan, W. L., and Bers, D. M. (1995). Fractional Sr Ca Release Is Regulated by Trigger Ca and Sr Ca Content in Cardiac Myocytes. *American Journal of Physiology-Cell Physiology* 268, C1313-C1319.
- Bea, S., Valdes-Mas, R., Navarro, A., Salaverria, I., Martin-Garcia, D., Jares, P., Gine, E., Pinyol, M., Royo, C., Nadeu, F., *et al.* (2013). Landscape of somatic mutations and clonal evolution in mantle cell lymphoma. *Proc Natl Acad Sci U S A* 110, 18250-18255.
- Blaumueller, C. M., Qi, H., Zagouras, P., and Artavanis-Tsakonas, S. (1997). Intracellular cleavage of Notch leads to a heterodimeric receptor on the plasma membrane. *Cell* 90, 281-291.
- Bleeker, N. P., Cornea, R. L., Thomas, D. D., and Xing, C. (2013). A novel SERCA inhibitor demonstrates synergy with classic SERCA inhibitors and targets multidrug-resistant AML. *Mol Pharm* 10, 4358-4366.
- Bocchi, L., Savi, M., Naponelli, V., Vilella, R., Sgarbi, G., Baracca, A., Solaini, G., Bettuzzi, S., Rizzi, F., and Stilli, D. (2018). Long-Term Oral Administration of Theaphephenon-E Improves Cardiomyocyte Mechanics and Calcium Dynamics by Affecting Phospholamban Phosphorylation and ATP Production. *Cell Physiol Biochem* 47, 1230-1243.
- Brini, M., and Carafoli, E. (2009). Calcium pumps in health and disease. *Physiol Rev* 89, 1341-1378.
- Brzozowa-Zasada, M., Piecuch, A., Michalski, M., Segiet, O., Kurek, J., Harabin-Slowinska, M., and Wojnicz, R. (2017). Notch and its oncogenic activity in human malignancies. *Eur Surg* 49, 199-209.

Bublitz, M., Kjellerup, L., Cohrt, K. O., Gordon, S., Mortensen, A. L., Clausen, J. D., Pallin, T. D., Hansen, J. B., Fuglsang, A. T., Dalby-Brown, W., and Winther, A. L. (2018). Tetrahydrocarbazoles are a novel class of potent P-type ATPase inhibitors with antifungal activity. *PLoS One* 13, e0188620.

Bublitz, M., Morth, J. P., and Nissen, P. (2011). P-type ATPases at a glance. *J Cell Sci* 124, 2515-2519.

Burghoorn, H. P., Soteropoulos, P., Paderu, P., Kashiwazaki, R., and Perlin, D. S. (2002). Molecular evaluation of the plasma membrane proton pump from *Aspergillus fumigatus*. *Antimicrob Agents Chemother* 46, 615-624.

Chemaly, E. R., Troncone, L., and Lebeche, D. (2018). SERCA control of cell death and survival. *Cell Calcium* 69, 46-61.

Chen, D., and Evans, P. A. (2017). A Concise, Efficient and Scalable Total Synthesis of Thapsigargin and Nortrilobolide from (R)-(-)-Carvone. *J Am Chem Soc* 139, 6046-6049.

Chidawanyika, T., Sergison, E., Cole, M., Mark, K., and Supattapone, S. (2018). SEC24A identified as an essential mediator of thapsigargin-induced cell death in a genome-wide CRISPR/Cas9 screen. *Cell Death Discov* 4, 115.

Chou, T. C. (2010). Drug combination studies and their synergy quantification using the Chou-Talalay method. *Cancer Res* 70, 440-446.

Christensen, S. B., Andersen, A., Poulsen, J. C., and Treiman, M. (1993). Derivatives of thapsigargin as probes of its binding site on endoplasmic reticulum Ca<sup>2+</sup> ATPase. Stereoselectivity and important functional groups. *FEBS Lett* 335, 345-348.

Christensen, S. B., Skytte, D. M., Denmeade, S. R., Dionne, C., Moller, J. V., Nissen, P., and Isaacs, J. T. (2009). A Trojan horse in drug development: targeting of thapsigargin towards prostate cancer cells. *Anticancer Agents Med Chem* 9, 276-294.

Chu, H., Smith, J. M., Felding, J., and Baran, P. S. (2017). Scalable Synthesis of (-)-Thapsigargin. *ACS Cent Sci* 3, 47-51.

Cid, A., Perona, R., and Serrano, R. (1987). Replacement of the promoter of the yeast plasma membrane ATPase gene by a galactose-dependent promoter and its physiological consequences. *Curr Genet* 12, 105-110.

Clark, J. H., Kinnear, N. P., Kalujnaia, S., Cramb, G., Fleischer, S., Jeyakumar, L. H., Wuytack, F., and Evans, A. M. (2010). Identification of functionally segregated sarcoplasmic reticulum calcium stores in pulmonary arterial smooth muscle. *J Biol Chem* 285, 13542-13549.

Clausen, J. D., Kjellerup, L., Cohrt, K. O., Hansen, J. B., Dalby-Brown, W., and Winther, A. L. (2017). Elucidation of antimicrobial activity and mechanism of action by N-substituted carbazole derivatives. *Bioorg Med Chem Lett* 27, 4564-4570.

Dally, S., Corvazier, E., Bredoux, R., Bobe, R., and Enouf, J. (2010). Multiple and diverse coexpression, location, and regulation of additional SERCA2 and SERCA3 isoforms in nonfailing and failing human heart. *J Mol Cell Cardiol* 48, 633-644.

Dally, S., Monceau, V., Corvazier, E., Bredoux, R., Raies, A., Bobe, R., del Monte, F., and Enouf, J. (2009). Compartmentalized expression of three novel sarco/endoplasmic reticulum Ca<sup>2+</sup>-ATPase 3 isoforms including the switch to ER stress, SERCA3f, in non-failing and failing human heart. *Cell Calcium* 45, 144-154.

De Ford, C., Heidersdorf, B., Haun, F., Murillo, R., Friedrich, T., Borner, C., and Merfort, I. (2016). The clerodane diterpene casearin J induces apoptosis of T-ALL cells through SERCA inhibition, oxidative stress, and interference with Notch1 signaling. *Cell Death Dis* 7, e2070.

De Strooper, B., Annaert, W., Cupers, P., Saftig, P., Craessaerts, K., Mumm, J. S., Schroeter, E. H., Schrijvers, V., Wolfe, M. S., Ray, W. J., et al. (1999). A presenilin-1-dependent gamma-secretase-like protease mediates release of Notch intracellular domain. *Nature* 398, 518-522.

DeAngelo, D. J., Stone, R.M., Silverman, L.B., and Aster, J.C. (2006). A phase I clinical trial of the Notch inhibitor MK-0752 in patients with T-cell acute lymphoblastic leukemia/lymphoma (T-ALL) and other leukemias. In *J Clin Oncol*.

Denmeade, S. R., and Isaacs, J. T. (2005). The SERCA pump as a therapeutic target: making a "smart bomb" for prostate cancer. *Cancer Biol Ther* 4, 14-22.

Denmeade, S. R., Jakobsen, C. M., Janssen, S., Khan, S. R., Garrett, E. S., Lilja, H., Christensen, S. B., and Isaacs, J. T. (2003). Prostate-specific antigen-activated thapsigargin prodrug as targeted therapy for prostate cancer. *J Natl Cancer Inst* 95, 990-1000.

Di Ianni, M., Baldoni, S., Rosati, E., Ciurnelli, R., Cavalli, L., Martelli, M. F., Marconi, P., Screpanti, I., and Falzetti, F. (2009). A new genetic lesion in B-CLL: a NOTCH1 PEST domain mutation. *Br J Haematol* 146, 689-691.

Doan, N. T., Paulsen, E. S., Sehgal, P., Moller, J. V., Nissen, P., Denmeade, S. R., Isaacs, J. T., Dionne, C. A., and Christensen, S. B. (2015). Targeting thapsigargin towards tumors. *Steroids* 97, 2-7.

Doody, R. S., Raman, R., Sperling, R. A., Seimers, E., Sethuraman, G., Mohs, R., Farlow, M., Iwatsubo, T., Vellas, B., Sun, X., *et al.* (2015). Peripheral and central effects of gamma-secretase inhibition by semagacestat in Alzheimer's disease. *Alzheimers Res Ther* 7, 36.

Drachmann, N. D., Olesen, C., Moller, J. V., Guo, Z., Nissen, P., and Bubltz, M. (2014). Comparing crystal structures of Ca(2+) -ATPase in the presence of different lipids. *FEBS J* 281, 4249-4262.

Dubois, C., Vanden Abeele, F., Sehgal, P., Olesen, C., Junker, S., Christensen, S. B., Prevarskaya, N., and Moller, J. V. (2013). Differential effects of thapsigargin analogues on apoptosis of prostate cancer cells: complex regulation by intracellular calcium. *FEBS J* 280, 5430-5440.

Ellisen, L. W., Bird, J., West, D. C., Soreng, A. L., Reynolds, T. C., Smith, S. D., and Sklar, J. (1991). TAN-1, the human homolog of the Drosophila notch gene, is broken by chromosomal translocations in T lymphoblastic neoplasms. *Cell* 66, 649-661.

Emsley, P., and Cowtan, K. (2004). Coot: model-building tools for molecular graphics. *Acta Crystallogr D Biol Crystallogr* 60, 2126-2132.

Evans, P. R., and Murshudov, G. N. (2013). How good are my data and what is the resolution? *Acta Crystallogr D Biol Crystallogr* 69, 1204-1214.

Extance, A. (2010). Alzheimer's failure raises questions about disease-modifying strategies. *Nat Rev Drug Discov* 9, 749-751.

Follini, E., Marchesini, M., and Roti, G. (2019). Strategies to Overcome Resistance Mechanisms in T-Cell Acute Lymphoblastic Leukemia. *Int J Mol Sci* 20.

Golde, T. E., Koo, E. H., Felsenstein, K. M., Osborne, B. A., and Miele, L. (2013). gamma-Secretase inhibitors and modulators. *Biochim Biophys Acta* 1828, 2898-2907.

Groeneweg, J. W., DiGloria, C. M., Yuan, J., Richardson, W. S., Growdon, W. B., Sathyanarayanan, S., Foster, R., and Rueda, B. R. (2014). Inhibition of notch signaling in combination with Paclitaxel reduces platinum-resistant ovarian tumor growth. *Front Oncol* 4, 171.

Hauptman, P. J., and Kelly, R. A. (1999). Digitalis. *Circulation* 99, 1265-1270.

Hill, J. E., Myers, A. M., Koerner, T. J., and Tzagoloff, A. (1986). Yeast/E. coli shuttle vectors with multiple unique restriction sites. *Yeast* 2, 163-167.

Horn, M., Kroef, V., Allmeroth, K., Schuller, N., Miethe, S., Peifer, M., Penninger, J. M., Elling, U., and Denzel, M. S. (2018). Unbiased compound-protein interface mapping and prediction of chemoresistance loci through forward genetics in haploid stem cells. *Oncotarget* 9, 9838-9851.

Inamdar, A. A., Goy, A., Ayoub, N. M., Attia, C., Oton, L., Taruvai, V., Costales, M., Lin, Y. T., Pecora, A., and Suh, K. S. (2016). Mantle cell lymphoma in the era of precision medicine-diagnosis, biomarkers and therapeutic agents. *Oncotarget* 7, 48692-48731.

Kabsch, W. (2010). Xds. *Acta Crystallogr D Biol Crystallogr* 66, 125-132.

Kjellerup, L., Gordon, S., Cohrt, K. O., Brown, W. D., Fuglsang, A. T., and Winther, A. L. (2017). Identification of Antifungal H(+)-ATPase Inhibitors with Effect on Plasma Membrane Potential. *Antimicrob Agents Chemother* 61.

Klinakis, A., Lobry, C., Abdel-Wahab, O., Oh, P., Haeno, H., Buonamici, S., van De Walle, I., Cathelin, S., Trimarchi, T., Araldi, E., *et al.* (2011). A novel tumour-suppressor function for the Notch pathway in myeloid leukaemia. *Nature* 473, 230-233.

Klodos, I., Esmann, M., and Post, R. L. (2002). Large-scale preparation of sodium-potassium ATPase from kidney outer medulla. *Kidney Int* 62, 2097-2100.

Knoechel, B., Bhatt, A., Pan, L., Pedomallu, C. S., Severson, E., Gutierrez, A., Dorfman, D. M., Kuo, F. C., Kluk, M., Kung, A. L., *et al.* (2015). Complete hematologic response of early T-cell progenitor acute lymphoblastic leukemia to the gamma-secretase inhibitor BMS-906024: genetic and epigenetic findings in an outlier case. *Cold Spring Harb Mol Case Stud* 1, a000539.

Kopan, R., and Ilagan, M. X. (2009). The canonical Notch signaling pathway: unfolding the activation mechanism. *Cell* 137, 216-233.

Kridel, R., Meissner, B., Rogic, S., Boyle, M., Telenius, A., Woolcock, B., Gunawardana, J., Jenkins, C., Cochrane, C., Ben-Neriah, S., *et al.* (2012). Whole transcriptome sequencing reveals recurrent NOTCH1 mutations in mantle cell lymphoma. *Blood* 119, 1963-1971.

La Starza, R., Barba, G., Demeyer, S., Pierini, V., Di Giacomo, D., Gianfelici, V., Schwab, C., Matteucci, C., Vicente, C., Cools, J., *et al.* (2016). Deletions of the long arm of chromosome 5 define subgroups of T-cell acute lymphoblastic leukemia. *Haematologica* 101, 951-958.

La Starza, R., Borga, C., Barba, G., Pierini, V., Schwab, C., Matteucci, C., Lema Fernandez, A. G., Leszl, A., Cazzaniga, G., Chiaretti, S., *et al.* (2014). Genetic profile of T-cell acute lymphoblastic leukemias with MYC translocations. *Blood* 124, 3577-3582.

Lawrence, M. S., Stojanov, P., Mermel, C. H., Robinson, J. T., Garraway, L. A., Golub, T. R., Meyerson, M., Gabriel, S. B., Lander, E. S., and Getz, G. (2014). Discovery and saturation analysis of cancer genes across 21 tumour types. *Nature* 505, 495-501.

Le Borgne, R. (2006). Regulation of Notch signalling by endocytosis and endosomal sorting. *Curr Opin Cell Biol* 18, 213-222.

Ley, S. V., Antonello, A., Balskus, E. P., Booth, D. T., Christensen, S. B., Cleator, E., Gold, H., Hogenauer, K., Hunger, U., Myers, R. M., *et al.* (2004). Synthesis of the thapsigargins. *Proc Natl Acad Sci U S A* 101, 12073-12078.

Li, Z. H., Qiu, M. Z., Zeng, Z. L., Luo, H. Y., Wu, W. J., Wang, F., Wang, Z. Q., Zhang, D. S., Li, Y. H., and Xu, R. H. (2012). Copper-transporting P-type adenosine triphosphatase (ATP7A) is associated with platinum-resistance in non-small cell lung cancer (NSCLC). *J Transl Med* 10, 21.

Lipskaia, L., Chemaly, E. R., Hadri, L., Lompre, A. M., and Hajjar, R. J. (2010). Sarcoplasmic reticulum Ca(2+) ATPase as a therapeutic target for heart failure. *Expert Opin Biol Ther* 10, 29-41.

Litzow, M. R., and Ferrando, A. A. (2015). How I treat T-cell acute lymphoblastic leukemia in adults. *Blood* 126, 833-841.

Liu, M., and Dudley, S. C., Jr. (2015). Role for the Unfolded Protein Response in Heart Disease and Cardiac Arrhythmias. *Int J Mol Sci* 17.

Lobry, C., Oh, P., and Aifantis, I. (2011). Oncogenic and tumor suppressor functions of Notch in cancer: it's NOTCH what you think. *J Exp Med* 208, 1931-1935.

Loewe, S. (1953). The problem of synergism and antagonism of combined drugs. *Arzneimittelforschung* 3, 285-290.

Logeat, F., Bessia, C., Brou, C., LeBail, O., Jarriault, S., Seidah, N. G., and Israel, A. (1998). The Notch1 receptor is cleaved constitutively by a furin-like convertase. *Proc Natl Acad Sci U S A* 95, 8108-8112.

Lu, M., Lawrence, D. A., Marsters, S., Acosta-Alvear, D., Kimmig, P., Mendez, A. S., Paton, A. W., Paton, J. C., Walter, P., and Ashkenazi, A. (2014). Opposing unfolded-protein-response signals converge on death receptor 5 to control apoptosis. *Science* 345, 98-101.

Lytton, J., Westlin, M., and Hanley, M. R. (1991). Thapsigargin inhibits the sarcoplasmic or endoplasmic reticulum Ca-ATPase family of calcium pumps. *J Biol Chem* 266, 17067-17071.

Ma, Z., Fan, C., Yang, Y., Di, S., Hu, W., Li, T., Zhu, Y., Han, J., Xin, Z., Wu, G., *et al.* (2016). Thapsigargin sensitizes human esophageal cancer to TRAIL-induced apoptosis via AMPK activation. *Sci Rep* 6, 35196.

Mahalingam, D., Cetnar, J., Wilding, G., Denmeade, S., Sarantopoulos, J., Kurman, M., and Carducci, M. (2013). Abstract B244: A first-in-human phase 1 clinical study of G-202, a thapsigargin-based Prostate-Specific Membrane Antigen (PSMA) activated prodrug, in patients with advanced solid tumors. *Molecular Cancer Therapeutics* 12, B244.

Mahalingam, D., Wilding, G., Denmeade, S., Sarantopoulos, J., Cosgrove, D., Cetnar, J., Azad, N., Bruce, J., Kurman, M., Allgood, V. E., and Carducci, M. (2016). Mipsagargin, a novel thapsigargin-based PSMA-activated prodrug: results of a first-in-man phase I clinical trial in patients with refractory, advanced or metastatic solid tumours. *Br J Cancer* 114, 986-994.

Marks, D. I., and Rowntree, C. (2017). Management of adults with T-cell lymphoblastic leukemia. *Blood* 129, 1134-1142.

McCoy, A. J. (2007). Solving structures of protein complexes by molecular replacement with Phaser. *Acta Crystallogr D Biol Crystallogr* 63, 32-41.

Meraviglia, V., Bocchi, L., Sacchetto, R., Florio, M. C., Motta, B. M., Corti, C., Weichenberger, C. X., Savi, M., D'Elia, Y., Rosato-Siri, M. D., *et al.* (2018). HDAC Inhibition Improves the Sarcoendoplasmic Reticulum Ca(2+)-ATPase Activity in Cardiac Myocytes. *Int J Mol Sci* 19.

Minowada, J., Kohno, K., Matsuo, Y., Drexler, H. G., Ohnuma, T., Tax, W. J., and Brenner, M. B. (1989). Characteristics of 27 human T-cell leukemia cell lines with/without T-cell receptors of T3-Ti alpha beta or T3-Ti gamma delta complex. *Haematol Blood Transfus* 32, 233-236.

Mukherjee, N., Almeida, A., Partyka, K. A., Lu, Y., Schwan, J. V., Lambert, K., Rogers, M., Robinson, W. A., Robinson, S. E., Applegate, A. J., *et al.* (2016). Combining a GSI and BCL-2 inhibitor to overcome melanoma's resistance to current treatments. *Oncotarget* 7, 84594-84607.

Orrenius, S., Zhivotovsky, B., and Nicotera, P. (2003). Regulation of cell death: the calcium-apoptosis link. *Nat Rev Mol Cell Biol* 4, 552-565.

Palomero, T., Lim, W. K., Odom, D. T., Sulis, M. L., Real, P. J., Margolin, A., Barnes, K. C., O'Neil, J., Neuberg, D., Weng, A. P., *et al.* (2006). NOTCH1 directly regulates c-MYC and activates a feed-forward-loop transcriptional network promoting leukemic cell growth. *Proc Natl Acad Sci U S A* 103, 18261-18266.

Parekh, A. B., and Putney, J. W., Jr. (2005). Store-operated calcium channels. *Physiol Rev* 85, 757-810.

Penton, A. L., Leonard, L. D., and Spinner, N. B. (2012). Notch signaling in human development and disease. *Semin Cell Dev Biol* 23, 450-457.

Periasamy, M., Bhupathy, P., and Babu, G. J. (2008). Regulation of sarcoplasmic reticulum Ca<sup>2+</sup> ATPase pump expression and its relevance to cardiac muscle physiology and pathology. *Cardiovasc Res* 77, 265-273.

Puente, X. S., Pinyol, M., Quesada, V., Conde, L., Ordonez, G. R., Villamor, N., Escaramis, G., Jares, P., Bea, S., Gonzalez-Diaz, M., *et al.* (2011). Whole-genome sequencing identifies recurrent mutations in chronic lymphocytic leukaemia. *Nature* 475, 101-105.

Pui, J. C., Allman, D., Xu, L., DeRocco, S., Karnell, F. G., Bakkour, S., Lee, J. Y., Kadesch, T., Hardy, R. R., Aster, J. C., and Pear, W. S. (1999). Notch1 expression in early lymphopoiesis influences B versus T lineage determination. *Immunity* 11, 299-308.

Quynh Doan, N. T., and Christensen, S. B. (2015). Thapsigargin, Origin, Chemistry, Structure-Activity Relationships and Prodrug Development. *Curr Pharm Des* 21, 5501-5517.

Riccio, O., van Gijn, M. E., Bezdek, A. C., Pellegrinet, L., van Es, J. H., Zimmer-Strobl, U., Strobl, L. J., Honjo, T., Clevers, H., and Radtke, F. (2008). Loss of intestinal crypt progenitor cells owing to inactivation of both Notch1 and Notch2 is accompanied by derepression of CDK inhibitors p27Kip1 and p57Kip2. *EMBO Rep* 9, 377-383.

Roti, G., Carlton, A., Ross, K. N., Markstein, M., Pajcini, K., Su, A. H., Perrimon, N., Pear, W. S., Kung, A. L., Blacklow, S. C., *et al.* (2013). Complementary genomic screens identify SERCA as a therapeutic target in NOTCH1 mutated cancer. *Cancer Cell* 23, 390-405.

Roti, G., Qi, J., Kitara, S., Sanchez-Martin, M., Saur Conway, A., Varca, A. C., Su, A., Wu, L., Kung, A. L., Ferrando, A. A., *et al.* (2017). Leukemia-specific delivery of mutant NOTCH1 targeted therapy. *J Exp Med*.

Roti, G., and Stegmaier, K. (2011). Targeting NOTCH1 in hematopoietic malignancy. *Crit Rev Oncog* 16, 103-115.

Roti, G., and Stegmaier, K. (2014). New Approaches to Target T-ALL. *Front Oncol* 4, 170.

Roy, M., Pear, W. S., and Aster, J. C. (2007). The multifaceted role of Notch in cancer. *Curr Opin Genet Dev* 17, 52-59.

Sachs, G. (1997). Proton pump inhibitors and acid-related diseases. *Pharmacotherapy* 17, 22-37.

Samimi, G., Safaei, R., Katano, K., Holzer, A. K., Rochdi, M., Tomioka, M., Goodman, M., and Howell, S. B. (2004). Increased expression of the copper efflux transporter ATP7A mediates resistance to cisplatin, carboplatin, and oxaliplatin in ovarian cancer cells. *Clin Cancer Res* 10, 4661-4669.

Savi, M., Bocchi, L., Mena, P., Dall'Asta, M., Crozier, A., Brighenti, F., Stilli, D., and Del Rio, D. (2017). In vivo administration of urolithin A and B prevents the occurrence of cardiac dysfunction in streptozotocin-induced diabetic rats. *Cardiovascular Diabetology* 16.

Schmitz, R., Wright, G. W., Huang, D. W., Johnson, C. A., Phelan, J. D., Wang, J. Q., Roulland, S., Kasbekar, M., Young, R. M., Shaffer, A. L., *et al.* (2018). Genetics and Pathogenesis of Diffuse Large B-Cell Lymphoma. *N Engl J Med* 378, 1396-1407.

Schott, A. F., Landis, M. D., Dontu, G., Griffith, K. A., Layman, R. M., Krop, I., Paskett, L. A., Wong, H., Dobrolecki, L. E., Lewis, M. T., *et al.* (2013). Preclinical and clinical studies of gamma secretase inhibitors with docetaxel on human breast tumors. *Clin Cancer Res* 19, 1512-1524.

Sehgal, P., Szalai, P., Olesen, C., Praetorius, H. A., Nissen, P., Christensen, S. B., Engedal, N., and Moller, J. V. (2017). Inhibition of the sarco/endoplasmic reticulum (ER) Ca(2+)-ATPase by thapsigargin analogs induces cell death via ER Ca(2+) depletion and the unfolded protein response. *J Biol Chem* 292, 19656-19673.



Seto-Young, D., Monk, B., Mason, A. B., and Perlin, D. S. (1997). Exploring an antifungal target in the plasma membrane H(+)-ATPase of fungi. *Biochim Biophys Acta* 1326, 249-256.

Sharma, A., Gadkari, R. A., Ramakanth, S. V., Padmanabhan, K., Madhumathi, D. S., Devi, L., Appaji, L., Aster, J. C., Rangarajan, A., and Dighe, R. R. (2015). A novel Monoclonal Antibody against Notch1 Targets Leukemia-associated Mutant Notch1 and Depletes Therapy Resistant Cancer Stem Cells in Solid Tumors. *Sci Rep* 5, 11012.

Sorrentino, C., Cuneo, A., and Roti, G. (2019). Therapeutic Targeting of Notch Signaling Pathway in Hematological Malignancies. *Mediterr J Hematol Infect Dis* 11, e2019037.

Sovolyova, N., Healy, S., Samali, A., and Logue, S. E. (2014). Stressed to death - mechanisms of ER stress-induced cell death. *Biol Chem* 395, 1-13.

Starza, R. L., Cambò, B., Pierini, A., Bornhauser, B., Montanaro, A., Bourquin, J.-P., Mecucci, C., and Roti, G. (2019). Venetoclax and Bortezomib in Relapsed/Refractory Early T-Cell Precursor Acute Lymphoblastic Leukemia. *JCO Precision Oncology*, 1-6.

Stransky, N., Egloff, A. M., Tward, A. D., Kostic, A. D., Cibulskis, K., Sivachenko, A., Kryukov, G. V., Lawrence, M. S., Sougnez, C., McKenna, A., *et al.* (2011). The mutational landscape of head and neck squamous cell carcinoma. *Science* 333, 1157-1160.

Szalai, P., Parys, J. B., Bultynck, G., Christensen, S. B., Nissen, P., Møller, J. V., and Engedal, N. (2018). Nonlinear relationship between ER Ca(2+) depletion versus induction of the unfolded protein response, autophagy inhibition, and cell death. *Cell Calcium* 76, 48-61.

Tadini-Buoninsegni, F., Sordi, G., Smeazzetto, S., Natile, G., and Arnesano, F. (2017). Effect of cisplatin on the transport activity of P11-type ATPases. *Metallomics* 9, 960-968.

Treiman, M., Caspersen, C., and Christensen, S. B. (1998). A tool coming of age: thapsigargin as an inhibitor of sarco-endoplasmic reticulum Ca(2+)-ATPases. *Trends Pharmacol Sci* 19, 131-135.

Twarog, N. R., Stewart, E., Hammill, C. V., and Shelat, A. A. (2016). BRAID: A Unifying Paradigm for the Analysis of Combined Drug Action. *Sci Rep* 6, 25523.

Twarog, N. R., Stewart, E., Hammill, C. V., and Shelat, A. A. (2018). Erratum: BRAID: A Unifying Paradigm for the Analysis of Combined Drug Action. *Sci Rep* 8, 46970.

van Es, J. H., van Gijn, M. E., Riccio, O., van den Born, M., Vooijs, M., Begthel, H., Cozijnsen, M., Robine, S., Winton, D. J., Radtke, F., and Clevers, H. (2005). Notch/gamma-secretase inhibition turns proliferative cells in intestinal crypts and adenomas into goblet cells. *Nature* 435, 959-963.

Wang, K., Li, M., and Hakonarson, H. (2010). ANNOVAR: functional annotation of genetic variants from high-throughput sequencing data. *Nucleic Acids Res* 38, e164.

Wang, M., and Kaufman, R. J. (2014). The impact of the endoplasmic reticulum protein-folding environment on cancer development. *Nat Rev Cancer* 14, 581-597.

Wang, Z., Da Silva, T. G., Jin, K., Han, X., Ranganathan, P., Zhu, X., Sanchez-Mejias, A., Bai, F., Li, B., Fei, D. L., *et al.* (2014). Notch signaling drives stemness and tumorigenicity of esophageal adenocarcinoma. *Cancer Res* 74, 6364-6374.

Weng, A. P., Ferrando, A. A., Lee, W., Morris, J. P. t., Silverman, L. B., Sanchez-Irizarry, C., Blacklow, S. C., Look, A. T., and Aster, J. C. (2004). Activating mutations of NOTCH1 in human T cell acute lymphoblastic leukemia. *Science* 306, 269-271.

Wilken, R., Veena, M. S., Wang, M. B., and Srivatsan, E. S. (2011). Curcumin: A review of anti-cancer properties and therapeutic activity in head and neck squamous cell carcinoma. *Mol Cancer* 10, 12.

Winther, A. M., Bubltz, M., Karlsen, J. L., Møller, J. V., Hansen, J. B., Nissen, P., and Buch-Pedersen, M. J. (2013). The sarcolipin-bound calcium pump stabilizes calcium sites exposed to the cytoplasm. *Nature* 495, 265-269.

Yano, M., Ikeda, Y., and Matsuzaki, M. (2005). Altered intracellular Ca<sup>2+</sup> handling in heart failure. *J Clin Invest* 115, 556-564.

Yatime, L., Buch-Pedersen, M. J., Musgaard, M., Morth, J. P., Lund Winther, A. M., Pedersen, B. P., Olesen, C., Andersen, J. P., Vilsen, B., Schiott, B., *et al.* (2009). P-type ATPases as drug targets: tools for medicine and science. *Biochim Biophys Acta* 1787, 207-220.

Yu, M., Lin, J., Khadeer, M., Yeh, Y., Inesi, G., and Hussain, A. (1999). Effects of various amino acid 256 mutations on sarcoplasmic/endoplasmic reticulum Ca<sup>2+</sup> ATPase function and their role in the cellular adaptive response to thapsigargin. *Arch Biochem Biophys* 362, 225-232.

Yu, M., Zhong, L., Rishi, A. K., Khadeer, M., Inesi, G., and Hussain, A. (1998). Specific substitutions at amino acid 256 of the sarcoplasmic/endoplasmic reticulum Ca<sup>2+</sup> transport ATPase mediate resistance to thapsigargin in thapsigargin-resistant hamster cells. *J Biol Chem* 273, 3542-3546.

Yuan, X., Wu, H., Xu, H., Xiong, H., Chu, Q., Yu, S., Wu, G. S., and Wu, K. (2015). Notch signaling: an emerging therapeutic target for cancer treatment. *Cancer Lett* 369, 20-27.

Zhong, L., and Inesi, G. (1998). Role of the S3 stalk segment in the thapsigargin concentration dependence of sarco-endoplasmic reticulum Ca<sup>2+</sup> ATPase inhibition. *J Biol Chem* 273, 12994-12998.

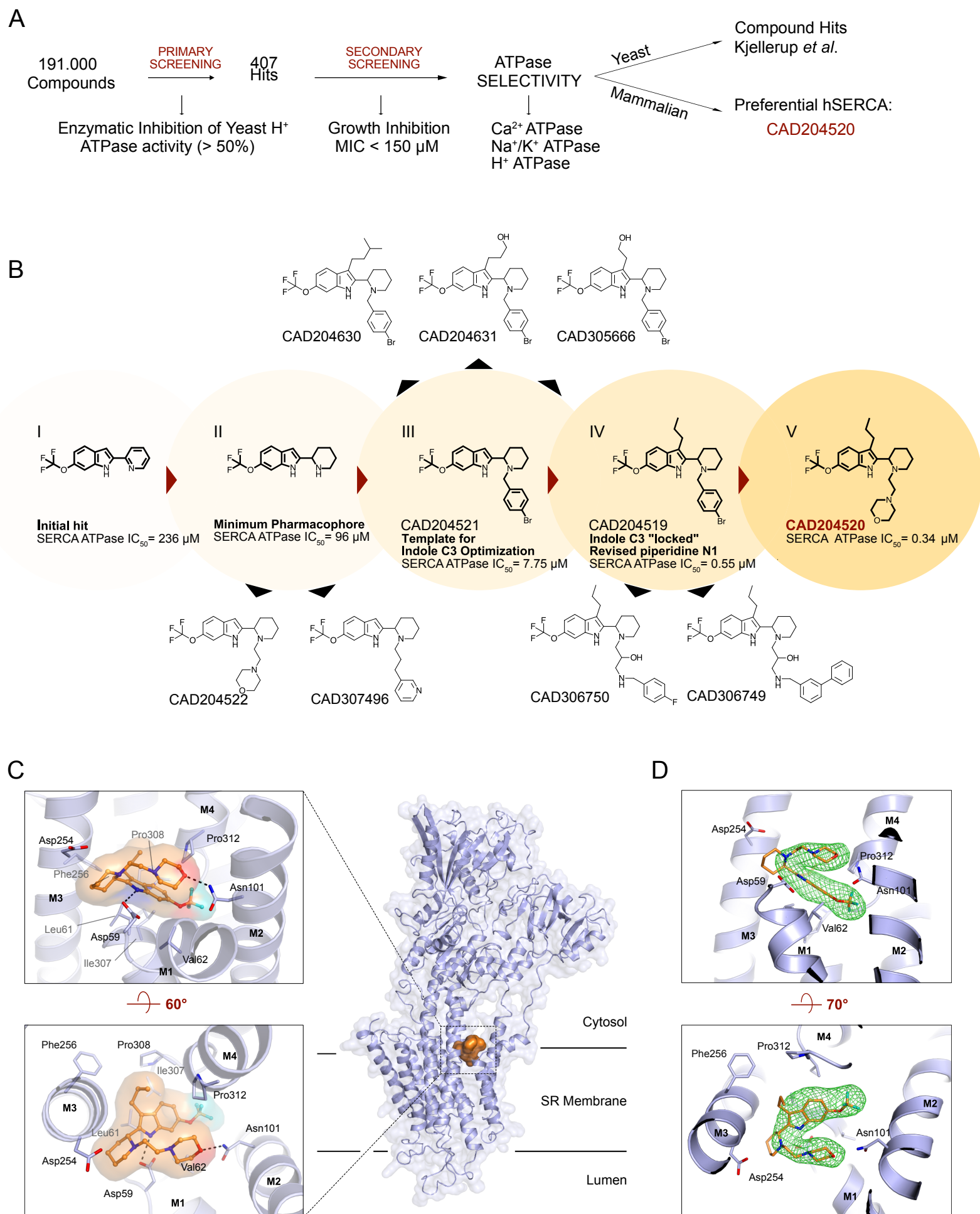


Figure 1

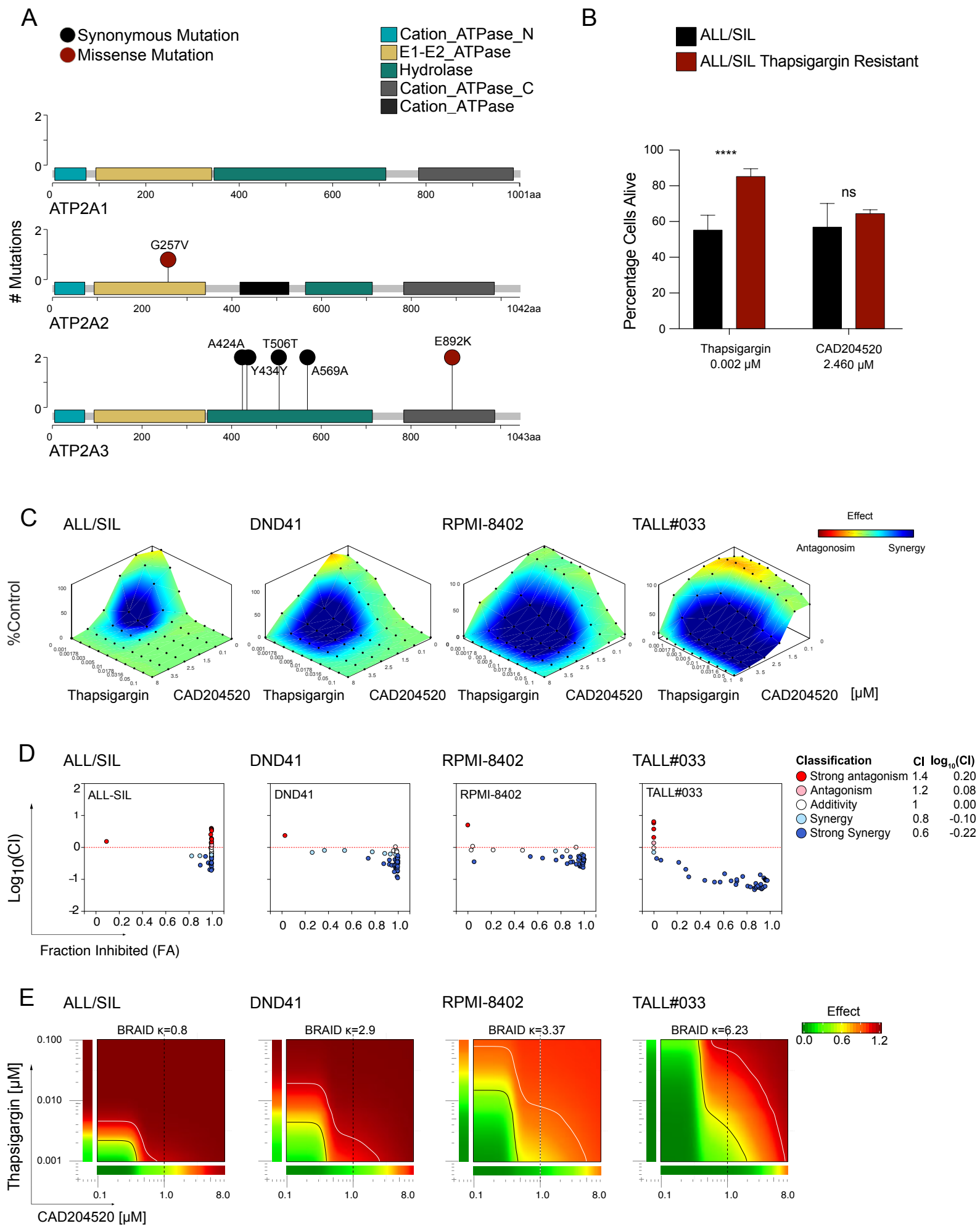


Figure 2

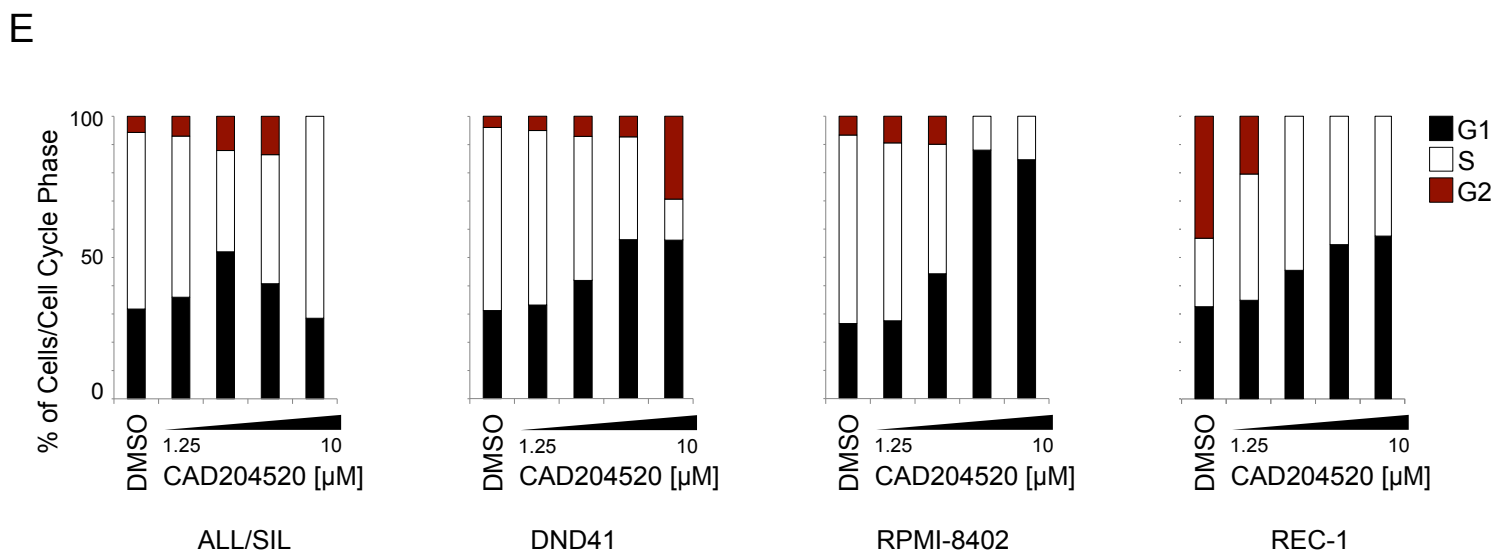
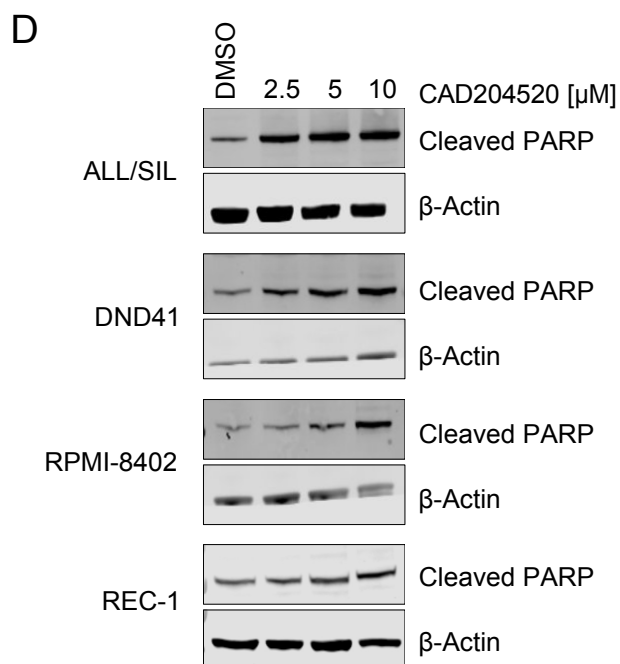
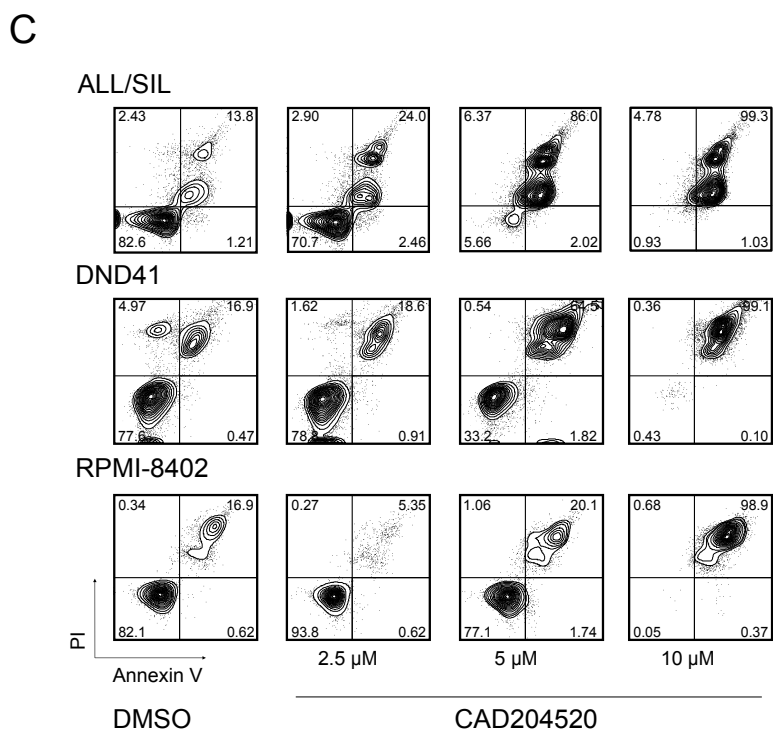
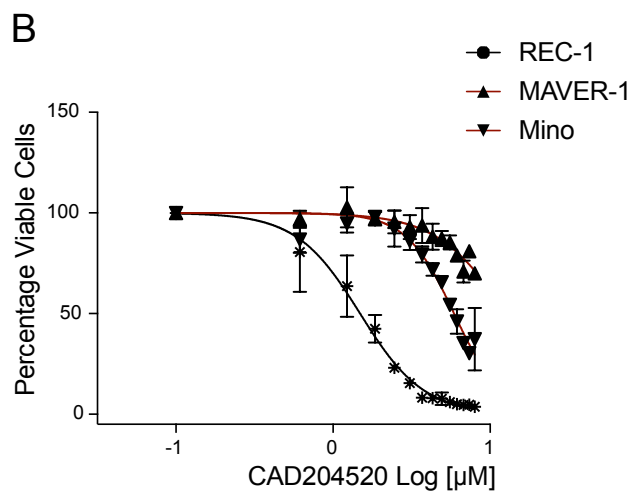
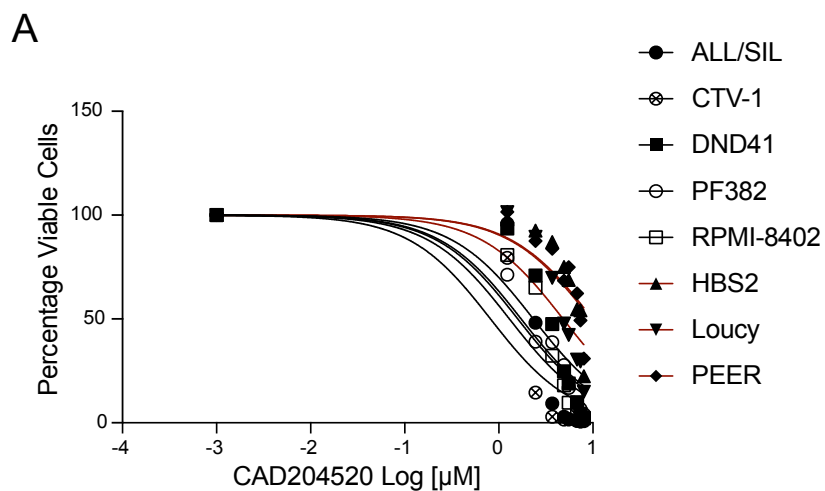


Figure 3

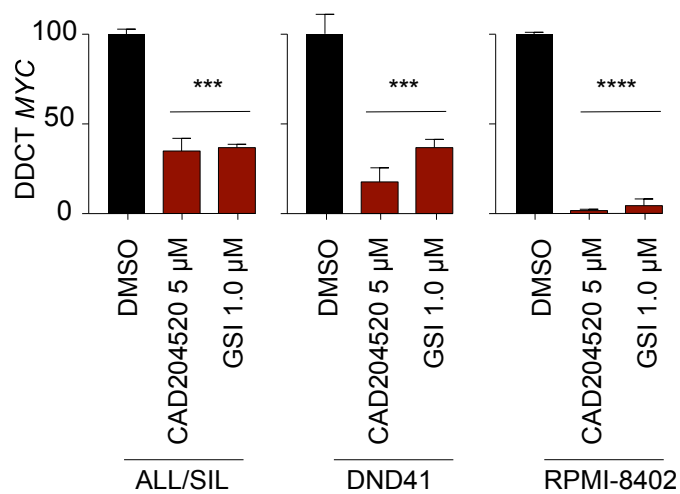
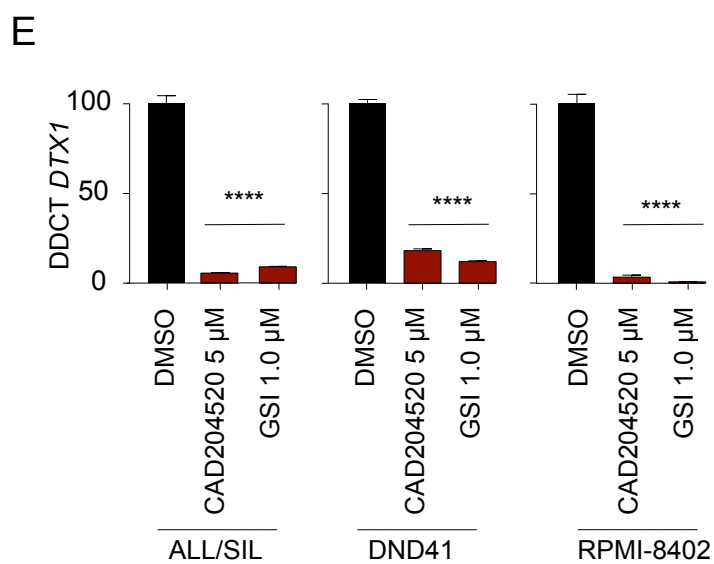
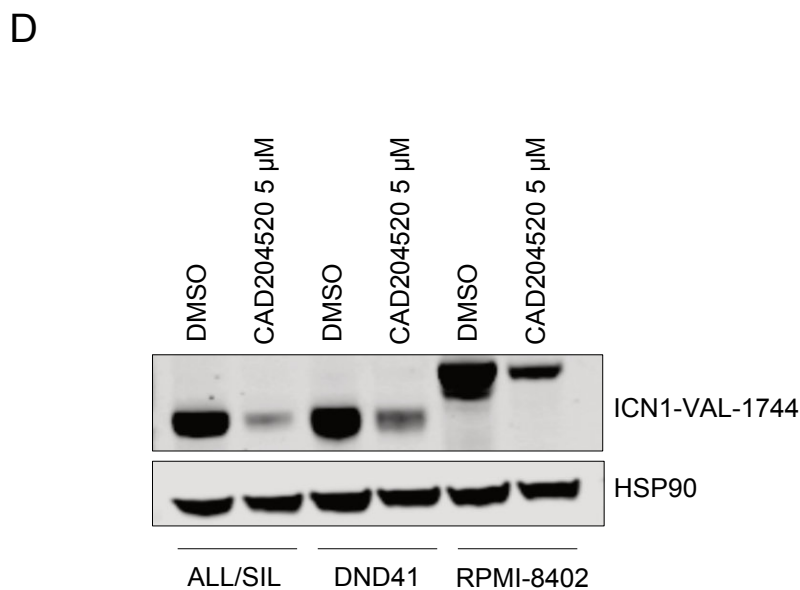
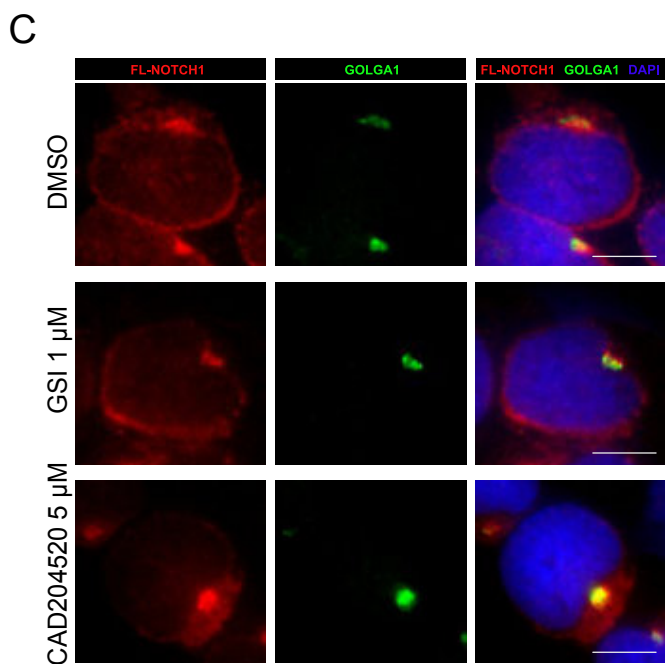
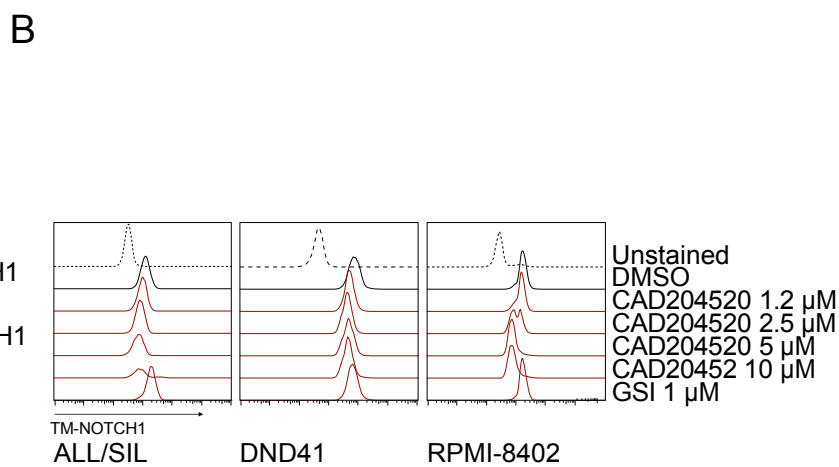
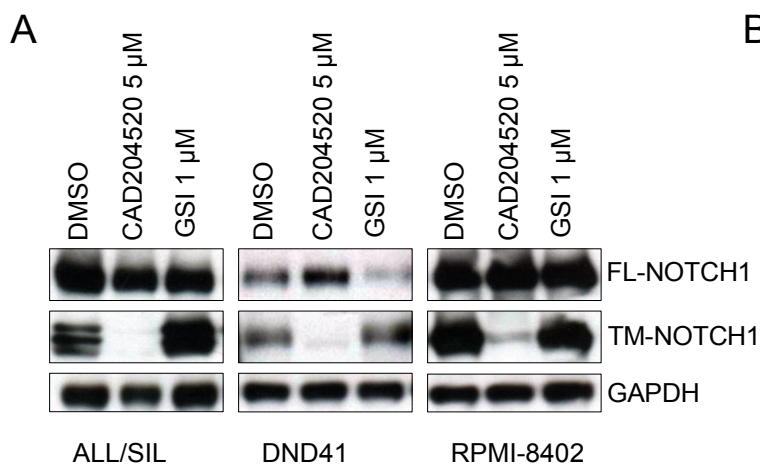
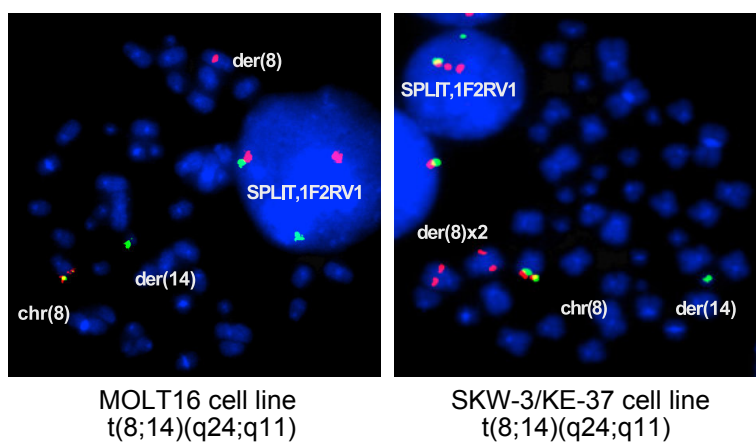
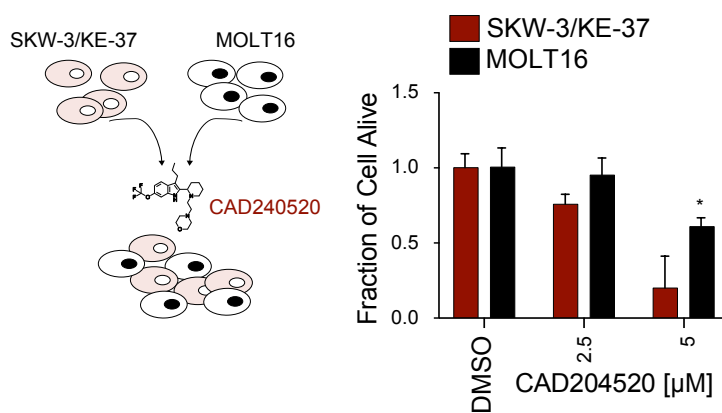


Figure 4

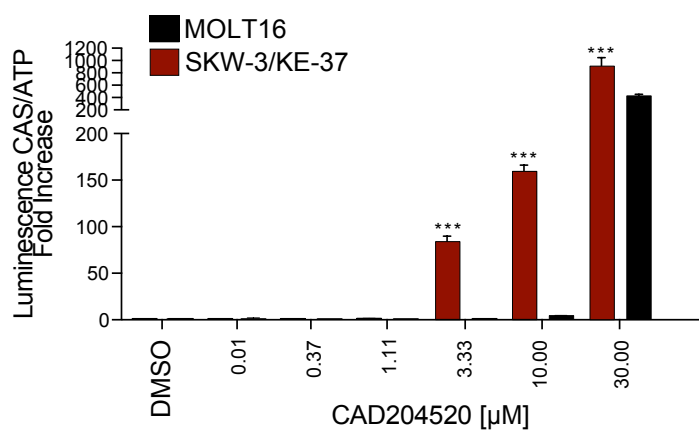
A



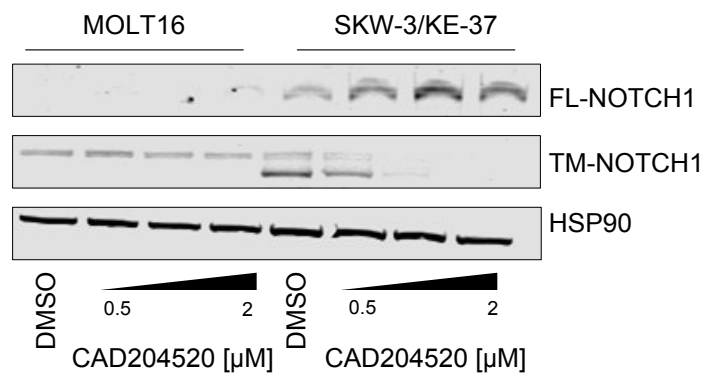
B



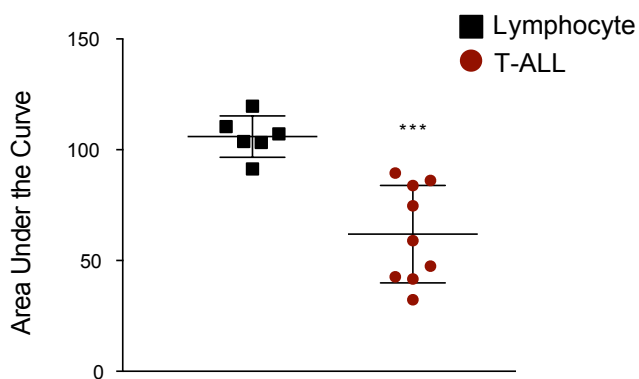
C



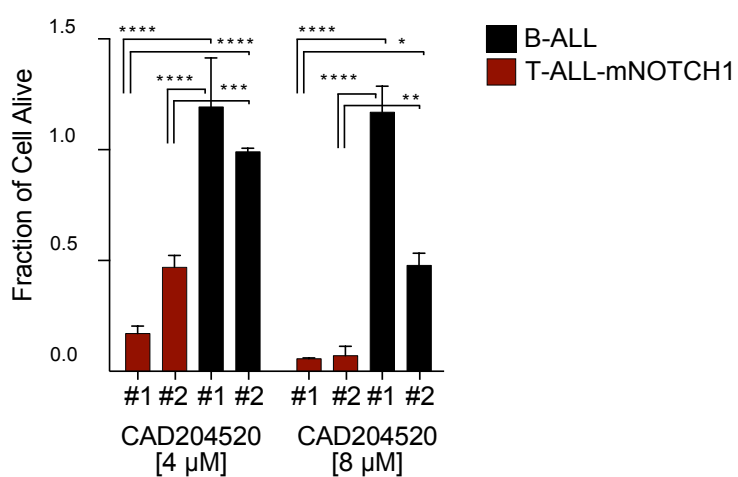
D



E



F





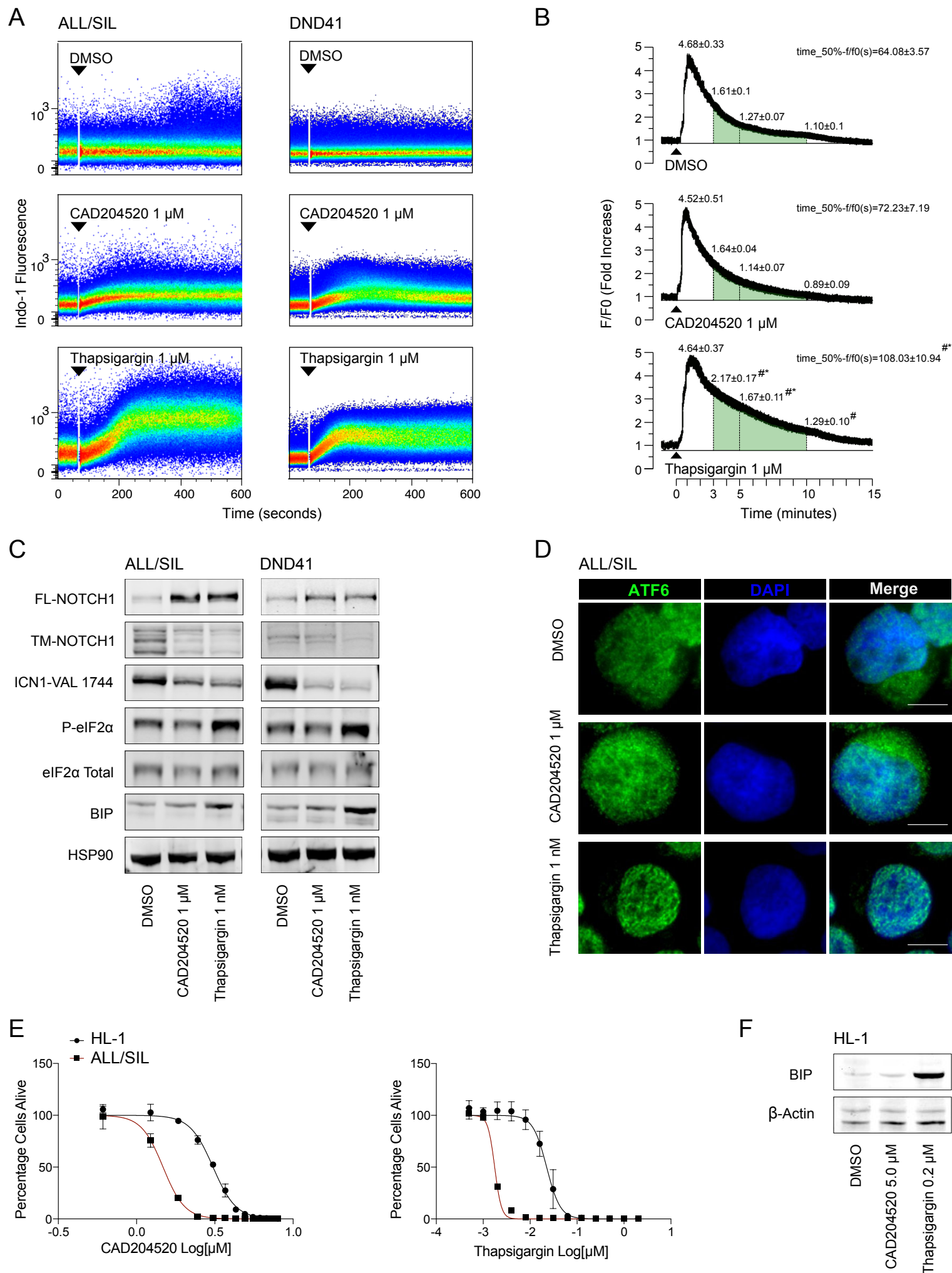


Figure 6



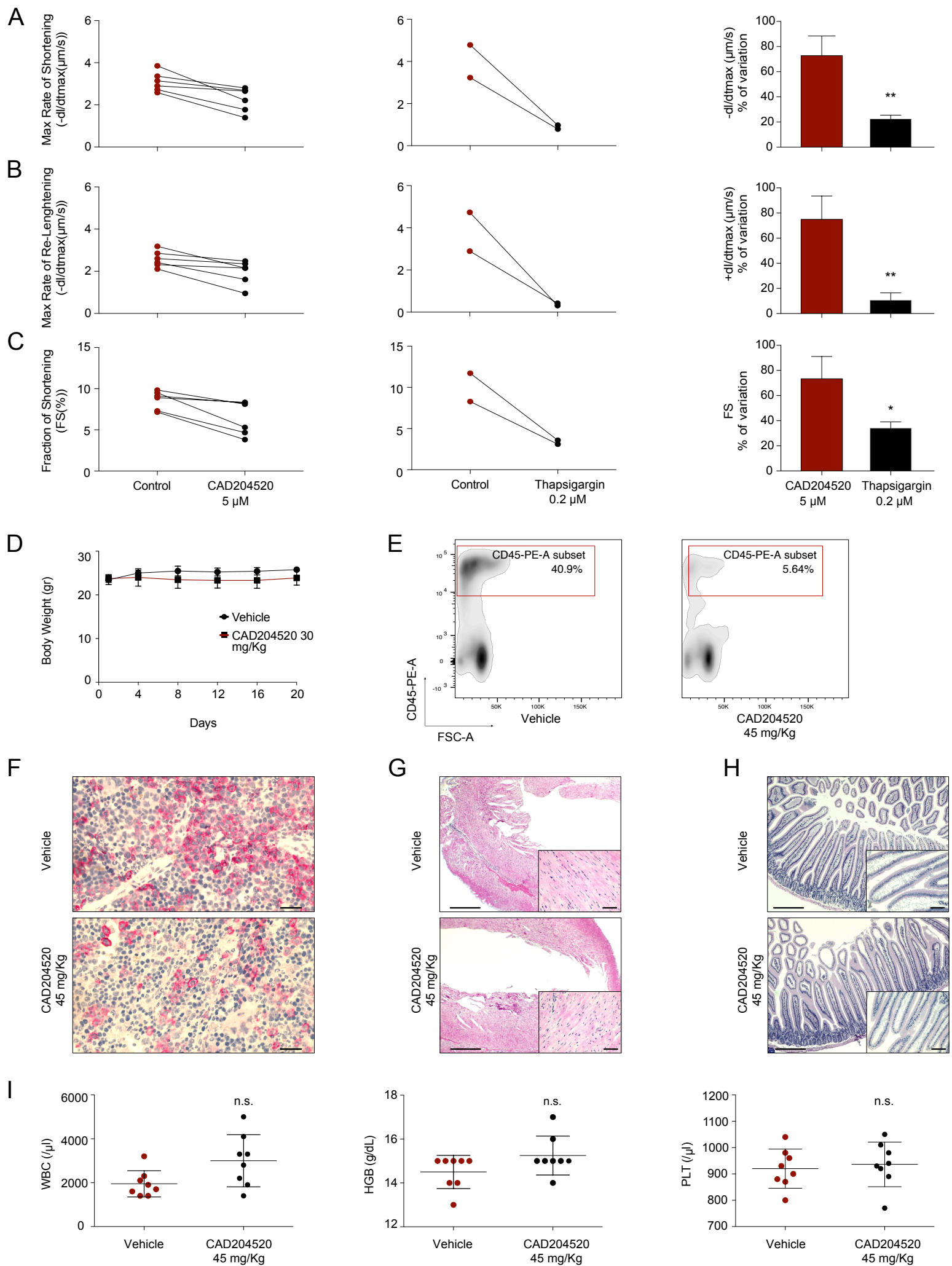


Figure 7

## KEY RESOURCES TABLE

The table highlights the genetically modified organisms and strains, cell lines, reagents, software, and source data **essential** to reproduce results presented in the manuscript. Depending on the nature of the study, this may include standard laboratory materials (i.e., food chow for metabolism studies), but the Table is **not** meant to be comprehensive list of all materials and resources used (e.g., essential chemicals such as SDS, sucrose, or standard culture media don't need to be listed in the Table). **Items in the Table must also be reported in the Method Details section within the context of their use.** The number of **primers and RNA sequences** that may be listed in the Table is restricted to no more than ten each. If there are more than ten primers or RNA sequences to report, please provide this information as a supplementary document and reference this file (e.g., See Table S1 for XX) in the Key Resources Table.

**Please note that ALL references cited in the Key Resources Table must be included in the References list.** Please report the information as follows:

- **REAGENT or RESOURCE:** Provide full descriptive name of the item so that it can be identified and linked with its description in the manuscript (e.g., provide version number for software, host source for antibody, strain name). In the Experimental Models section, please include all models used in the paper and describe each line/strain as: model organism: name used for strain/line in paper: genotype. (i.e., Mouse: OXTR<sup>fl/fl</sup>; B6.129(SJL)-Oxtr<sup>tm1.1Wsy/J</sup>). In the Biological Samples section, please list all samples obtained from commercial sources or biological repositories. Please note that software mentioned in the Methods Details or Data and Software Availability section needs to be also included in the table. See the sample Table at the end of this document for examples of how to report reagents.
- **SOURCE:** Report the company, manufacturer, or individual that provided the item or where the item can be obtained (e.g., stock center or repository). For materials distributed by Addgene, please cite the article describing the plasmid and include "Addgene" as part of the identifier. If an item is from another lab, please include the name of the principal investigator and a citation if it has been previously published. If the material is being reported for the first time in the current paper, please indicate as "this paper." For software, please provide the company name if it is commercially available or cite the paper in which it has been initially described.
- **IDENTIFIER:** Include catalog numbers (entered in the column as "Cat#" followed by the number, e.g., Cat#3879S). Where available, please include unique entities such as [RRIDs](#), Model Organism Database numbers, accession numbers, and PDB or CAS IDs. For antibodies, if applicable and available, please also include the lot number or clone identity. For software or data resources, please include the URL where the resource can be downloaded. Please ensure accuracy of the identifiers, as they are essential for generation of hyperlinks to external sources when available. Please see the Elsevier [list of Data Repositories](#) with automated bidirectional linking for details. When listing more than one identifier for the same item, use semicolons to separate them (e.g. Cat#3879S; RRID: AB\_2255011). If an identifier is not available, please enter "N/A" in the column.
  - **A NOTE ABOUT RRIDs:** We highly recommend using RRIDs as the identifier (in particular for antibodies and organisms, but also for software tools and databases). For more details on how to obtain or generate an RRID for existing or newly generated resources, please [visit the RII](#) or [search for RRIDs](#).

Please use the empty table that follows to organize the information in the sections defined by the subheading, skipping sections not relevant to your study. Please do not add subheadings. To add a row, place the cursor at the end of the row above where you would like to add the row, just outside the right border of the table. Then press the ENTER key to add the row. Please delete empty rows. Each entry must be on a separate row; do not list multiple items in a single table cell. Please see the sample table at the end of this document for examples of how reagents should be cited.

REAGENT or RESOURCE	SOURCE	IDENTIFIER
<b>Antibodies</b>		
Rabbit monoclonal anti-Cleaved NOTCH1 (Val1744) (D3B8)	Cell Signaling	Cat# 4147; RRID: AB_2153348
Rabbit polyclonal anti-Cleaved NOTCH1 (Val1744)	Cell Signaling	Cat# 2421; RRID: AB_2314204
Goat polyclonal anti-NOTCH1 (C20)	Santa Cruz	Cat# sc-6014; RRID: AB_650336
Mouse monoclonal anti-NOTCH1	R&D Systems	Cat# FAB5317P; RRID: AB_1602927
Mouse monoclonal anti-NOTCH1 (A6)	Abcam	Cat# ab44986; RRID: AB_776840
Rabbit polyclonal anti-Cleaved PARP (Asp214)	Cell Signaling	Cat# 9541; RRID: AB_331427
Mouse monoclonal anti- $\beta$ -Actin (8H10D10)	Cell Signaling	Cat# 3700; RRID: AB_2242334
Mouse monoclonal anti-GADPH (A3)	Santa Cruz	Cat# sc-137179; RRID: AB_2232048
Mouse monoclonal anti-HSP90 (4F-10)	Santa Cruz	Cat# sc-69703; RRID: AB_2121191
Rabbit monoclonal anti-SERCA2 (D51B11)	Cell Signaling	Cat# 9580
Mouse monoclonal anti-SERCA3 (PL/IM430)	Santa Cruz	Cat# sc-81759; RRID: AB_1129372
Rabbit monoclonal anti-BIP (C50B12)	Cell Signaling	Cat# 3177; RRID: AB_2119845
Rabbit polyclonal anti-phospho eIF2 $\alpha$ (Ser51)	Cell Signaling	Cat# 9721; RRID: AB_330951
Rabbit polyclonal anti-eIF2 $\alpha$	Cell Signaling	Cat# 9722; RRID: AB_2230924
Mouse polyclonal anti-GOLGA1	Sigma-Aldrich	Cat# SAB1409131
Rabbit polyclonal anti-ATF6	Abcam	Cat# ab37149; RRID: AB_725571
Mouse monoclonal anti-human CD45 PE(HI30)	BD Biosciences	Cat# 560975; RRID: AB_2033960
Mouse monoclonal anti-human CD45 leucocyte common antigen (2B11+PD7/26)	Agilent	Cat# IS75130; RRID: AB_2661839
Goat polyclonal anti-Mouse IgG IRDye 680LT	LI-COR	Cat# 925-68020; RRID: AB_2687826
Goat polyclonal anti-Rabbit IgG IRDye 800CW	LI-COR	Cat# 925-32211; RRID: AB_2651127
Goat polyclonal anti-Rabbit IgG IRDye 680RD	LI-COR	Cat# 925-68071; RRID: AB_2721181
Goat polyclonal anti-Mouse IgG Alexa Fluor 488	Invitrogen	Cat# A-11029; RRID: AB_138404
Goat polyclonal anti-Rabbit IgG Alexa Fluor 568	Invitrogen	Cat# A-11036; RRID: AB_143011
<b>Bacterial and Virus Strains</b>		
pCMV-VSV-G packaging vector	Addgene	Cat# 8454; RRID: Addgene_8454
pCMV-delta R8.91	Laboratory of Kimberley Stegmaier (DFCI/Broad)	N/A
pXPR-011 expressing vector	Addgene	Cat# 59702; RRID: Addgene_59702

Biological Samples		
Primary samples	This paper	Parma and Perugia University Hospitals
Chemicals, Peptides, and Recombinant Proteins		
Rabbit sarcoplasmic reticulum membranes	Andersen et al., 1985	N/A
Tris	Sigma-Aldrich	Cat# 252859
MOPS	Sigma-Aldrich	Cat# M1254
KCl	Sigma-Aldrich	Cat# P3911
MgCl <sub>2</sub>	Sigma-Aldrich	Cat# 208377
MgSO <sub>4</sub>	Sigma-Aldrich	Cat# 746452
CaCl <sub>2</sub>	Sigma-Aldrich	Cat# C1016
NaOH	Sigma-Aldrich	Cat# S8045
NaCl	Sigma-Aldrich	Cat# S9888
NaN <sub>3</sub>	Sigma-Aldrich	Cat# 71289
Na <sub>2</sub> MoO <sub>4</sub>	Sigma-Aldrich	Cat# 243655
NaAsO <sub>2</sub>	Sigma-Aldrich	Cat# S7400
NaH <sub>2</sub> PO <sub>4</sub>	Sigma-Aldrich	Cat# S3139
NaHCO <sub>3</sub>	Sigma-Aldrich	Cat# S6014
Sodium citrate dihydrate	Sigma-Aldrich	Cat# W302600
Sodium DOC	Sigma-Aldrich	Cat# D6750
Sodium pyruvate	Sigma-Aldrich	Cat# P8574
KNO <sub>3</sub>	Sigma-Aldrich	Cat# P8394
K <sub>2</sub> CO <sub>3</sub>	Sigma-Aldrich	Cat# P5833
PtO <sub>2</sub>	Sigma-Aldrich	Cat# 206032
2-bromopyridine	Sigma-Aldrich	Cat# B80100
EGTA	Sigma-Aldrich	Cat# E3889
HEPES	Sigma-Aldrich	Cat# 54457
Glycerol	Sigma-Aldrich	Cat# G7893
TNP-ATP	Sigma-Aldrich	Cat# SLM07040
C12E8	Sigma-Aldrich	Cat# P8925
PEG	Sigma-Aldrich	Cat# 8074911000
MPD	Sigma-Aldrich	Cat# 112100
DMF	Sigma-Aldrich	Cat# 227056
Ammonium heptamolybdate tetrahydrate	Sigma-Aldrich	Cat# 431346
Glacial acetic acid	Merk	Cat# 1005706
L-Ascorbic acid	Sigma-Aldrich	Cat# A5960
Dextrose	Sigma-Aldrich	Cat# D8066
Triton X-100	Sigma-Aldrich	Cat# T9284
Tween-80	Sigma-Aldrich	Cat# P1754
Taurine	Sigma-Aldrich	Cat# T0625
CuI	Sigma-Aldrich	Cat# 03140
Creatine	Sigma-Aldrich	Cat# C0780
Collagenase type II	Worthington Biochemical	Cat# LS004194
Protease type XIV	Sigma-Aldrich	Cat# P5147
DCM	Sigma-Aldrich	Cat# 4104976
DIPEA	Sigma-Aldrich	Cat# 03439
Ethanol	Sigma-Aldrich	Cat# 443611

Ethyl acetate	Sigma-Aldrich	Cat# 270989
Methanol	Sigma-Aldrich	Cat# 34860
CH <sub>3</sub> CN	Sigma-Aldrich	Cat# L010010
Dichloromethane	Supelco	Cat# DX0831
Triethylamine	Sigma-Aldrich	Cat# 90335
Paraformaldehyde 4%	ThermoFisher Scientific	Cat# 28908
Diethyl ether	Supelco	Cat# 1070625000
NMP	Sigma-Aldrich	Cat# 238634
MDAP	Sigma-Aldrich	Cat# 03439
Sarco/Endoplasmatic reticulum (SR) membranes	Claus E. Olesen and Jesper V. Møller, Aarhus University	N/A
Pig kidney Na <sup>+</sup> , K <sup>+</sup> -ATPase	Natalya Fedosova, Aarhus University	N/A
Fetal bovine serum (FBS)	ThermoFisher Scientific	Cat# MT10270-106
RPMI 1640	ThermoFisher Scientific	Cat# MT10040CV
Dulbecco's modified eagle medium (DMEM)	ThermoFisher Scientific	Cat# 11965-084
Claycomb medium	Sigma-Aldrich	Cat# 51800C
Penicillin-streptomycin	ThermoFisher Scientific	Cat# 3MT30002CI
L-Glutamine	ThermoFisher Scientific	Cat# 25030081
Norepinephrine [(±)- Arterenol]	Sigma-Aldrich	Cat# A0937
L-Ascorbic acid	Sigma-Aldrich	Cat# A7506
Gelatine from bovine skin	Sigma-Aldrich	Cat# G9391
Fibronectin bovine plasma	Sigma-Aldrich	Cat# F1141
DMSO	Sigma-Aldrich	Cat# 276855
Hydroxypropyl-methylcellulose (HPMC)	Shin-Etsu Chemical Co	Cat# SR-44439
Hematoxylin	Sigma-Aldrich	Cat# H3136
Eosin Y dye	Sigma-Aldrich	Cat# E4009
DAPT	Selleckchem	Cat# S2215
Thapsigargin	Enzo Biochem, Inc.	Cat# BML-PE180-0005
CAD204520	CaDo Biotechnology lvs	N/A
DAPI	Sigma-Aldrich	Cat# D9542
FLUO3 AM	Invitrogen	Cat# F1241
Propidium iodide	Sigma-Aldrich	Cat# P4170
Indo1 AM	ThermoFisher Scientific	Cat# 1223
Critical Commercial Assays		
ATP-lite assay	PerkinElmer	Cat# 6016943
DC protein assay kit	Bio-Rad	Cat# 5000111
CellTiter-Glo ATP assay	Promega Corporation	Cat# G7573
Annexin V Apoptosis Detection Kit APC	eBioscience	Cat# 88-8007-74
LIVE/DEAD Fixable Far Red Dead Cell Stain	Invitrogen	Cat# L34973

Promega Maxwell® kit	Promega Corporation	Cat# AS1010
Agilent SureSelect Human all exon kit	Agilent Technologies	N/A
AMPure XP system	Beckman Coulter	N/A
Agilent high sensitivity DNA assay	Agilent Technologies	N/A
FuGENE 6 protocol	Promega Corporation	Cat# E2691
Deposited Data		
SERCA-Tg complex, molecular replacement model	Drachmann <i>et al.</i> , 2014	PDB: 4UU0
SERCA-CAD204520 complex structure	This study	PDB: 6YAA
Experimental Models: Cell Lines		
DND-41	DMSZ	Cat# ACC-525; RRID: CVCL_2022
MOLT16	DMSZ	Cat# ACC-29; RRID: CVCL_1424
REC-1	DMSZ	Cat# ACC-584; RRID: CVCL_1884
Mino	DMSZ	Cat# ACC-687; RRID: CVCL_1872
PF382	DMSZ	Cat# ACC-38; RRID: CVCL_1641
RPMI-8402	DMSZ	Cat# ACC-290; RRID: CVCL_1667
SKW-3/KE-37	DMSZ	Cat# ACC-53; RRID: CVCL_2197
CTV-1	DMSZ	Cat# ACC-40; RRID: CVCL_1150
Loucy	DMSZ	Cat# ACC-394; RRID: CVCL_1380
PEER	DMSZ	Cat# ACC-6; RRID: CVCL_1913
HSB2 (CCRF-HSB-2)	DMSZ	Cat# ACC-435; RRID: CVCL_1859
ALL/SIL	Laboratory of Kimberley Stegmaier (DFCI/Broad)	N/A
ALL/SIL thapsigargin resistant	This paper	University of Parma
MAVER-1	Laboratory of Elena Muraro (C.R.O., National Cancer Institute, Aviano, Italy)	N/A
293T (HEK293T)	DMSZ	Cat# ACC-635; RRID: CVCL_0063
HL-1	Laboratory of Michele Miragoli (University of Parma, Parma, Italy)	N/A
Experimental Models: Organisms/Strains		
Mouse: Crl: CD1(ICR) Mus Musculus	Aurigene	N/A
Mouse: BALB/cAnNCrl Mus Musculus	Aurigene	N/A
Mouse: NOD- <i>scid</i> IL2Rgamma <sup>null</sup> Mus Musculus	The Jackson labs	Cat# 005557; RRID: IMSR_JAX:005557



Rat: Wistar Rattus Norvegicus	Charles River Laboratories	Cat# 13508588; RRID: RGD_13508588
Yeast: Saccharomyces cerevisiae RS72	ATCC	Cat# 9763
Oligonucleotides		
RT-PCR Primers for <i>RPL13A</i> gene	Applied Biosystems	Cat# Hs01926559_g1
RT-PCR Primers for <i>Myc</i> gene	Applied Biosystems	Cat# Hs00153401_m1
RT-PCR Primers for <i>DTX1</i> gene	Applied Biosystems	Cat# Hs00269995_m1
Software and Algorithms		
XDS	Kabsch, 2010	<a href="http://xds.mpimf-heidelberg.mpg.de/">http://xds.mpimf-heidelberg.mpg.de/</a>
AIMLESS	Evans and Murshudov, 2013	<a href="http://www.ccp4.ac.uk/html/aimless.html">http://www.ccp4.ac.uk/html/aimless.html</a>
PHASER	McCoy, 2007	<a href="http://www.phaser.com/">http://www.phaser.com/</a>
PHENIX	Adams et al., 2010	<a href="https://www.phenix-online.org/">https://www.phenix-online.org/</a>
Pymol Version 2.0	Molecular Graphics System, Schrödinger, LLC	<a href="https://pymol.org/2/">https://pymol.org/2/</a>
GraphPad Prism Version 7.0a	GraphPad Software Inc.	<a href="https://www.graphpad.com/scientific-software/prism/">https://www.graphpad.com/scientific-software/prism/</a>
ImageJ Version 1.52q	NIH	<a href="http://rsbweb.nih.gov/ij/">http://rsbweb.nih.gov/ij/</a>
FlowJo Version10	Tree Star LLC	<a href="https://www.flowjo.com/">https://www.flowjo.com/</a>
SAMtool	Genome Research Limited	<a href="http://www.htslib.org/">http://www.htslib.org/</a>
Burrows-Wheeler aligner (B.W.A.)	Li H. and Durbin R. 2009	<a href="http://bio-bwa.sourceforge.net/">http://bio-bwa.sourceforge.net/</a>
MatLab R2018a	MathWorks Inc.	<a href="https://it.mathworks.com/products/matlab.html">https://it.mathworks.com/products/matlab.html</a>
Analyst 1.6.1 Software	AB Sciex Pte.Ltd.	<a href="https://sciex.com/">https://sciex.com/</a>

#### TABLE FOR AUTHOR TO COMPLETE

Please upload the completed table as a separate document. **Please do not add subheadings to the Key Resources Table.** If you wish to make an entry that does not fall into one of the subheadings below, please contact your handling editor. (**NOTE:** For authors publishing in *Current Biology*, please note that references within the KRT should be in numbered style, rather than Harvard.)

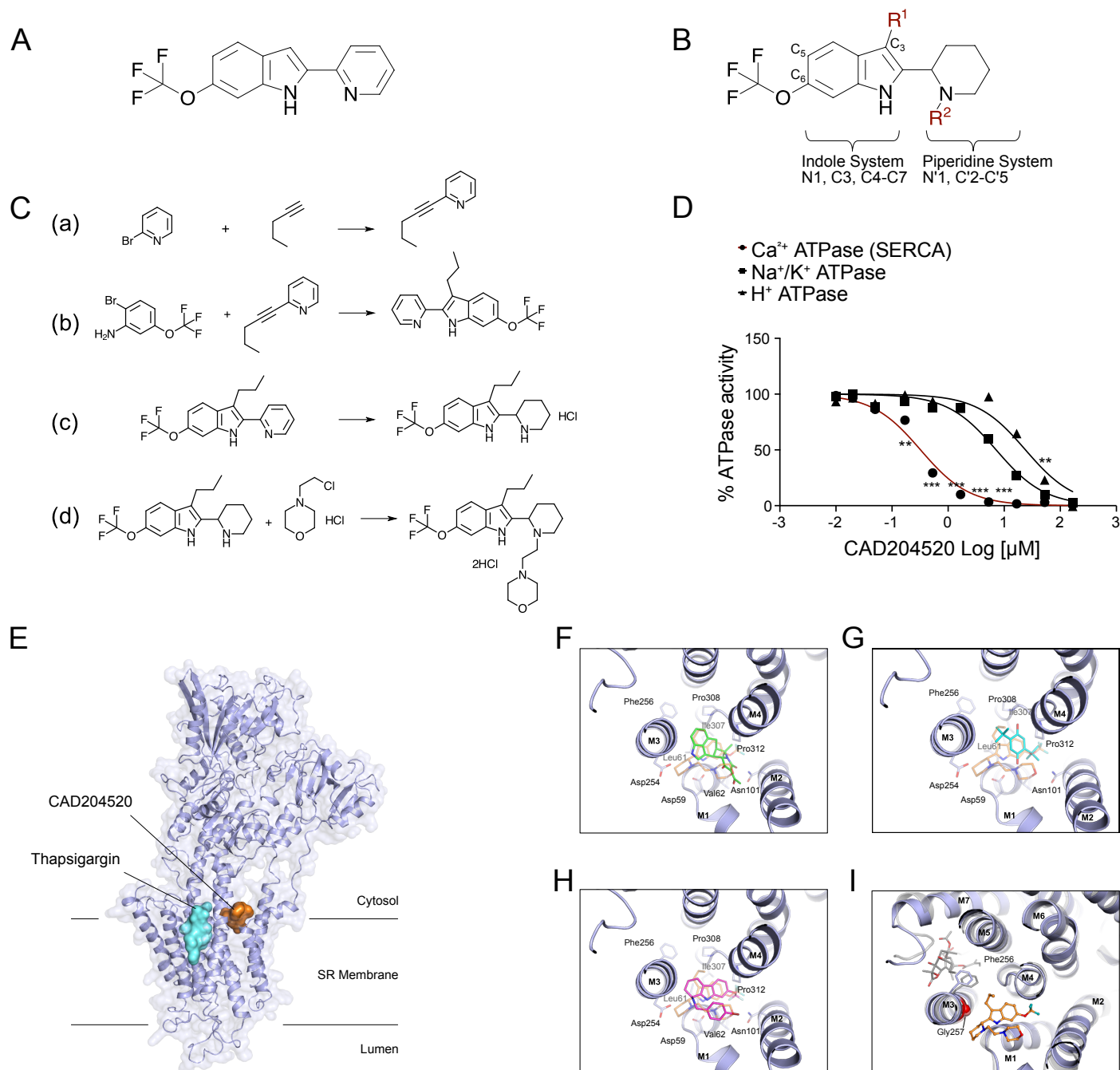


**Figure S1 (Related to Figure 1 and Table S1): Synthesis route, activity and binding mode of CAD204520**

**A** Chemical structure of the initial hit compound: 2-(2-pyridyl)-6-(trifluoromethoxy)-1H-indole **B** Schematic representation for medicinal chemistry optimization. R1 and R2 substitutions are indicated. **C** Synthesis route of CAD204520 (4-[2-[2-[3-propyl-6-(trifluoromethoxy)-1H-indol-2-yl]-1-piperidyl]ethyl]morpholine). Synthetic route (a) to (e) is depicted and described in the methods section. **D** Determination of the protein ATP hydrolysis activity in the presence of compound CAD204520 at pH 7. The figure displays ATPase activity determined by measuring the amount of liberated phosphate from ATP hydrolysis. Data is presented as a fitted curve which has been normalized to the maximal enzyme activity with subtraction of background signal from spontaneous hydrolysis of ATP. Error bars denote the mean  $\pm$  SD (standard deviation) of 3 replicates. Statistical significance (\*\* $P \leq 0.01$ ; \*\*\* $P \leq 0.001$ ) was determined by two-way ANOVA using Bonferroni's correction for multiple comparison testing. **E** Binding sites of CAD204520 and thapsigargin. Superposition of the SERCA-CAD204520 complex with SERCA-thapsigargin (PDB ID: 2AGV). The binding sites are both in the transmembrane region, separated by transmembrane helix M3. Thapsigargin is shown as cyan surface representation. **F** Superposition of SERCA-CAD204520 with SERCA-CPA (PDB ID 3FGO), viewed roughly along the membrane normal. CAD204520 and CPA are shown as orange and green sticks, respectively. **G** Superposition of SERCA-CAD204520 with SERCA-BHQ (PDB ID 2AGV) viewed roughly along the membrane normal. CAD204520 and BHQ are shown as orange and light blue, respectively. **H** Superposition of SERCA-CAD204520 with SERCA-Cpd7 (PDB ID 5NCQ), viewed along the membrane plane. CAD204520 and Cpd7 are shown as orange and magenta sticks, respectively. **I** Binding sites of CAD204520 and thapsigargin, as seen roughly along the membrane normal. Superposition of SERCA bound to CAD204520 (light blue cartoon and orange sticks, respectively) with SERCA bound to thapsigargin (grey cartoon and sticks, respectively). Glycine257, which is mutated to valine in the thapsigargin resistant mutant, is indicated by a red sphere. In the SERCA-thapsigargin complex, Phe256 has undergone a displacement that is likely to be impaired by a valine residue in position 257.



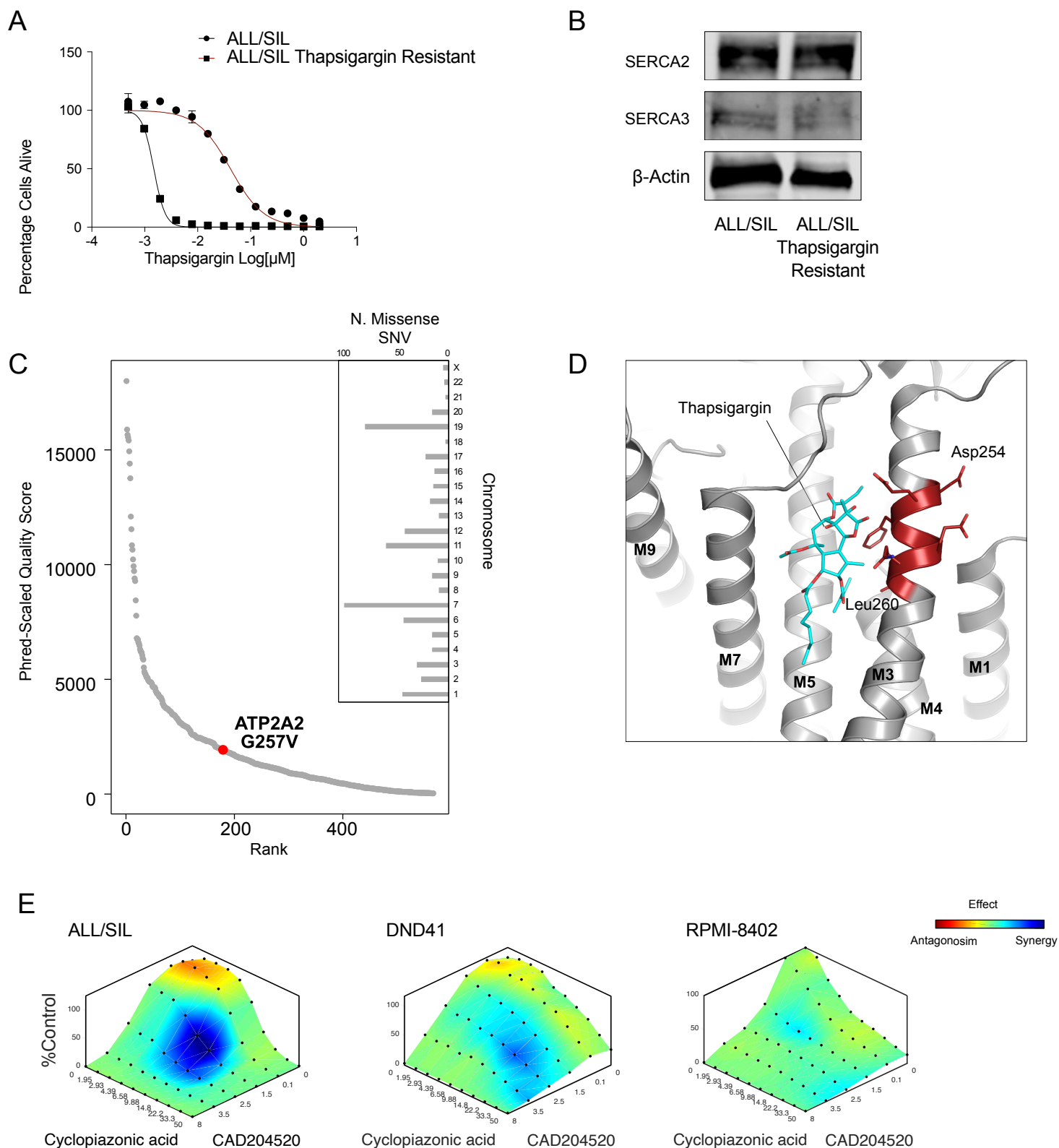


**Figure S2 (Related to Figure 2): Identification of a thapsigargin resistant T-ALL cell line**

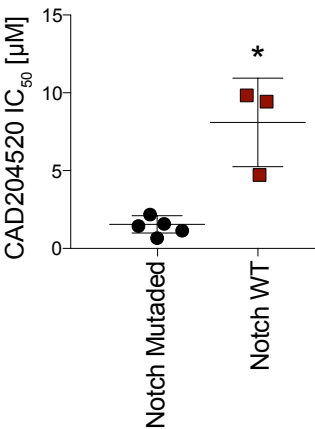
**A**) Effects of Thapsigargin (left) and CAD204520 (right) on cell viability after 72 hours of treatments in ALL/SIL and ALL/SIL thapsigargin-resistant cell lines. Error bars denote  $\pm$  SD of a minimum of 2 replicates. **B**) Western blot showing the expression of SERCA2 and SERCA3 in naïve and resistant ALL/SIL. -actin was used as a loading control. **C**) Phred-scale analysis of exonic single nucleotide variation (SNV) occurring in the ALL/SIL thapsigargin resistant cell line. Inset shows number (N.) of variation (SNV) occurring per chromosome. **D**) Thapsigargin resistance mutation hot spot region on helix M3. Thapsigargin and SERCA residues 254-260 are shown in stick representation and colored cyan and red, respectively. **E**) Surface plots analysis of ALL/SIL, DND41 and RPMI-8402 T-ALL cells lines and a primary NOTCH1 mutated T-ALL sample treated vehicle, CAD204520, cyclopiazonic acid, or CAD204520 plus cyclopiazonic acid. Each point represents an independent measurement representative of three biological replicates. Plots were generated using Combeneft script by MATLAB R2018 and represent the Loewe (dose-effect based approach) analysis. A color scale bar represents level of drug antagonism or synergism.

A

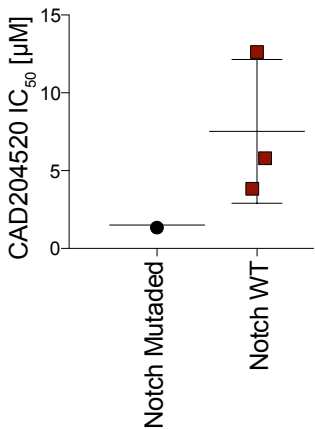
T-ALL Cell Line	NOTCH Protein Domains		CAD204520 IC <sub>50</sub> [μM]
	Heterodimerization (HD)	Proline, Glutamic Acid, Serine and Threonine (PEST)	
ALL/SIL	Mutated	Mutated	2.1
DND41	Mutated	Mutated	3.1
RPMI-8402	Mutated	WT	2.5
PF382	Mutated	Mutated	1.5
SKW-3/KE-37	WT	Mutated	1.5
PEER	WT	WT	9.9
Loucy	WT	WT	4.8
MOLT16	WT	WT	2.3
HSB2	WT	WT	9.5
CTV-1	WT	Mutated	0.8
REC-1	WT	Mutated	1.4
MAVER-1	WT	WT	12.7
Mino	WT	Mutated*	5.9

\* PEST domain mutation p.Q2487\* (exon 34). The effect of this mutation is to be considered ligand-dependent. E. Silkenstedt, F. Arenas, B. Colom-Sanmarti et al. Notch1 signaling in *NOTCH1*-mutated mantle cell lymphoma depends on *Delta-Like* ligand 4 and is a potential target for specific antibody therapy. J. Exp. Clin. Cancer Res, 2019. **38**(1), 446.

B



C



D

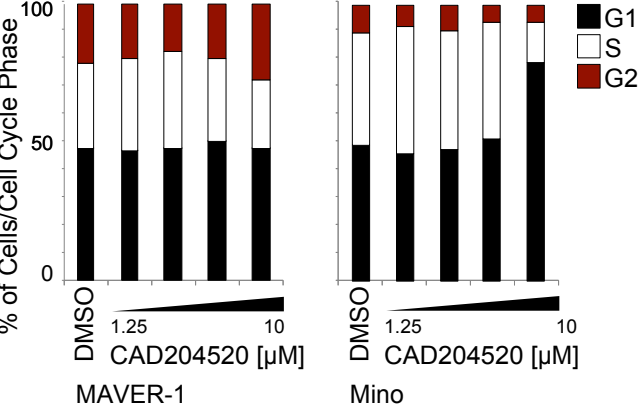


**Figure S3 (Related to Figure 3): Effect of CAD204520 on NOTCH1 wild type T-ALL and MCL lines**

**A)** Table representing NOTCH1 mutational status in T-ALL and MCL lines. **B)** Scatter dot plot representing IC<sub>50</sub> [μM] of CAD204520 in NOTCH1 mutated (n=5) or NOTCH1 WT (n=3) T-ALL or in NOTCH1 mutated (n=1) or NOTCH1 WT (n=3) MCL (shown in **C**) cell line. Statistical significance (\*P ≤ 0.05) was determined by a non-parametric t-test (Mann-Whitney). **D)** Effect of CAD204520 treatments on cycling MAVER-1 and MINO cells. Percentage of DNA content following four days of treatment with the indicated concentrations of CAD204520 on each cell cycle phase is indicated. A minimum of 20,000 events was collected for each condition.

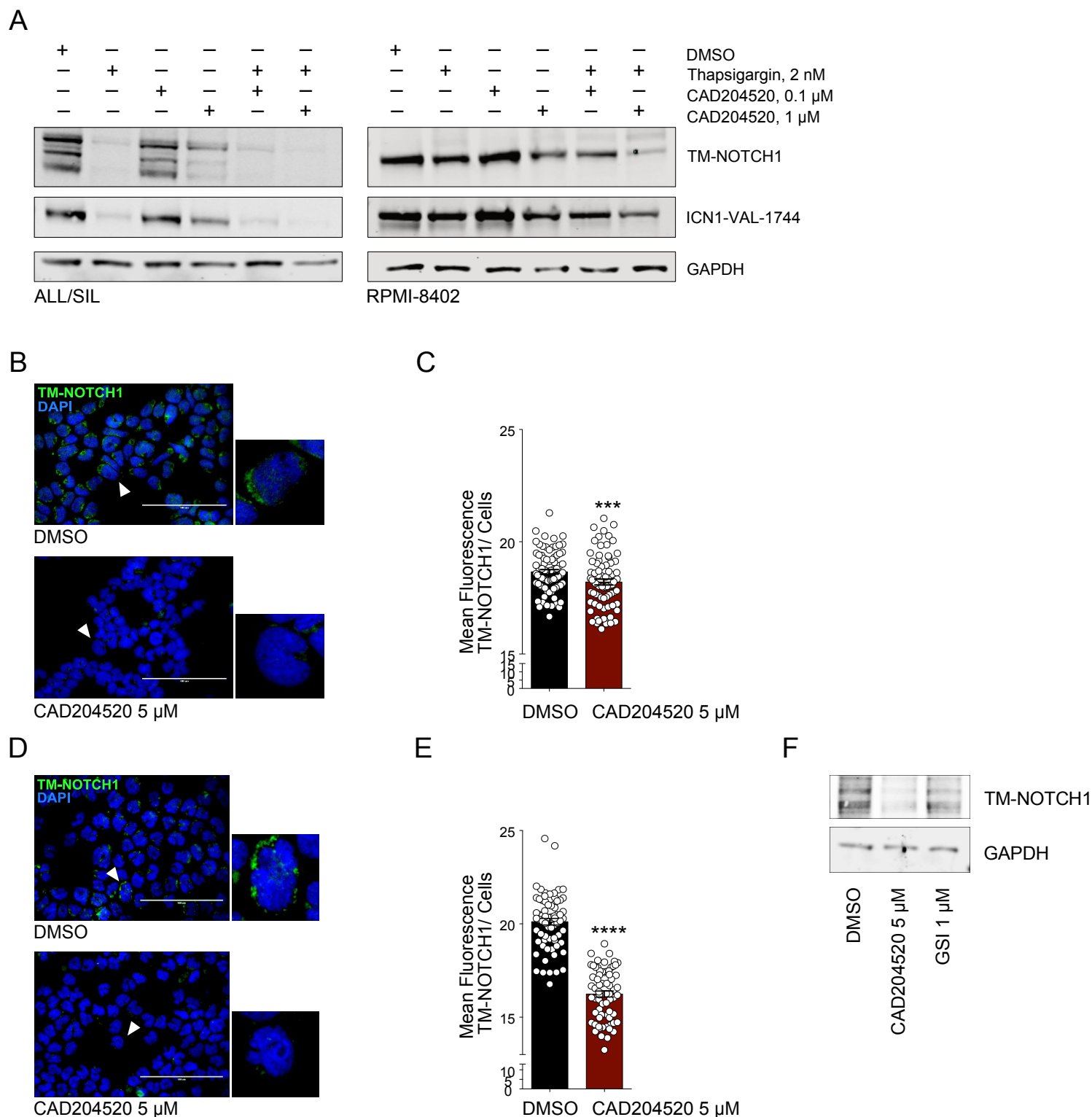


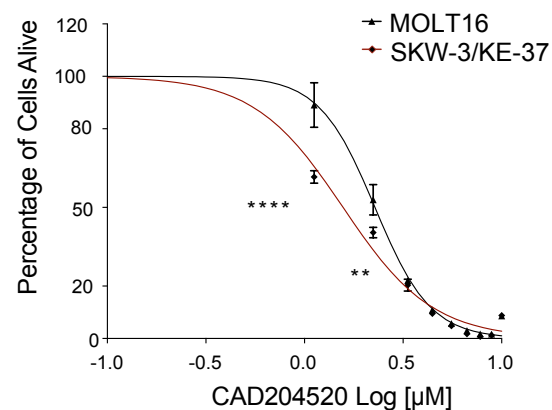
**Figure S4 (Related to Figure 4): Effects of CAD204520 on NOTCH1 trafficking**

**A)** Effect of CAD204520 and thapsigargin treatment for 24 hours on NOTCH1 (N1) processing and activation in T-ALL cell lines. The immunoblot was incubated with an antibody against the C-terminus of NOTCH1 that recognizes the transmembrane subunit (TM) and an antibody that recognizes the cleaved NOTCH1 (ICN1). GAPDH was used as a loading control. **B)** Effect of 24 hours of CAD204520 on NOTCH1 cell surface staining as assessed by immunofluorescence in DND41 T-ALL cells. Scale bars: 100  $\mu$ m. **C)** Quantitative immunofluorescence analysis of NOTCH1 surface signal in DND41 cells after 24 hours of CAD204520 treatment. Error bars denote the mean  $\pm$  standard deviation (SD) of fluorescence of 70 single cells/nuclei (arbitrary units); Statistical significance among groups was determined by unpaired t-test ( $***P \leq 0.001$ ). **D)** Effect of 24 hours of CAD204520 on NOTCH1 cell surface staining as assessed by immunofluorescence in REC-1 T-ALL cells. Scale bars: 100  $\mu$ m. **E)** Quantitative immunofluorescence analysis of NOTCH1 surface signal in REC-1 cells after 24 hours of CAD204520 treatment. Error bars denote the mean  $\pm$  standard deviation (SD) of fluorescence of 70 single cells/nuclei (arbitrary units); Statistical significance among groups was determined by unpaired t-test ( $***P \leq 0.001$ ). **F)** Effect of 24 hours treatment of CAD204520 on NOTCH1 (N1) processing and activation in REC-1 cell line. The blot was incubated with an antibody against the C-terminus of NOTCH1 that recognizes the NOTCH1 transmembrane subunit (TM). GAPDH was used as a loading control.

A

CELL LINES	GENOMIC PROFILE
MOLT16	<i>SIL-TAL1</i> t(3;11)(p21;p13)/ <i>LMO2</i> translocation with non- <i>TR@</i> partner t(8;14)(q24;q32)/ <i>TRAD@-MYC</i> <i>CDKN2AB</i> biallelic deletion <i>PTEN</i> c.735-736insCTTA p.P246fs*12 (exon 7)
SKW-3/KE-37	t(8;11)(p11-12;p13)/ <i>LMO2</i> translocation with non- <i>TR@</i> partner t(8;14)(q24;q32)/ <i>TRAD@-MYC</i> <i>CDKN2AB</i> biallelic deletion <i>PTEN</i> biallelic deletion <i>NOTCH1</i> c7375C>T p.Q2459* (exon 34)

B



C

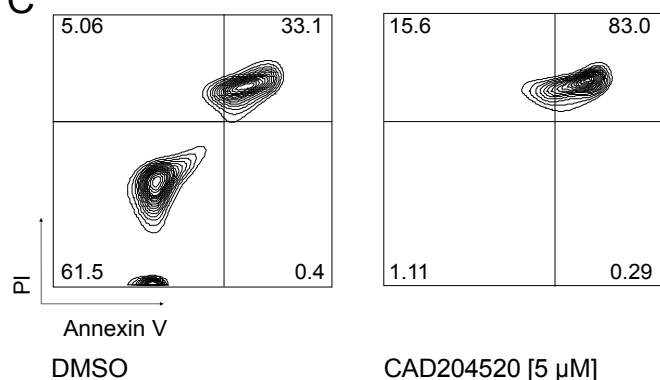


**Figure S5 (Related to Figure 5): Genomic characterization of MOLT16 and SKW-3/KE-37 T-ALL cell lines**

**A)** Genomic characterization of MOLT16 and SKW-3/KE-37 T-ALL cell line. The karyotype and the mutational analysis are indicated. **B)** Effects of CAD204520 on cell viability after 72 hours of treatments in MOLT16 and SKW/KE-37 T-ALL cell lines. Error bars denote  $\pm$  SD of 2 replicates. Statistical significance among groups was determined by 2-way ANOVA (\*\* $P \leq 0.01$ , \*\*\* $P \leq 0.001$ ). **C)** Pro-apoptotic effect of CAD204520 treatment. Annexin V/propidium iodide staining of primary NOTCH1 mutated T-ALL cells following 72 hours of treatment with the indicated concentrations of CAD204520. A minimum of 20,000 events was collected for each condition.

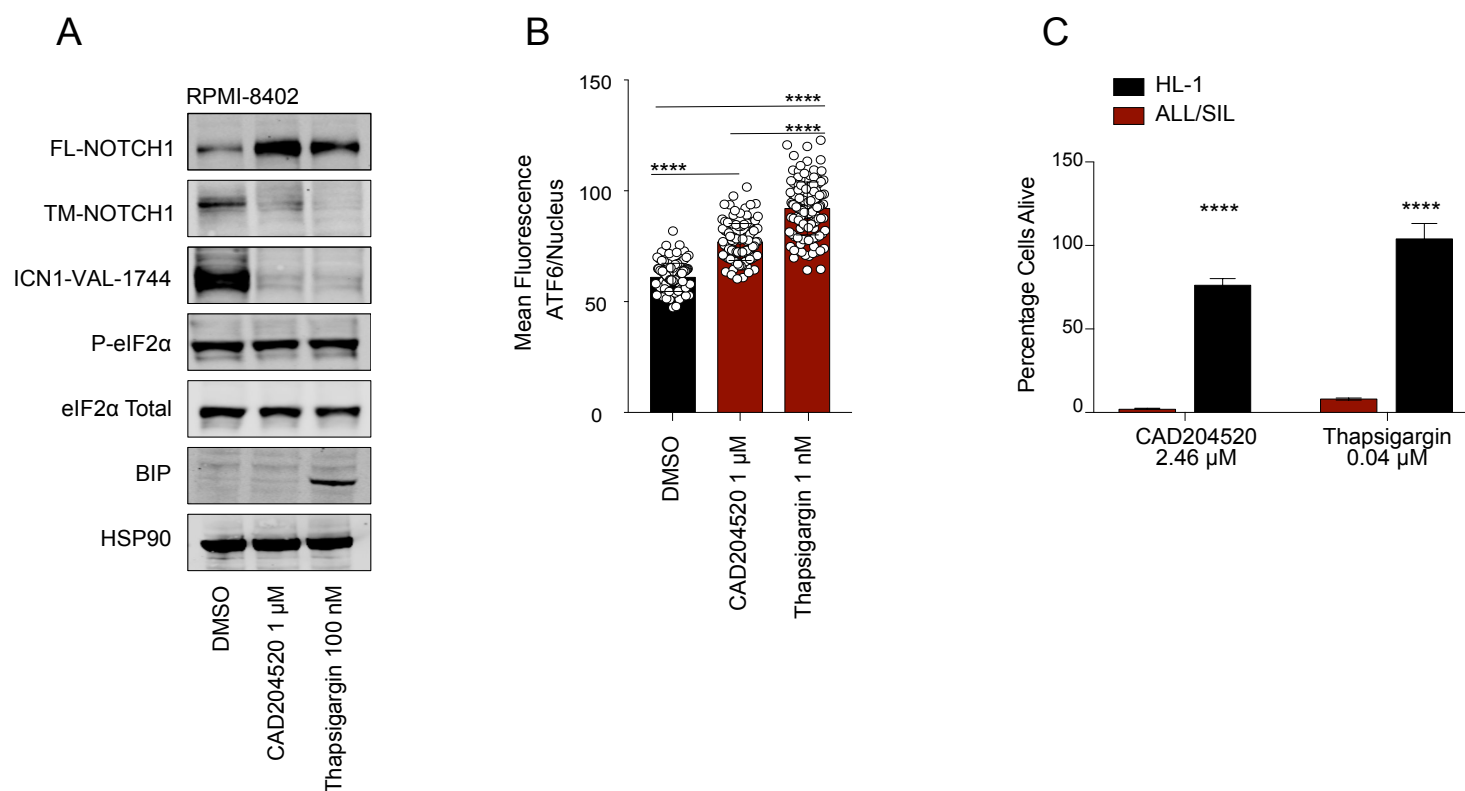


**Figure S6 (Related to Figure 6): Consequences of CAD204520 on UPR pathway**

**A)** Effect of CAD204520 and thapsigargin treatment for 24 hours in RPMI-8402 cell lines. The immunoblot was stained with an antibody against the C-terminus of NOTCH1 that recognizes the furin-processed NOTCH1 transmembrane subunit (TM) and the unprocessed NOTCH1 precursor (FL), an antibody that recognizes the cleaved NOTCH1 (ICN1), and antibodies that recognize the activation of the UPR pathway. P-eIF2, eIF2, total BiP. HSP90 was used as a loading control. **B)** Quantitative immunofluorescence analysis of nuclear ATF6 signal in ALL/SIL cells after 24 hours of CAD204520 treatment. Error bars denote the mean  $\pm$  standard deviation (SD) of fluorescence of 70 single cells/nuclei (arbitrary units); Statistical significance among groups was determined using one-way ANOVA with Bonferroni's correction for multiple comparison testing ( $***P \leq 0.001$ ). **C)** Effect of CAD204520 and thapsigargin treatment in HL-1 and ALL/SIL cell lines. Histograms show percentage of cell alive after 72 hours of treatment at indicates doses. Error bar denotes the mean  $\pm$  SD of a minimum of three replicates. Statistical significance among groups ( $****P \leq 0.0001$ ) was determined by 2-way ANOVA.

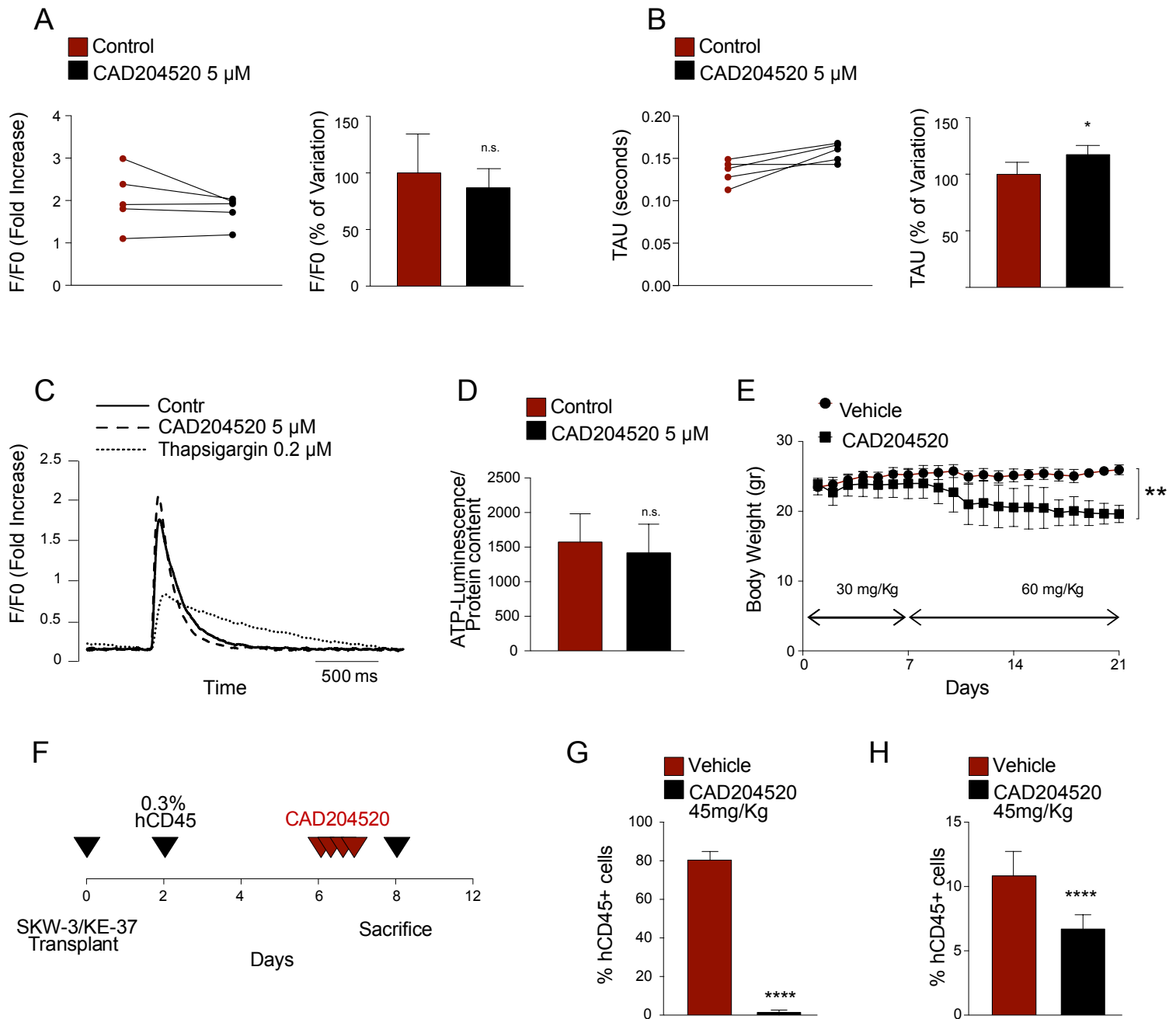


**Figure S7 (Related to Figure 7): Preclinical toxicity and activity of CAD204520**

**A-B left panels):** Effect of CAD204520 treatment on rat cardiomyocyte calcium transients. Single experiments are represented by two dots interconnected by a solid line. Specifically, the line between dots connects the quantification of the amplitude of the calcium transient (A: F/F0) and the time required for cytosolic calcium removal (B: TAU), before and after the CAD204520 (5  $\mu$ M) treatment compared to control (Control). **A-B right panels):** Mean percentage variation of CAD204520 treated cardiomyocytes on the same parameters. Graph bars: mean  $\pm$  SD of the 5 CAD204520 treated cardiomyocyte groups. Statistical significance comparing CAD204520 treated cells vs. Control cells (\* $P$  < 0.05) was determined by a non-parametric t-test (Mann-Whitney). **C)** Representative examples of calcium transients (normalized traces: fold increase) recorded from control (solid line), CAD204520 (5  $\mu$ M) (dashed line), and thapsigargin (0.2  $\mu$ M) (dotted line) ventricular myocytes. **D)** ATP Luminescence induction normalized to cellular protein content in rat cardiomyocytes treated either with CAD204520 or vehicle (Control). Error bars denote the mean  $\pm$  SD of 6 replicates. Statistical significance comparing CAD204520 treated cells vs. vehicle treated cells (not significant = n.s.) was determined by a non-parametric t-test (Mann-Whitney). **E)** Effect of administration of CAD204520 on body weight. Error bars denote the mean  $\pm$  SD of 6 replicates. Animals were treated for 6 days with 30mg/Kg of CAD204520 and subsequently treated with 60 mg/Kg daily. Statistical significance (\*\* $P$   $\leq$  0.01) was determined by a 2-way ANOVA analysis. **F)** Representative schema of CAD204520 in vivo studies. **G)** Effect of CAD204520 on T-ALL leukemia burden in a SKW-3/KE-37 xenografted murine model. Anti-leukemic activity of CAD204520 assessed by measuring hCD45+ cells after 4 days of CAD204520 treatment (45 mg/kg/OS BID) or vehicle (tween-80 0.5% w/v and HPMC 1.0% w/v). Error bars denote the mean  $\pm$  SD of 9 CAD204520 treated animals or the mean  $\pm$  SD of 8 replicates vehicles treated mice. Statistical significance for treated vs. vehicle (\*\*\*\* $P$   $\leq$  0.0001) was determined by non-parametric t-test (Mann-Whitney). **H)** Antileukemic activity of CAD204520 in hCD45+ spleen infiltrating cells in a SKW-3/KE-37 xenografted murine model after 5 days of CAD204520 treatment (45 mg/kg/OS BID) or vehicle (tween-80 0.5% w/v and HPMC 1.0% w/v). The number of hCD45+ cells per field were represented as percentage relative to vehicle control. Error bars denote the mean  $\pm$  SD of 13 fields from 2 mice treated with CAD204520 or the mean  $\pm$  SD of 12 fields from 3 vehicle treated mice. Statistical significance for treated vs. vehicle (\*\*\*\* $P$   $\leq$  0.0001) was determined by non-parametric t-test (Mann-Whitney).

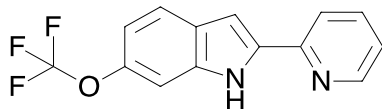
Compound	Structure	ATP hydrolysis IC <sub>50</sub> [μM]			SERCA Ligand Efficiency Index (LE)
		H <sup>+</sup> -ATPase	Na <sup>+</sup> ,K <sup>+</sup> -ATPase	Ca <sup>2+</sup> -ATPase (SERCA)	
CAD204522		126.80 ±14.94	22.56 ±5.48	30.14 ±5.61	0.20
CAD307496		37.68 ±6.22	20.09 ±2.76	58.86 ±6.50	0.21
CAD204521		21.81 ±4.50	0.28 ±0.07	7.75 ±1.68	0.26
CAD204630		>333	0.04 ±0.01	1.56 ±0.45	0.25
CAD204631		71.25 ±18.00	3.16 ±0.41	18.00 ±3.25	0.21
CAD305666		9.74 ±1.67	0.39 ±0.20	1.03 ±0.22	0.27
CAD204519		84.22 ±24.37	0.01 ±0.02	0.55 ±0.12	0.28
CAD204520		26.90 ±2.98	8.30 ±0.95	0.34 ±0.03	0.29
CAD306749		7.75 ±2.69	0.59 ±0.17	0.32 ±0.19	0.22
CAD306750		16.80 ±2.68	1.21 ±0.37	2.62 ±0.83	0.22

**Table S1 (Related to Figure 1 and Figure S1): H<sup>+</sup>, Na/K<sup>+</sup>, Ca<sup>2+</sup> ATP hydrolysis of 2-(2-pyridyl)-6-(trifluoromethoxy)-1H-indole derivatives**

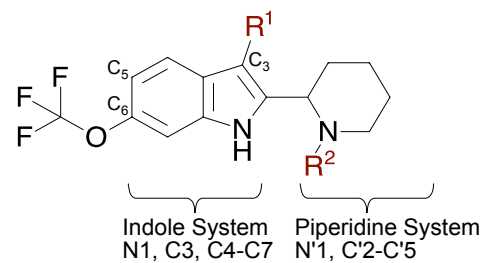
Data of compounds fitted to the pharmacophore model. ATPase hydrolysis activity toward H<sup>+</sup>, Ca<sup>2+</sup> and Na<sup>+</sup>/K<sup>+</sup>-ATPase is indicated as the half maximal inhibitory concentration (IC<sub>50</sub>) and expressed in μM. The ligand efficiency index is equal to LE = 1.4(-logIC<sub>50</sub>)/N. N is the number of non-hydrogen atoms.



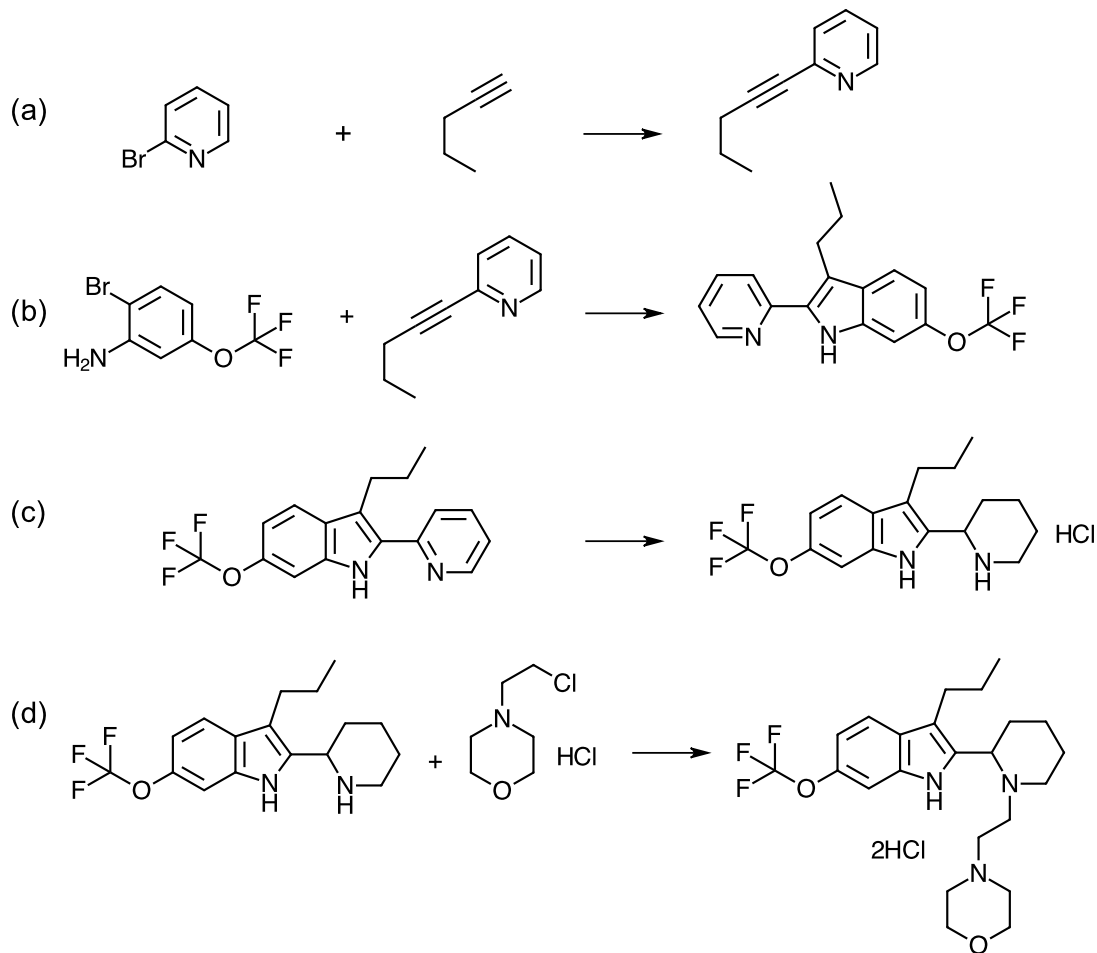
A



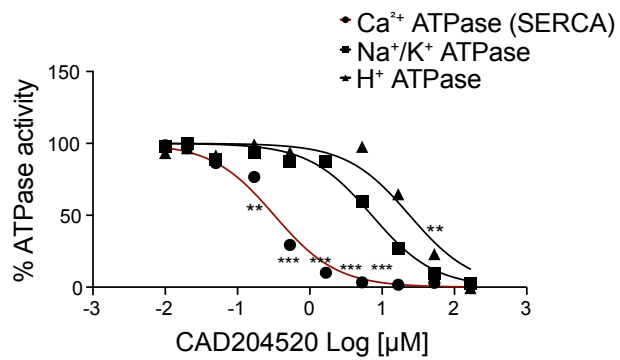
B



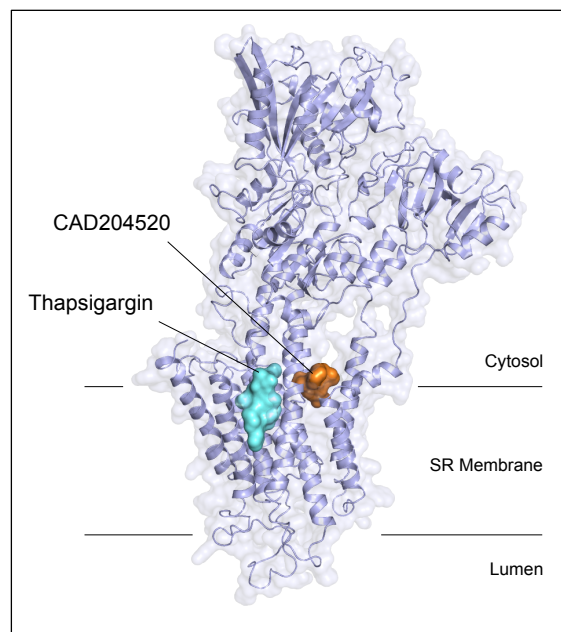
C



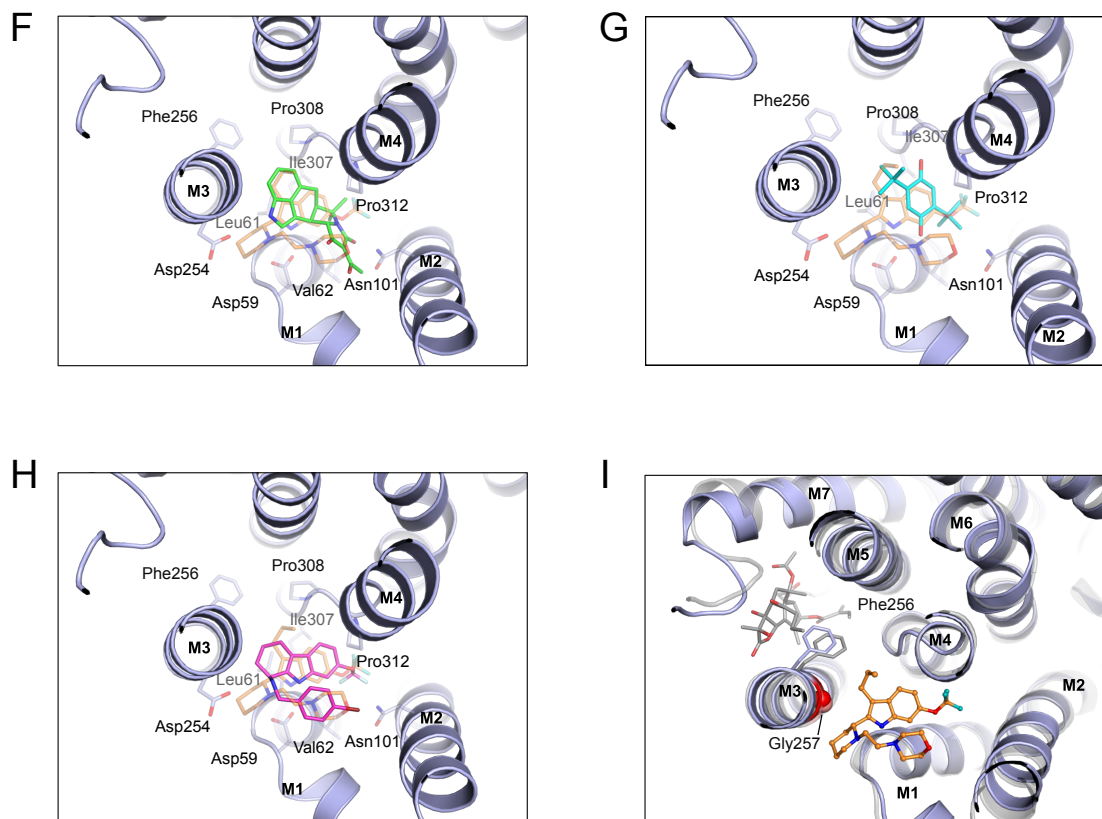
D



E

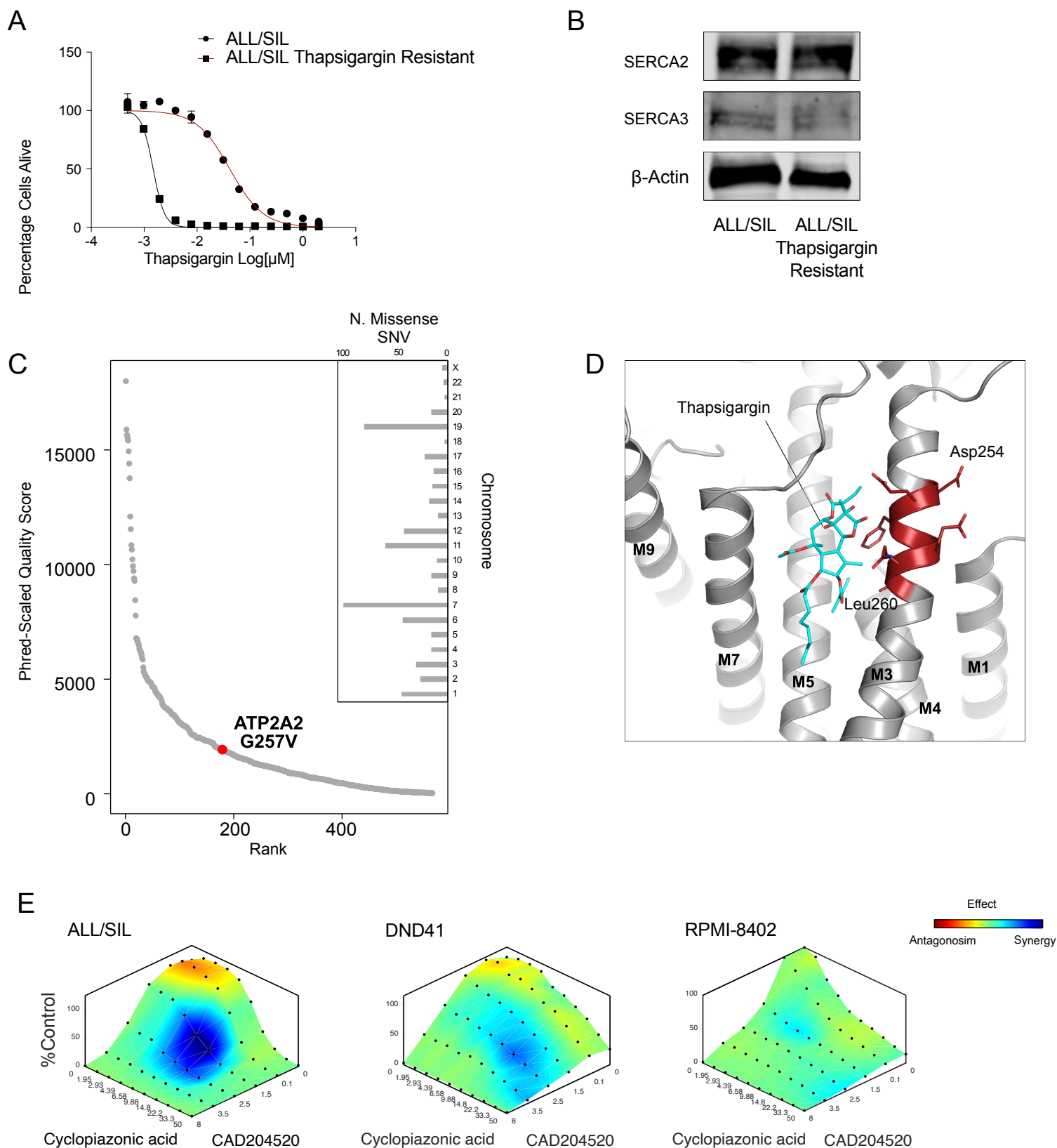






**Supplementary Figure S1 (Related to Figure 1 and Table 1): Synthesis route, activity and binding mode of CAD204520**

**A)** Chemical structure of the initial hit compound: 2-(2-pyridyl)-6-(trifluoromethoxy)-1H-indole **B)** Schematic representation for medicinal chemistry optimization. R1 and R2 substitutions are indicated. **C)** Synthesis route of CAD204520 (4-[2-[2-[3-propyl-6-(trifluoromethoxy)-1H-indol-2-yl]-1-piperidyl]ethyl]morpholine). Synthetic route (a) to (e) is depicted and described in the methods section. **D)** Determination of the protein ATP hydrolysis activity in the presence of compound CAD204520 at pH 7. The figure displays ATPase activity determined by measuring the amount of liberated phosphate from ATP hydrolysis. Data is presented as a fitted curve which has been normalized to the maximal enzyme activity with subtraction of background signal from spontaneous hydrolysis of ATP. Error bars denote the mean  $\pm$  SD (standard deviation) of 3 replicates. Statistical significance (\*\* $P \leq 0.01$ ; \*\*\* $P \leq 0.001$ ) was determined by two-way ANOVA using Bonferroni's correction for multiple comparison testing. **E)** Binding sites of CAD204520 and thapsigargin. Superposition of the SERCA-CAD204520 complex with SERCA-thapsigargin (PDB ID: 2AGV). The binding sites are both in the transmembrane region, separated by transmembrane helix M3. Thapsigargin is shown as cyan surface representation. **F)** Superposition of SERCA-CAD204520 with SERCA-CPA (PDB ID 3FGO), viewed roughly along the membrane normal. CAD204520 and CPA are shown as orange and green sticks, respectively. **G)** Superposition of SERCA-CAD204520 with SERCA-BHQ (PDB ID 2AGV) viewed roughly along the membrane normal. CAD204520 and BHQ are shown as orange and light blue, respectively. **H)** Superposition of SERCA-CAD204520 with SERCA-Cpd7 (PDB ID 5NCQ), viewed along the membrane plane. CAD204520 and Cpd7 are shown as orange and magenta sticks, respectively. **I)** Binding sites of CAD204520 and thapsigargin, as seen roughly along the membrane normal. Superposition of SERCA bound to CAD204520 (light blue cartoon and orange sticks, respectively) with SERCA bound to thapsigargin (grey cartoon and sticks, respectively). Glycine257, which is mutated to valine in the thapsigargin resistant mutant, is indicated by a red sphere. In the SERCA-thapsigargin complex, Phe256 has undergone a displacement that is likely to be impaired by a valine residue in position 257.



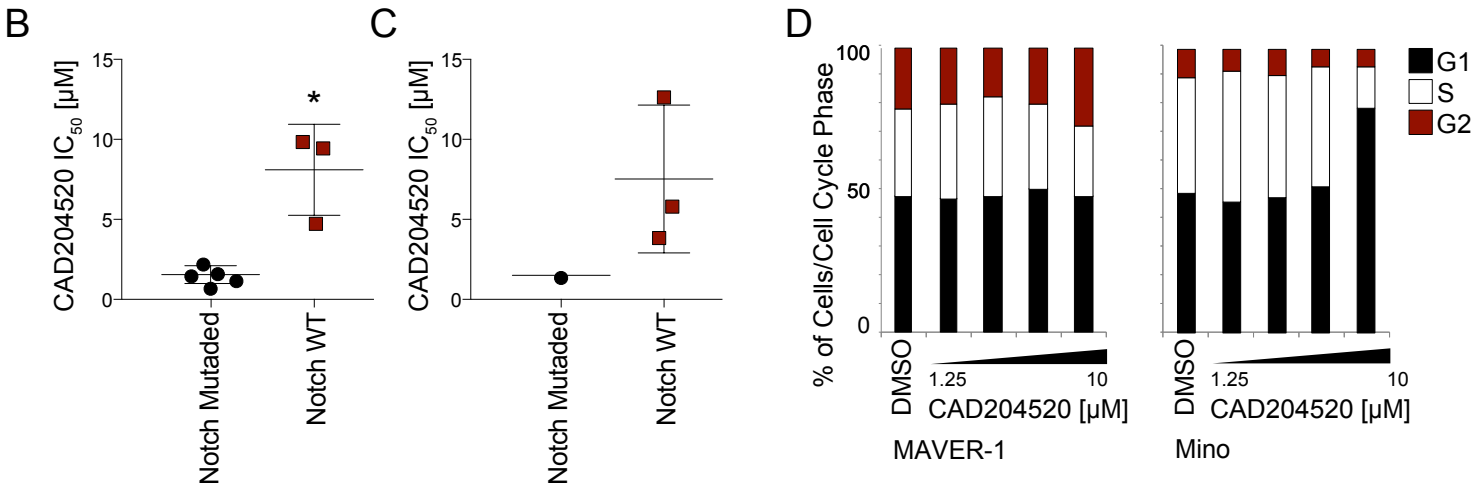
**Supplementary Figure S2 (Related to Figure 2): Identification of a thapsigargin resistant T-ALL cell line**

**A)** Effects of Thapsigargin (left) and CAD204520 (right) on cell viability after 72 hours of treatments in ALL/SIL and ALL/SIL thapsigargin-resistant cell lines. Error bars denote  $\pm$  SD of a minimum of 2 replicates. **B)** Western blot showing the expression of SERCA2 and SERCA3 in naïve and resistant ALL/SIL. -actin was used as a loading control. **C)** Phred-scale analysis of exonic single nucleotide variation (SNV) occurring in the ALL/SIL thapsigargin resistant cell line. Inset shows number (N.) of variation (SNV) occurring per chromosome. **D)** Thapsigargin resistance mutation hot spot region on helix M3. Thapsigargin and SERCA residues 254-260 are shown in stick representation and colored cyan and red, respectively. **E)** Surface plots analysis of ALL/SIL, DND41 and RPMI-8402 T-ALL cells lines and a primary NOTCH1 mutated T-ALL sample treated vehicle, CAD204520, cyclopiazonic acid, or CAD204520 plus cyclopiazonic acid. Each point represents an independent measurement representative of three biological replicates. Plots were generated using Combeneft script by MATLAB R2018 and represent the Loewe (dose-effect based approach) analysis. A color scale bar represents level of drug antagonism or synergism.

A

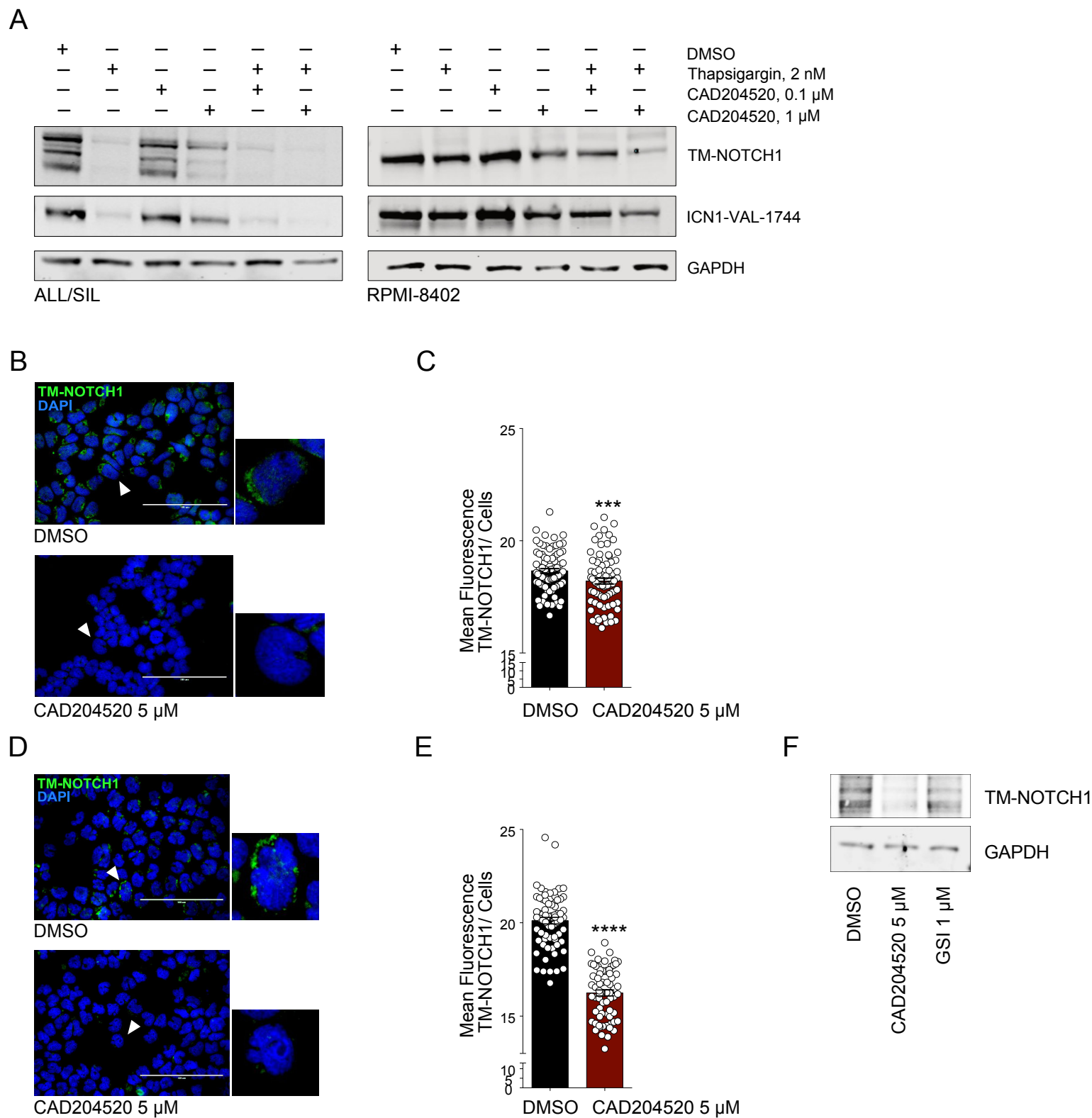
T-ALL Cell Line	NOTCH Protein Domains		CAD204520 IC <sub>50</sub> [μM]
	Heterodimerization (HD)	Proline, Glutamic Acid, Serine and Threonine (PEST)	
ALL/SIL	Mutated	Mutated	2.1
DND41	Mutated	Mutated	3.1
RPMI-8402	Mutated	WT	2.5
PF382	Mutated	Mutated	1.5
SKW-3/KE-37	WT	Mutated	1.5
PEER	WT	WT	9.9
Loucy	WT	WT	4.8
MOLT16	WT	WT	2.3
HSB2	WT	WT	9.5
CTV-1	WT	Mutated	0.8
REC-1	WT	Mutated	1.4
MAVER-1	WT	WT	12.7
Mino	WT	Mutated*	5.9

\* PEST domain mutation p.Q2487\* (exon 34). The effect of this mutation is to be considered ligand-dependent. E. Silkenstedt, F. Arenas, B. Colom-Sanmarti et al. Notch1 signaling in *NOTCH1*-mutated mantle cell lymphoma depends on *Delta-Like* ligand 4 and is a potential target for specific antibody therapy. J. Exp. Clin. Cancer Res, 2019. **38**(1), 446.



**Supplementary Figure S3 (Related to Figure 3): Effect of CAD204520 on NOTCH1 wild type T-ALL and MCL lines**

**A)** Table representing NOTCH1 mutational status in T-ALL and MCL lines. **B)** Scatter dot plot representing IC<sub>50</sub> [μM] of CAD204520 in NOTCH1 mutated (n=5) or NOTCH1 WT (n=3) T-ALL or in NOTCH1 mutated (n=1) or NOTCH1 WT (n=3) MCL (shown in **C**) cell line. Statistical significance (\*P ≤ 0.05) was determined by a non-parametric t-test (Mann-Whitney). **D)** Effect of CAD204520 treatments on cycling MAVER-1 and MINO cells. Percentage of DNA content following four days of treatment with the indicated concentrations of CAD204520 on each cell cycle phase is indicated. A minimum of 20,000 events was collected for each condition.



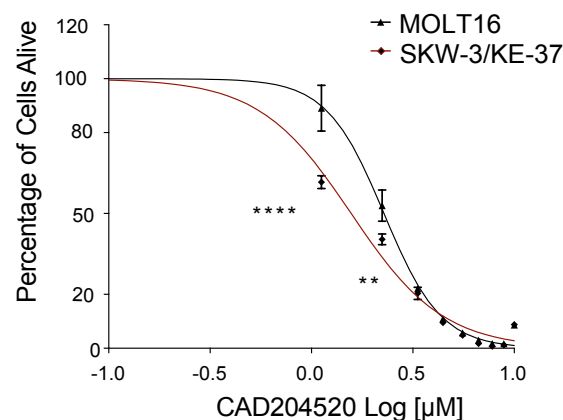
**Supplementary Figure S4 (Related to Figure 4): Effects of CAD204520 on NOTCH1 trafficking**

**A)** Effect of CAD204520 and thapsigargin treatment for 24 hours on NOTCH1 (N1) processing and activation in T-ALL cell lines. The immunoblot was incubated with an antibody against the C-terminus of NOTCH1 that recognizes the transmembrane subunit (TM) and an antibody that recognizes the cleaved NOTCH1 (ICN1). GAPDH was used as a loading control. **B)** Effect of 24 hours of CAD204520 on NOTCH1 cell surface staining as assessed by immunofluorescence in DND41 T-ALL cells. Scale bars: 100  $\mu$ m. **C)** Quantitative immunofluorescence analysis of NOTCH1 surface signal in DND41 cells after 24 hours of CAD204520 treatment. Error bars denote the mean  $\pm$  standard deviation (SD) of fluorescence of 70 single cells/nuclei (arbitrary units); Statistical significance among groups was determined by unpaired t-test ( $***P \leq 0.001$ ). **D)** Effect of 24 hours of CAD204520 on NOTCH1 cell surface staining as assessed by immunofluorescence in REC-1 T-ALL cells. Scale bars: 100  $\mu$ m. **E)** Quantitative immunofluorescence analysis of NOTCH1 surface signal in REC-1 cells after 24 hours of CAD204520 treatment. Error bars denote the mean  $\pm$  standard deviation (SD) of fluorescence of 70 single cells/nuclei (arbitrary units); Statistical significance among groups was determined by unpaired t-test ( $***P \leq 0.001$ ). **F)** Effect of 24 hours treatment of CAD204520 on NOTCH1 (N1) processing and activation in REC-1 cell line. The blot was incubated with an antibody against the C-terminus of NOTCH1 that recognizes the NOTCH1 transmembrane subunit (TM). GAPDH was used as a loading control.

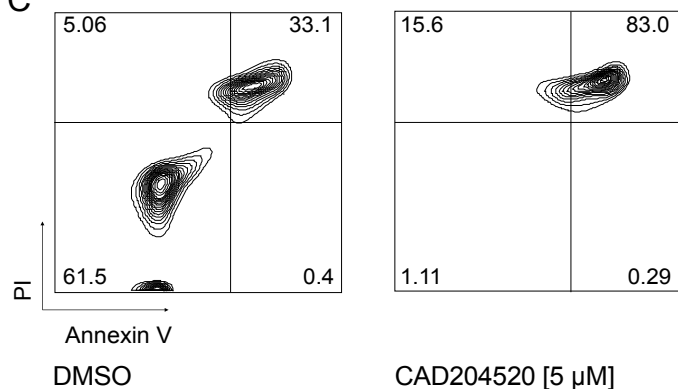
A

CELL LINES	GENOMIC PROFILE
MOLT16	<i>SIL-TAL1</i> t(3;11)(p21;p13)/ <i>LMO2</i> translocation with non- <i>TR@</i> partner t(8;14)(q24;q32)/ <i>TRAD@-MYC</i> <i>CDKN2AB</i> biallelic deletion <i>PTEN</i> c.735-736insCTTA p.P246fs*12 (exon 7)
SKW-3/KE-37	t(8;11)(p11-12;p13)/ <i>LMO2</i> translocation with non- <i>TR@</i> partner t(8;14)(q24;q32)/ <i>TRAD@-MYC</i> <i>CDKN2AB</i> biallelic deletion <i>PTEN</i> biallelic deletion <i>NOTCH1</i> c7375C>T p.Q2459* (exon 34)

B

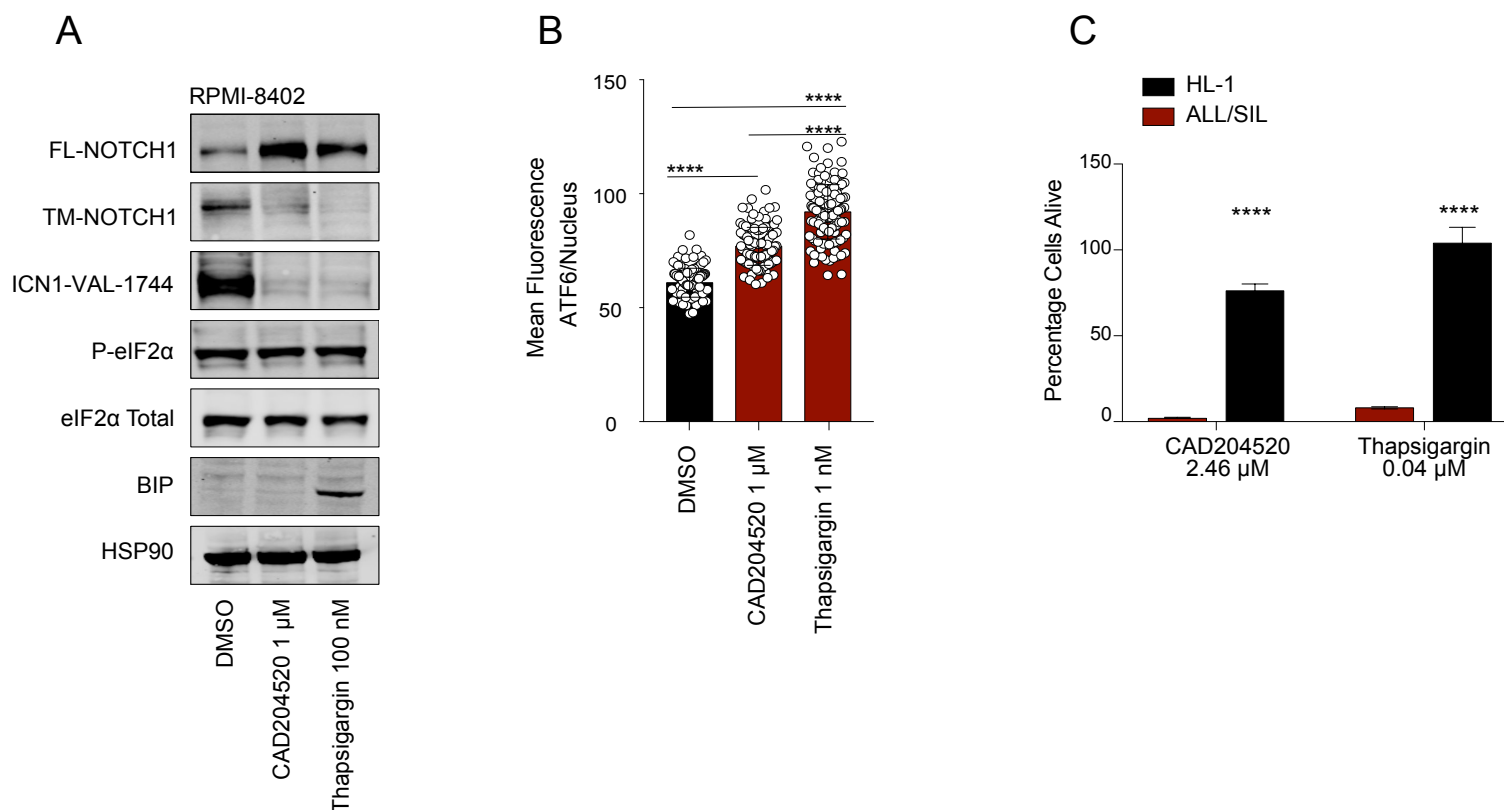


C



### Supplementary Figure S5 (Related to Figure 5): Genomic characterization of MOLT16 and SKW-3/KE-37 T-ALL cell lines

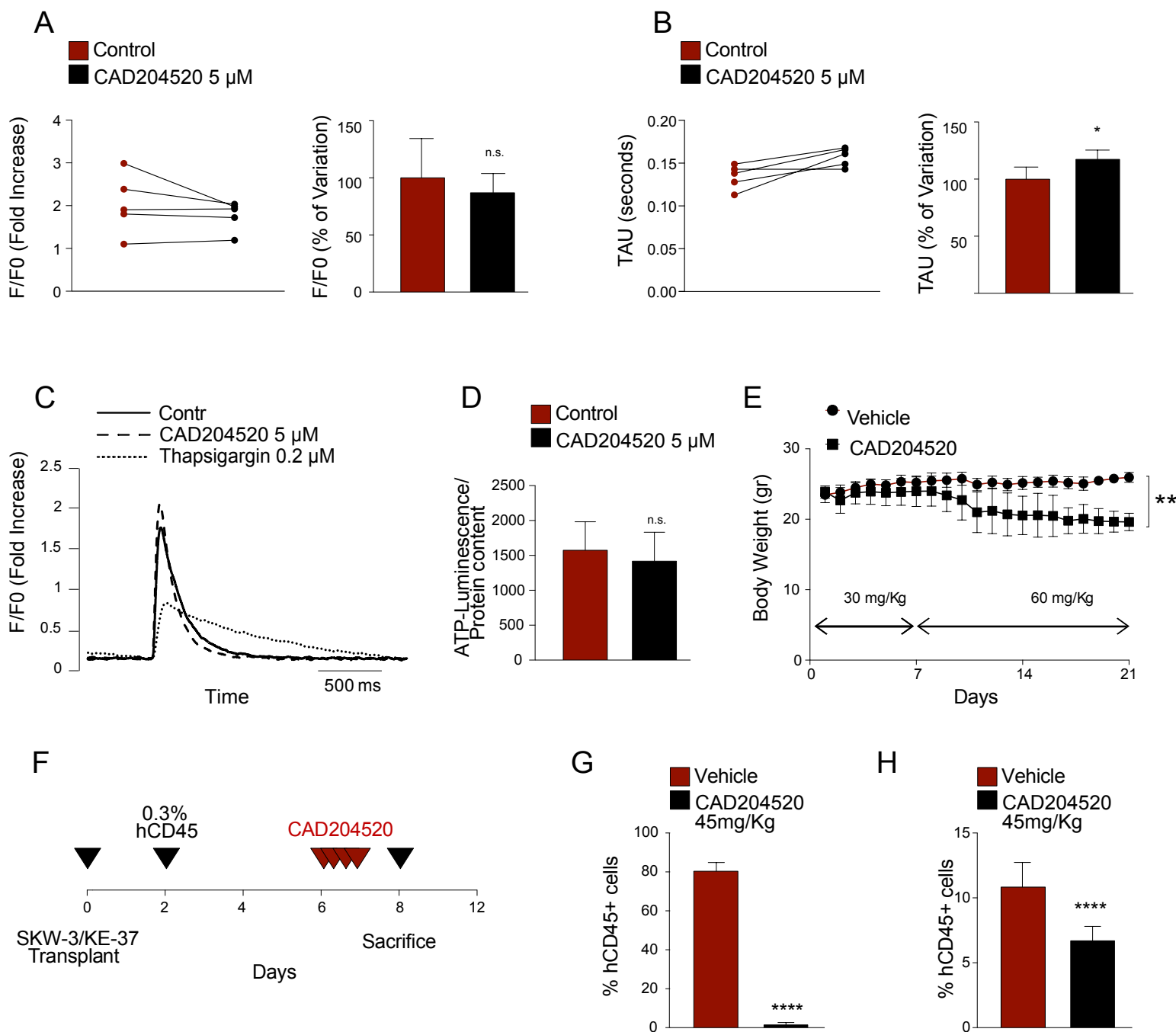
**A)** Genomic characterization of MOLT16 and SKW-3/KE-37 T-ALL cell line. The karyotype and the mutational analysis are indicated. **B)** Effects of CAD204520 on cell viability after 72 hours of treatments in MOLT16 and SKW/KE-37 T-ALL cell lines. Error bars denote  $\pm$  SD of 2 replicates. Statistical significance among groups was determined by 2-way ANOVA (\*\* $P \leq 0.01$ , \*\*\* $P \leq 0.001$ ). **C)** Pro-apoptotic effect of CAD204520 treatment. Annexin V/propidium iodide staining of primary NOTCH1 mutated T-ALL cells following 72 hours of treatment with the indicated concentrations of CAD204520. A minimum of 20,000 events was collected for each condition.



#### Supplementary Figure S6 (Related to Figure 6): Consequences of CAD204520 on UPR pathway

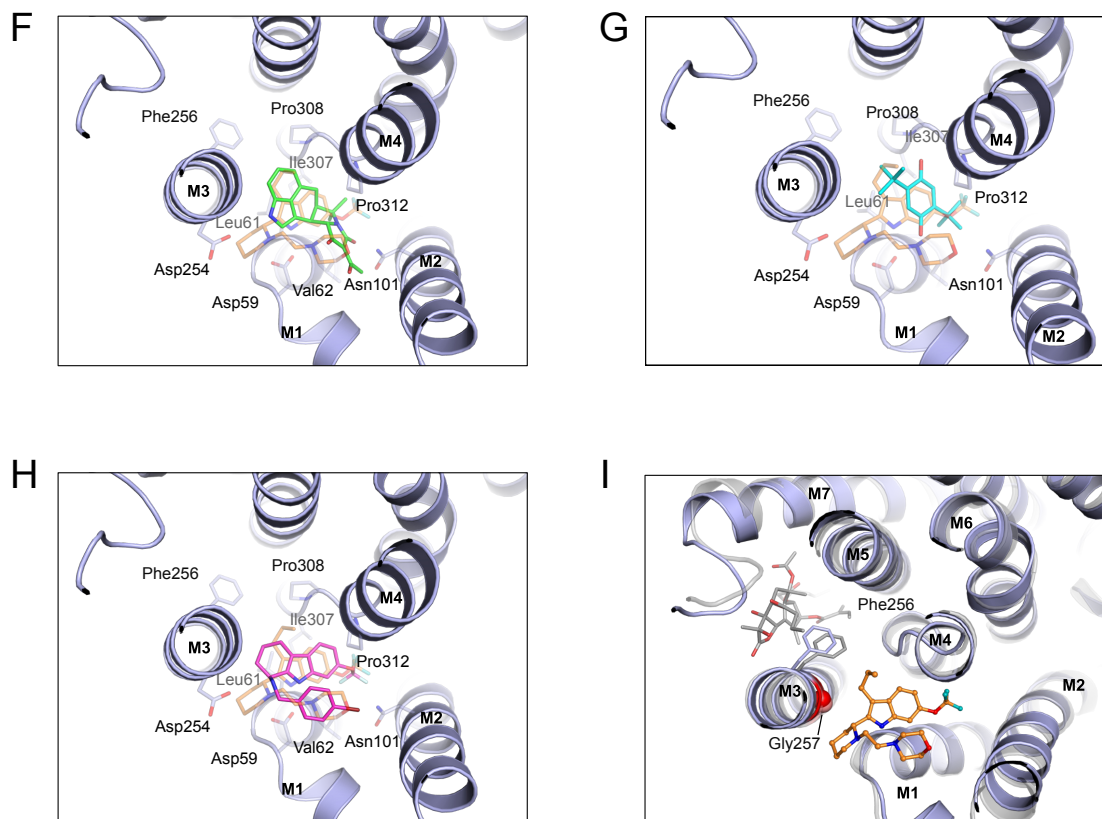
**A)** Effect of CAD204520 and thapsigargin treatment for 24 hours in RPMI-8402 cell lines. The immunoblot was stained with an antibody against the C-terminus of NOTCH1 that recognizes the furin-processed NOTCH1 transmembrane subunit (TM) and the unprocessed NOTCH1 precursor (FL), an antibody that recognizes the cleaved NOTCH1 (ICN1), and antibodies that recognize the activation of the UPR pathway. P-eIF2, eIF2, total BiP. HSP90 was used as a loading control. **B)** Quantitative immunofluorescence analysis of nuclear ATF6 signal in ALL/SIL cells after 24 hours of CAD204520 treatment. Error bars denote the mean  $\pm$  standard deviation (SD) of fluorescence of 70 single cells/nuclei (arbitrary units); Statistical significance among groups was determined using one-way ANOVA with Bonferroni's correction for multiple comparison testing ( $***P \leq 0.001$ ). **C)** Effect of CAD204520 and thapsigargin treatment in HL-1 and ALL/SIL cell lines. Histograms show percentage of cell alive after 72 hours of treatment at indicates doses. Error bar denotes the mean  $\pm$  SD of a minimum of three replicates. Statistical significance among groups ( $****P \leq 0.0001$ ) was determined by 2-way ANOVA.





### Supplementary Figure S7 (Related to Figure 7): Preclinical toxicity and activity of CAD204520

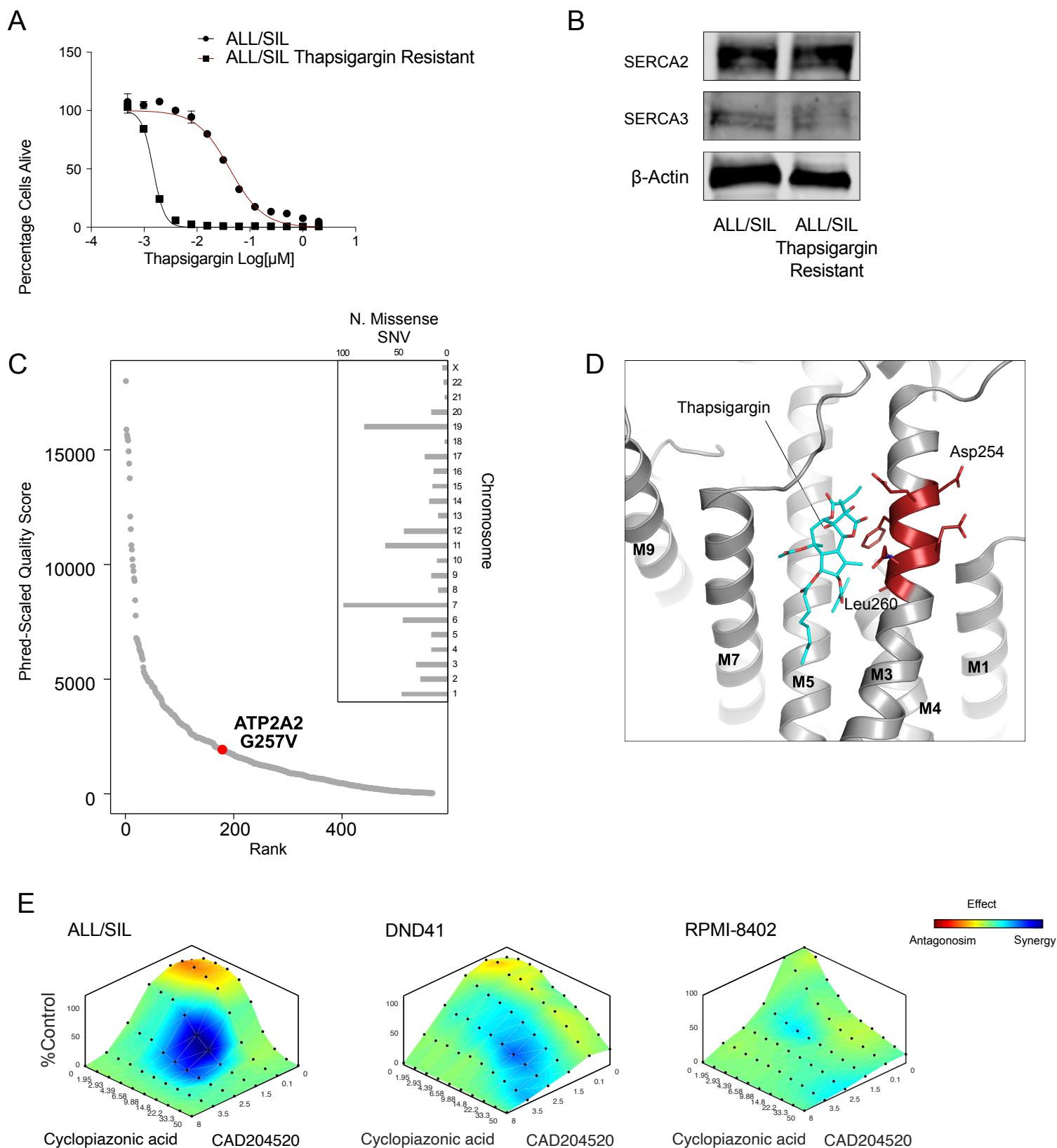
**A-B left panels:** Effect of CAD204520 treatment on rat cardiomyocyte calcium transients. Single experiments are represented by two dots interconnected by a solid line. Specifically, the line between dots connects the quantification of the amplitude of the calcium transient (A: F/F0) and the time required for cytosolic calcium removal (B: TAU), before and after the CAD204520 (5  $\mu$ M) treatment compared to control (Control). **A-B right panels:** Mean percentage variation of CAD204520 (CAD204520) on the same parameters. Graph bars: mean  $\pm$  SD of the 5 CAD204520 treated cardiomyocyte groups. Statistical significance comparing CAD204520 treated cells vs. Control cells (\* $P$  < 0.05) was determined by a non-parametric t-test (Mann-Whitney). **C)** Representative examples of calcium transients (normalized traces: fold increase) recorded from control (solid line), CAD204520 (5  $\mu$ M) (dashed line), and thapsigargin (0.2  $\mu$ M) (dotted line) ventricular myocytes. **D)** ATP Luminescence induction normalized to cellular protein content in rat cardiomyocytes treated either with CAD204520 or vehicle (Control). Error bars denote the mean  $\pm$  SD of 6 replicates. Statistical significance comparing CAD204520 treated cells vs. vehicle treated cells (not significant = n.s.) was determined by a non-parametric t-test (Mann-Whitney). **E)** Effect of administration of CAD204520 on body weight. Error bars denote the mean  $\pm$  SD of 6 replicates. Animals were treated for 6 days with 30mg/Kg of CAD204520 and subsequently treated with 60 mg/Kg daily. Statistical significance (\*\* $P$   $\leq$  0.01) was determined by a 2-way ANOVA analysis. **F)** Representative schema of CAD204520 in vivo studies. **G)** Effect of CAD204520 on T-ALL leukemia burden in a SKW-3/KE-37 xenografted murine model. Anti-leukemic activity of CAD204520 assessed by measuring hCD45+ cells after 4 days of CAD204520 treatment (45 mg/kg/OS BID) or vehicle (tween-80 0.5% w/v and HPMC 1.0% w/v). Error bars denote the mean  $\pm$  SD of 9 CAD204520 treated animals or the mean  $\pm$  SD of 8 replicates vehicles treated mice. Statistical significance for treated vs. vehicle (\*\*\*\* $P$   $\leq$  0.0001) was determined by non-parametric t-test (Mann-Whitney). **H)** Antileukemic activity of CAD204520 in hCD45+ spleen infiltrating cells in a SKW-3/KE-37 xenografted murine model after 5 days of CAD204520 treatment (45 mg/kg/OS BID) or vehicle (tween-80 0.5% w/v and HPMC 1.0% w/v). The number of hCD45+ cells per field were represented as percentage relative to vehicle control. Error bars denote the mean  $\pm$  SD of 13 fields from 2 mice treated with CAD204520 or the mean  $\pm$  SD of 12 fields from 3 vehicle treated mice. Statistical significance for treated vs. vehicle (\*\*\*\* $P$   $\leq$  0.0001) was determined by non-parametric t-test (Mann-Whitney).



**Supplementary Figure S1 (Related to Figure 1 and Table 1): Synthesis route, activity and binding mode of CAD204520**

**A)** Chemical structure of the initial hit compound: 2-(2-pyridyl)-6-(trifluoromethoxy)-1H-indole **B)** Schematic representation for medicinal chemistry optimization. R1 and R2 substitutions are indicated. **C)** Synthesis route of CAD204520 (4-[2-[2-[3-propyl-6-(trifluoromethoxy)-1H-indol-2-yl]-1-piperidyl]ethyl]morpholine). Synthetic route (a) to (e) is depicted and described in the methods section. **D)** Determination of the protein ATP hydrolysis activity in the presence of compound CAD204520 at pH 7. The figure displays ATPase activity determined by measuring the amount of liberated phosphate from ATP hydrolysis. Data is presented as a fitted curve which has been normalized to the maximal enzyme activity with subtraction of background signal from spontaneous hydrolysis of ATP. Error bars denote the mean  $\pm$  SD (standard deviation) of 3 replicates. Statistical significance (\*\* $P \leq 0.01$ ; \*\*\* $P \leq 0.001$ ) was determined by two-way ANOVA using Bonferroni's correction for multiple comparison testing. **E)** Binding sites of CAD204520 and thapsigargin. Superposition of the SERCA-CAD204520 complex with SERCA-thapsigargin (PDB ID: 2AGV). The binding sites are both in the transmembrane region, separated by transmembrane helix M3. Thapsigargin is shown as cyan surface representation. **F)** Superposition of SERCA-CAD204520 with SERCA-CPA (PDB ID 3FGO), viewed roughly along the membrane normal. CAD204520 and CPA are shown as orange and green sticks, respectively. **G)** Superposition of SERCA-CAD204520 with SERCA-BHQ (PDB ID 2AGV) viewed roughly along the membrane normal. CAD204520 and BHQ are shown as orange and light blue, respectively. **H)** Superposition of SERCA-CAD204520 with SERCA-Cpd7 (PDB ID 5NCQ), viewed along the membrane plane. CAD204520 and Cpd7 are shown as orange and magenta sticks, respectively. **I)** Binding sites of CAD204520 and thapsigargin, as seen roughly along the membrane normal. Superposition of SERCA bound to CAD204520 (light blue cartoon and orange sticks, respectively) with SERCA bound to thapsigargin (grey cartoon and sticks, respectively). Glycine257, which is mutated to valine in the thapsigargin resistant mutant, is indicated by a red sphere. In the SERCA-thapsigargin complex, Phe256 has undergone a displacement that is likely to be impaired by a valine residue in position 257.





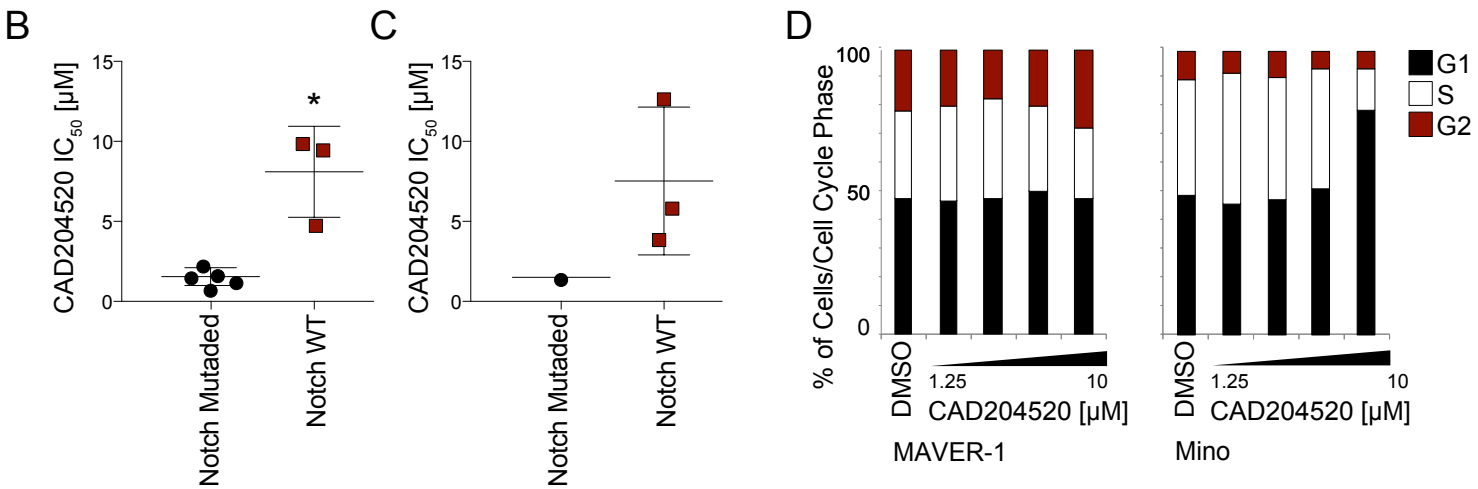
**Supplementary Figure S2 (Related to Figure 2): Identification of a thapsigargin resistant T-ALL cell line**

**A)** Effects of Thapsigargin (left) and CAD204520 (right) on cell viability after 72 hours of treatments in ALL/SIL and ALL/SIL thapsigargin-resistant cell lines. Error bars denote  $\pm$  SD of a minimum of 2 replicates. **B)** Western blot showing the expression of SERCA2 and SERCA3 in naïve and resistant ALL/SIL. -actin was used as a loading control. **C)** Phred-scale analysis of exonic single nucleotide variation (SNV) occurring in the ALL/SIL thapsigargin resistant cell line. Inset shows number (N.) of variation (SNV) occurring per chromosome. **D)** Thapsigargin resistance mutation hot spot region on helix M3. Thapsigargin and SERCA residues 254-260 are shown in stick representation and colored cyan and red, respectively. **E)** Surface plots analysis of ALL/SIL, DND41 and RPMI-8402 T-ALL cells lines and a primary NOTCH1 mutated T-ALL sample treated vehicle, CAD204520, cyclopiazonic acid, or CAD204520 plus cyclopiazonic acid. Each point represents an independent measurement representative of three biological replicates. Plots were generated using Combeneft script by MATLAB R2018 and represent the Loewe (dose-effect based approach) analysis. A color scale bar represents level of drug antagonism or synergism.

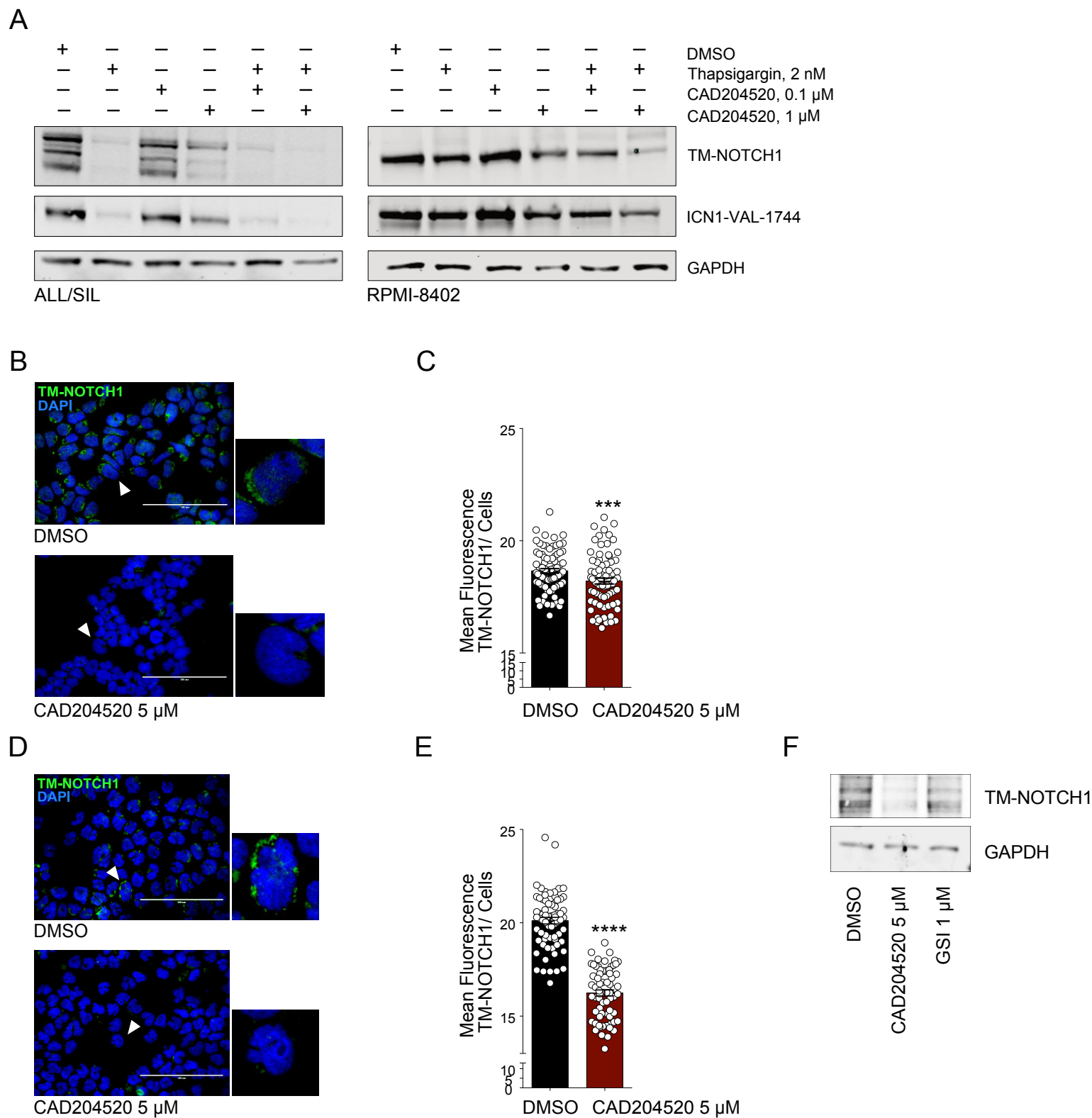
A

T-ALL Cell Line	NOTCH Protein Domains		CAD204520 IC <sub>50</sub> [μM]
	Heterodimerization (HD)	Proline, Glutamic Acid, Serine and Threonine (PEST)	
ALL/SIL	Mutated	Mutated	2.1
DND41	Mutated	Mutated	3.1
RPMI-8402	Mutated	WT	2.5
PF382	Mutated	Mutated	1.5
SKW-3/KE-37	WT	Mutated	1.5
PEER	WT	WT	9.9
Loucy	WT	WT	4.8
MOLT16	WT	WT	2.3
HSB2	WT	WT	9.5
CTV-1	WT	Mutated	0.8
REC-1	WT	Mutated	1.4
MAVER-1	WT	WT	12.7
Mino	WT	Mutated*	5.9

\* PEST domain mutation p.Q2487\* (exon 34). The effect of this mutation is to be considered ligand-dependent. E. Silkenstedt, F. Arenas, B. Colom-Sanmarti et al. Notch1 signaling in *NOTCH1*-mutated mantle cell lymphoma depends on *Delta-Like* ligand 4 and is a potential target for specific antibody therapy. J. Exp. Clin. Cancer Res, 2019. **38**(1), 446.



**Supplementary Figure S3 (Related to Figure 3): Effect of CAD204520 on NOTCH1 wild type T-ALL and MCL lines**  
**A)** Table representing NOTCH1 mutational status in T-ALL and MCL lines. **B)** Scatter dot plot representing IC<sub>50</sub> [μM] of CAD204520 in NOTCH1 mutated (n=5) or NOTCH1 WT (n=3) T-ALL or in NOTCH1 mutated (n=1) or NOTCH1 WT (n=3) MCL (shown in **C**) cell line. Statistical significance (\*P ≤ 0.05) was determined by a non-parametric t-test (Mann-Whitney). **D)** Effect of CAD204520 treatments on cycling MAVER-1 and MINO cells. Percentage of DNA content following four days of treatment with the indicated concentrations of CAD204520 on each cell cycle phase is indicated. A minimum of 20,000 events was collected for each condition.



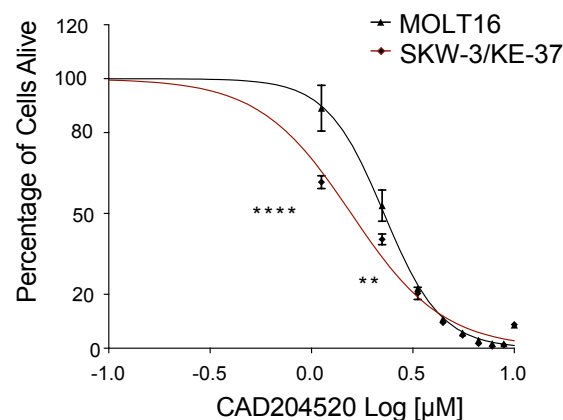
#### Supplementary Figure S4 (Related to Figure 4): Effects of CAD204520 on NOTCH1 trafficking

**A)** Effect of CAD204520 and thapsigargin treatment for 24 hours on NOTCH1 (N1) processing and activation in T-ALL cell lines. The immunoblot was incubated with an antibody against the C-terminus of NOTCH1 that recognizes the transmembrane subunit (TM) and an antibody that recognizes the cleaved NOTCH1 (ICN1). GAPDH was used as a loading control. **B)** Effect of 24 hours of CAD204520 on NOTCH1 cell surface staining as assessed by immunofluorescence in DND41 T-ALL cells. Scale bars: 100  $\mu$ m. **C)** Quantitative immunofluorescence analysis of NOTCH1 surface signal in DND41 cells after 24 hours of CAD204520 treatment. Error bars denote the mean  $\pm$  standard deviation (SD) of fluorescence of 70 single cells/nuclei (arbitrary units); Statistical significance among groups was determined by unpaired t-test ( $***P \leq 0.001$ ). **D)** Effect of 24 hours of CAD204520 on NOTCH1 cell surface staining as assessed by immunofluorescence in REC-1 T-ALL cells. Scale bars: 100  $\mu$ m. **E)** Quantitative immunofluorescence analysis of NOTCH1 surface signal in REC-1 cells after 24 hours of CAD204520 treatment. Error bars denote the mean  $\pm$  standard deviation (SD) of fluorescence of 70 single cells/nuclei (arbitrary units); Statistical significance among groups was determined by unpaired t-test ( $***P \leq 0.001$ ). **F)** Effect of 24 hours treatment of CAD204520 on NOTCH1 (N1) processing and activation in REC-1 cell line. The blot was incubated with an antibody against the C-terminus of NOTCH1 that recognizes the NOTCH1 transmembrane subunit (TM). GAPDH was used as a loading control.

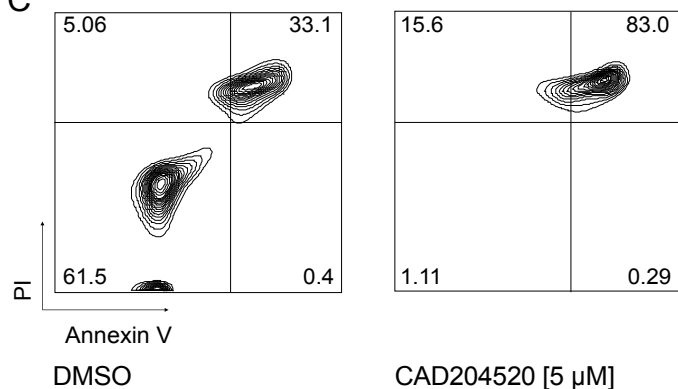
A

CELL LINES	GENOMIC PROFILE
MOLT16	<i>SIL-TAL1</i> t(3;11)(p21;p13)/ <i>LMO2</i> translocation with non- <i>TR@</i> partner t(8;14)(q24;q32)/ <i>TRAD@-MYC</i> <i>CDKN2AB</i> biallelic deletion <i>PTEN</i> c.735-736insCTTA p.P246fs*12 (exon 7)
SKW-3/KE-37	t(8;11)(p11-12;p13)/ <i>LMO2</i> translocation with non- <i>TR@</i> partner t(8;14)(q24;q32)/ <i>TRAD@-MYC</i> <i>CDKN2AB</i> biallelic deletion <i>PTEN</i> biallelic deletion <i>NOTCH1</i> c7375C>T p.Q2459* (exon 34)

B

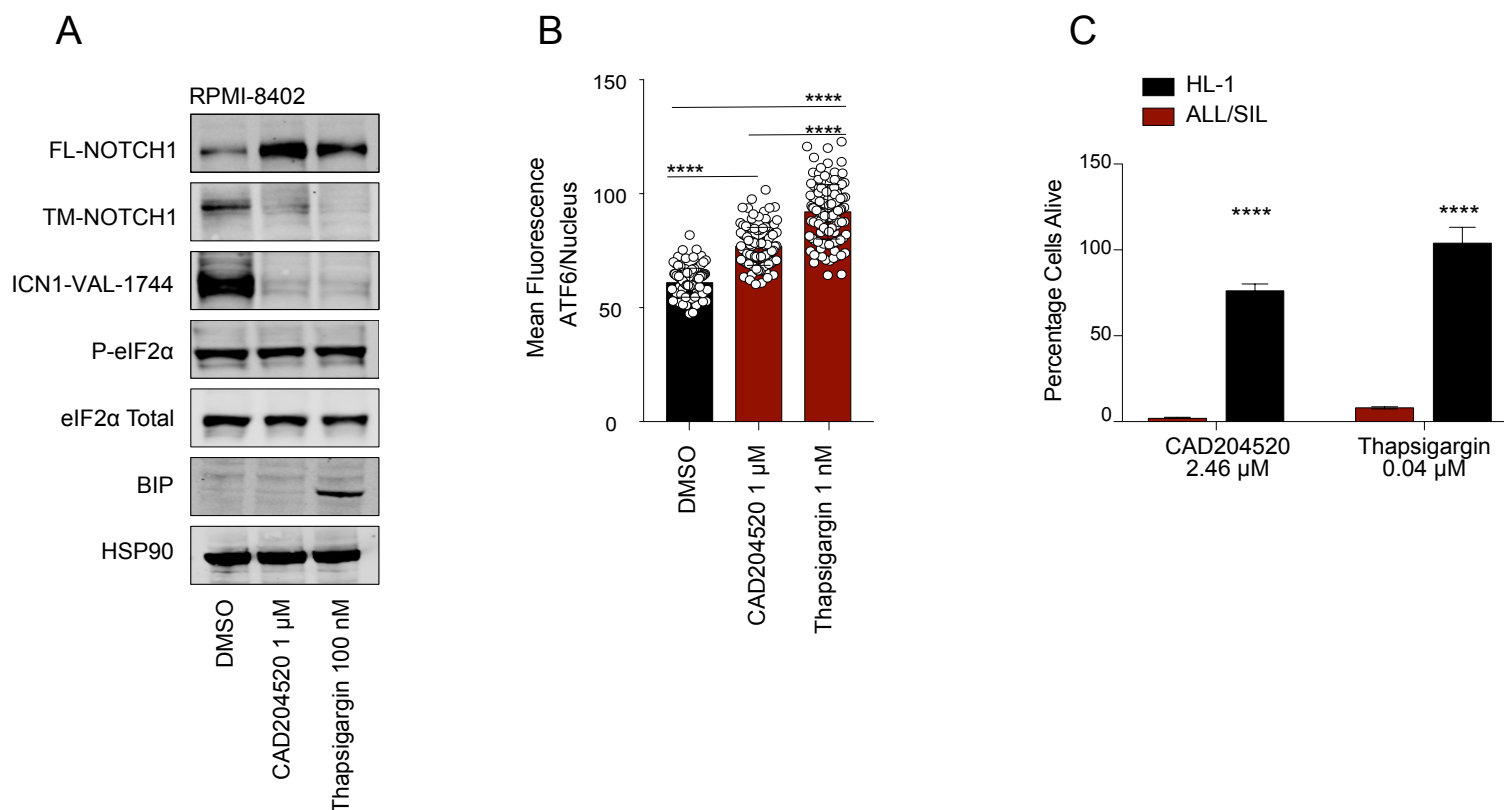


C



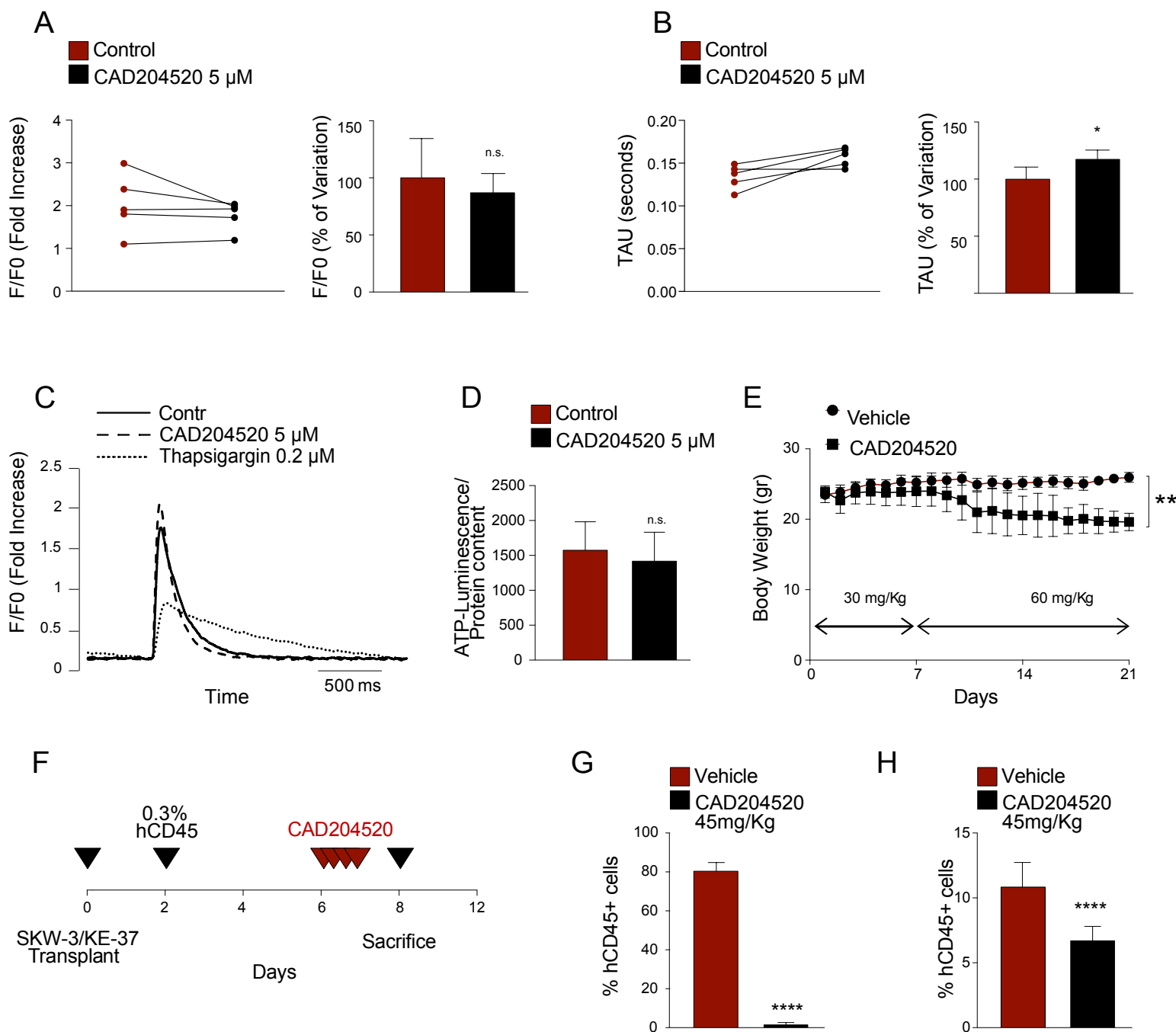
### Supplementary Figure S5 (Related to Figure 5): Genomic characterization of MOLT16 and SKW-3/KE-37 T-ALL cell lines

**A)** Genomic characterization of MOLT16 and SKW-3/KE-37 T-ALL cell line. The karyotype and the mutational analysis are indicated. **B)** Effects of CAD204520 on cell viability after 72 hours of treatments in MOLT16 and SKW/KE-37 T-ALL cell lines. Error bars denote  $\pm$  SD of 2 replicates. Statistical significance among groups was determined by 2-way ANOVA (\*\* $P \leq 0.01$ , \*\*\* $P \leq 0.001$ ). **C)** Pro-apoptotic effect of CAD204520 treatment. Annexin V/propidium iodide staining of primary NOTCH1 mutated T-ALL cells following 72 hours of treatment with the indicated concentrations of CAD204520. A minimum of 20,000 events was collected for each condition.



#### Supplementary Figure S6 (Related to Figure 6): Consequences of CAD204520 on UPR pathway

**A)** Effect of CAD204520 and thapsigargin treatment for 24 hours in RPMI-8402 cell lines. The immunoblot was stained with an antibody against the C-terminus of NOTCH1 that recognizes the furin-processed NOTCH1 transmembrane subunit (TM) and the unprocessed NOTCH1 precursor (FL), an antibody that recognizes the cleaved NOTCH1 (ICN1), and antibodies that recognize the activation of the UPR pathway. P-eIF2, eIF2, total BiP. HSP90 was used as a loading control. **B)** Quantitative immunofluorescence analysis of nuclear ATF6 signal in ALL/SIL cells after 24 hours of CAD204520 treatment. Error bars denote the mean  $\pm$  standard deviation (SD) of fluorescence of 70 single cells/nuclei (arbitrary units); Statistical significance among groups was determined using one-way ANOVA with Bonferroni's correction for multiple comparison testing ( $***P \leq 0.001$ ). **C)** Effect of CAD204520 and thapsigargin treatment in HL-1 and ALL/SIL cell lines. Histograms show percentage of cell alive after 72 hours of treatment at indicates doses. Error bar denotes the mean  $\pm$  SD of a minimum of three replicates. Statistical significance among groups ( $****P \leq 0.0001$ ) was determined by 2-way ANOVA.



### Supplementary Figure S7 (Related to Figure 7): Preclinical toxicity and activity of CAD204520

**A-B left panels:** Effect of CAD204520 treatment on rat cardiomyocyte calcium transients. Single experiments are represented by two dots interconnected by a solid line. Specifically, the line between dots connects the quantification of the amplitude of the calcium transient (A: F/F0) and the time required for cytosolic calcium removal (B: TAU), before and after the CAD204520 (5  $\mu$ M) treatment compared to control (Control). **A-B right panels:** Mean percentage variation of CAD204520 (CAD204520) on the same parameters. Graph bars: mean  $\pm$  SD of the 5 CAD204520 treated cardiomyocyte groups. Statistical significance comparing CAD204520 treated cells vs. Control cells (\* $P$  < 0.05) was determined by a non-parametric t-test (Mann-Whitney). **C)** Representative examples of calcium transients (normalized traces: fold increase) recorded from control (solid line), CAD204520 (5  $\mu$ M) (dashed line), and thapsigargin (0.2  $\mu$ M) (dotted line) ventricular myocytes. **D)** ATP Luminescence induction normalized to cellular protein content in rat cardiomyocytes treated either with CAD204520 or vehicle (Control). Error bars denote the mean  $\pm$  SD of 6 replicates. Statistical significance comparing CAD204520 treated cells vs. vehicle treated cells (not significant = n.s.) was determined by a non-parametric t-test (Mann-Whitney). **E)** Effect of administration of CAD204520 on body weight. Error bars denote the mean  $\pm$  SD of 6 replicates. Animals were treated for 6 days with 30mg/Kg of CAD204520 and subsequently treated with 60 mg/Kg daily. Statistical significance (\*\* $P$   $\leq$  0.01) was determined by a 2-way ANOVA analysis. **F)** Representative schema of CAD204520 in vivo studies. **G)** Effect of CAD204520 on T-ALL leukemia burden in a SKW-3/KE-37 xenografted murine model. Anti-leukemic activity of CAD204520 assessed by measuring hCD45+ cells after 4 days of CAD204520 treatment (45 mg/kg/OS BID) or vehicle (tween-80 0.5% w/v and HPMC 1.0% w/v). Error bars denote the mean  $\pm$  SD of 9 CAD204520 treated animals or the mean  $\pm$  SD of 8 replicates vehicles treated mice. Statistical significance for treated vs. vehicle (\*\*\*\* $P$   $\leq$  0.0001) was determined by non-parametric t-test (Mann-Whitney). **H)** Antileukemic activity of CAD204520 in hCD45+ spleen infiltrating cells in a SKW-3/KE-37 xenografted murine model after 5 days of CAD204520 treatment (45 mg/kg/OS BID) or vehicle (tween-80 0.5% w/v and HPMC 1.0% w/v). The number of hCD45+ cells per field were represented as percentage relative to vehicle control. Error bars denote the mean  $\pm$  SD of 13 fields from 2 mice treated with CAD204520 or the mean  $\pm$  SD of 12 fields from 3 vehicle treated mice. Statistical significance for treated vs. vehicle (\*\*\*\* $P$   $\leq$  0.0001) was determined by non-parametric t-test (Mann-Whitney).